Fall 2013

Halloysite nanotube composites for sustained release of antimocrobial agents (antiseptics and antibiotics)

Wenbo Wei

HALLOYSITE NANOTUBE COMPOSITES FOR SUSTAINED RELEASE OF ANTIMICROBIAL AGENTS (ANTISEPTICS AND ANTIBIOTICS)

by

Wenbo Wei, B.S.

A Dissertation Presented in Partial Fulfillment
of the Requirements of the Degree
Doctor of Philosophy

COLLEGE OF ENGINEERING AND SCIENCE
LOUISIANA TECH UNIVERSITY

November 2013

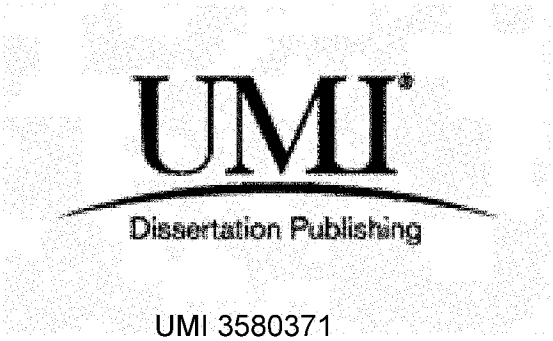

ProQuest LLC
789 East Eisenhower Parkway
P.O. Box 1346
Ann Arbor, MI 48106-1346

LOUISIANA TECH UNIVERSITY

THE GRADUATE SCHOOL

July 18, 2013

Date

We hereby recommend that the dissertation prepared under our supervision by Wenbo Wei, B.S.

entitled HALLOYSITE NANOTUBE COMPOSITES FOR SUSTAINED RELEASE OF ANTIMICROBIAL AGENTS (ANTISEPTICS AND ANTIBIOTICS)

be accepted in partial fulfillment of the requirements for the Degree of Doctor of Philosophy in Biomedical Engineering

Yuri Lvov
Supervisor of Dissertation Research

Head of Department
Biomedical Engingeering
Department

Recommendation concurred in:

Advisory Committee

Approved:
Director of Graduate Studies

Approved:
Dean of the Graduate School

Dean of the College

GS Form 13a
(6/07)

ABSTRACT

Encapsulation of antimicrobial agents (simple antiseptics and more specific antibiotics) within micro-scale and nano-scale containers may provide prolonged and more evenly distributed drug release. One of such containers proposed at Louisiana Tech is natural halloysite clay nanotubes. Halloysite is an aluminosilicate tube with a length of approximately 1 μm, outer diameter of approximately 50 nm, and internal lumen of 15 nm. The chemical composition of halloysite is similar to more common clay–kaolinite, and it can be described as rolled sheets of kaolinite. Halloysite, loaded with drugs inside its lumen, has shown aqueous release of the loaded chemicals over 10-20 hours and, with formation of the tube-end stoppers, for days. Typical loading efficiency for drugs is 5-10 wt%. An attractive aspect of halloysite nanotubes is an economically viable, green and biocompatible material. However, the size of halloysite clay tube is not in the safe size range(less than 1 μm) for injection.

In this study, halloysite tubes were used as nanocontainers loaded with antiseptics and antibiotics, and the controlled release of these drugs was monitored. The popular antiseptic brilliant green was loaded into halloysite at 5 wt% and provided sustained release over 24 hours. The release profile was fitted with an exponential first-order curve time rate of approximately 3.5 hours. Measurement of antibacterial efficiency of the brilliant green tubule nano-formulation on *S. aureus* bacterial culture demonstrated that

the antibacterial action was extended up to 72 hours (as compared with 4-5 hours activity for non-encapsulated brilliant green). In order to further decrease the release rate, tube-ending stoppers were developed. The formation of benzotriazole-copper coating on halloysite nanotubes provided additional encapsulation and slowed release of the loaded substances to 100-200 hours.

Silver ions have strong antimicrobial efficiency, and we used halloysite as a silver carrier. First, we developed template synthesis of 15 nm diameter silver nanorods inside the tube lumen and, second, spherical 5-10 nm diameter silver nanoparticles on the nanotube external surface. The composites of silver nanorods encased in halloysite tubes with the polymer paint were prepared, and the composite coating enhanced antimicrobial activity and increased the tensile strength. An additional advantage was that the coating containing 5 wt% silver-loaded halloysite did not change color after light exposure, contrary to the sample prepared with unshelled silver nanoparticles (so, we described protective core-shell effect). Halloysite nanotube templates have an additional potential for scalable manufacturing of ceramic encapsulated metal nanorods for composite materials.

In the next stage of this research project, we studied loading and slow release of two antibiotics (ciprofloxacin and gentamicin) from halloysite nanotubes. First, we demonstrated enhanced efficiency of antibiotics loaded in these clay nanotubes for multidrug-resistant gangrene bacteria (longer time action). Afterwards, we developed doping of bone cements (polymethylmethacrylate and tricalcium phosphates) with 5-8 wt% of antibiotics loaded halloysite. This approach allowed us synergetic improvement of adhesivity and strength of the bone composites in combination with

longer time (200 hours) antibiotics release. This is the time typically needed for after surgery treatment of implant-bone conjunctions (bone glue).

Orthopedic grade polymethylmethacrylate (PMMA) bone cement, admixed with prophylactic antibiotics (e.g. gentamicin), is widely used in hip and knee replacement surgery. For cement loaded with antibiotics, there is a critical need to improve its structural integrity and to control antibiotic release. In particular, preventing reaction of the drug with the cement during its polymerization is important. The resulting composite material has a significantly larger material strength and adhesion on cow bone surface and provides sustained release of antibiotics loaded within the halloysite lumen. Besides, the addition of halloysite significantly (ca. 20 ° C) reduces the PMMA polymerization temperature. When added directly, many common antibiotics have carbonyl groups that react with monomers or decompose during free radical polymerization. This construct allows separation of antibiotics from other components of the cement and hence provides a larger choice of antibiotics. In future work, antibiotics combinations in the nanotubes could be mixed in the cement with enhanced antibacterial action for a customized, sustained, "a la carte" multiple drug delivery. Halloysite nanotubes have no cytotoxic effects placing halloysite on par with other well-known materials, such as bioactive glass, silica and hydroxyapatite.

APPROVAL FOR SCHOLARLY DISSEMINATION

The author grants to the Prescott Memorial Library of Louisiana Tech University the right to reproduce, by appropriate methods, upon request, any or all portions of this Dissertation. It is understood that "proper request" consists of the agreement, on the part of the requesting party, that said reproduction is for his personal use and that subsequent reproduction will not occur without written approval of the author of this Dissertation. Further, any portions of the Dissertation used in books, papers, and other works must be appropriately referenced to this Dissertation.

Finally, the author of this Dissertation reserves the right to publish freely, in the literature, at any time, any or all portions of this Dissertation.

Author Wenbo Wei

Date 10/28/2013

DEDICATION

To my wife Zhiju Tie, my son Allen T. Wei and my family.

TABLE OF CONTENTS

LIST OF TABLES

LIST OF FIGURES

ACKNOWLEDGMENTS

I wish to express my sincere gratitude and appreciation to my advisor Dr. Yuri Lvov. His guidance, encouragement and trust have supported me throughout all aspects of my doctoral education and research. I would like to thank my committee members: Dr. Mark DeCoster, Dr. Steven A. Jones, Dr. David Mills, and Dr. Bryant Hollins for their time and contributions.

I am grateful to Dr. Zhiguo Zheng who introduced me to Dr. Yuri Lvov's research group. I want to thank Dr. Anne Hollister (LSU-Health Center, Shreveport), Dr. Elshad Abdullayev and Dr. Tatsiana Shutava for their invaluable help and experience in my research. I am thankful to Medical Technologies (Arlington, TN, USA) for providing polymethylmethacrylate cement, Orthoset 3; to Applied Minerals, Inc, NY for providing halloysite; and to Dr. Anne Hollister (LSU Health Science Center) for providing a titanium implant. I also want to thank Dr. Rebecca Giorno (Louisiana Tech University) and Renata Minullina for help growing bacteria culture. I acknowledge Dr. Shraddha Patel who started the research on brilliant green loading into halloysite.

A number of fellow graduate students: Yafei Zhao, Anupam Joshi, Xingcai Zhang, Pravin Pattekari, and Gaurav Parekh, whom I have been closely working with, gave me much useful advice and assistance, and I want to take this opportunity to thank all of them.

CHAPTER 1

INTRODUCTION

1.1 Motivation and Background

Advancing medical technology is improving longevity and quality of life, making people feel happier. However, much of the tissue in our bodies, such as heart, liver, lung and bones, has only limited ability to reproduce when damaged. To repair these tissues, tissue engineering becomes more and more important. Among other tissues, bones can be replaced with inorganic materials (implants). Ceramics, metals and plastics have been used as bone implants, but neither compares with the original bone. Therefore, bone cement, a new material, will be examined for minor bone repair and connection of implants to bones.

Advances in surgical techniques and population longevity have both increased the need for and the number of orthopedic and dental procedures worldwide [1-3]. The greater number of high risk individuals in the patient population has also led to an increase in the need for additional operations due to device/implant failure or infection. Revision procedures are also needed in the case of complicating conditions, such as bone infection and re-sorption, loss of bone mass, bone cancer reoccurrence or failure of new bone tissue to grow.

Antibiotics mixed in bone cement are widely used in hip and knee surgery to treat or prevent infection. However, there is a restricted choice of antibiotics to be mixed with

polymethylmethacrylate (PMMA) and calcium phosphate (CP) cements because they are often inactivated during composite formulation (e.g., MMA polymerization), and are released over a short time period. In addition, adding antibiotics will decrease the strength of PMMA and CP cements. Thus, there is a critical need to improve antibiotic activity and release time from the bone cements without losing its strength.

1.2 Objectives

First, we are introducing the concept of natural halloysite clay tubule nanocontainers that will be loaded with different antiseptics and antibiotics for longer active release times. Second, we doped antibiotic loaded halloysite into bone cements (polymethylmethacrylate-PMMA or calcium phosphate-CP) for their antimicrobial protection during the most dangerous first two-week period (standard time) after implant surgery. This construct allows the antibiotics to be separated from the polymerization step allows a broader range of antibiotics that would otherwise be incompatible with the polymerization step. Many common antibiotics have carbonyl groups that react with MMA or decompose during free radical polymerization. Polyelectrolyte tube encapsulation and stopper formation at the tube ends will optimize the release rate within a few days to ten days. Antibiotic combinations could be mixed in the cement with enhanced antibacterial action for a customized, "a la carte" multiple drug delivery over a sustained period. Halloysite doping will preserve cement strength and increase bone and implant adhesiveness. The tensile strength of halloysite-antibiotic composites does not deteriorate, as compared with pure cement. Clay nanotubes have shown no cytotoxic effects (up to a very high concentration of 0.8 mg/ml) placing halloysite on par with other well-known materials, such as bioactive glass and hydroxyapatite.

We loaded halloysite tubes with different antibiotics and dope them into PMMA or CP cement powder at a 5-8 wt% ratio (0.6-1 wt% antibiotic content in the composite). Halloysite loaded with antibiotics provides a simple method for their combinations in base cements. The clay tubes isolate the drugs and serve as containers for sustained release which is controlled by the tube openings. To extend drug release, the tube will be encapsulated with polyelectrolytes, urea-formaldehyde or benzotriazole cross-linking. Antibiotics-loaded halloysite admixed in PMMA or CP will provide sustained release up to 100-250 hours, and with enhanced release at crack locations in the cement. The new nanocomposite bone cement may incorporate any number of desired medical factors (singly or in combination) including antibiotics, anti-inflammatories, and imaging agents.

1.3 Outline of Dissertation

Chapter 1 introduces the motivation and some background information about this research work. The research goal and the organization of this dissertation are shown.

Chapter 2 gives a brief literature review covering the knowledge needed for this dissertation: halloysite clay nanotube description, loading and release of bioactive chemicals from halloysite, antiseptics and antibiotics loading into clay nanotubes and their additional encapsulation to extend drug release from tens to hundreds of hours, halloysite-polymer mixtures and bone cement composites: PMMA and CP bone cement.

Chapter 3 gives research methods and instrumentations for experimentation and analysis.

Chapter 4 describes using simple drug-antiseptics loading into halloysite tubes and slow release. Additional tube-end stopper formation increases the release time and

improves drug loading efficiency. The comparison of the enhanced antibacterial efficiency of drug loaded halloysite and free drugs are presented.

Chapter 5 describes the method of using halloysite nanotubes as a template to synthesize alternative antimicrobial-silver nanorods inside the halloysite lumen. The paint composite, doped with core-shell silver nanorods, presents extended antibacterial properties and protection from light exposure.

Chapter 6 demonstrates the advantages of making PMMA and CP bone cement composites with antibiotics loaded halloysite. The composites show a slow release of loaded gentamicin of hundreds of hours, and enhance the mechanical properties of the cement, such as tensile strength, adhesive strength to bone and titanium nail, and lowering the polymerization temperature. For tricalcium phosphate-CP bone cement, anoutstanding8 times tensile strength increase was demonstrated, which is especially important for this relatively mechanically weak bone implant.

Chapter 7 concludes the results of the dissertation, and recommends some future works.

CHAPTER 2

LITERATURE REVIEW

2.1 Bone Cement

Bone cement has been used very successfully to anchor artificial joints (hip joints, knee joints, shoulder and elbow joints) for more than 50 years. The bone cement fills the free space between the prosthesis and the bone and plays the important role of an elastic zone, such that the mechanical properties become very important to ensure that the artificial implant remains in place over the long term.

2.1.1 Polymethylmethacrylate (PMMA) Bone Cement

Polymethylmethacrylate (PMMA) bone cement has been used in orthopedic surgery since 1958 [1-3].Its biocompatibility and mechanical properties have made it a remarkable and indispensable tool in orthopedic repair, specifically in joint replacement arthroplasty. During surgery, PMMA is added to fill the void between the implant and the bone providing a stable construct. PMMA is commonly used for fixation in hip and knee replacement surgery.

The two-stage knee arthroplasty revision for infection, with implant removal and an interval of antibiotic therapy before implant replacement, was invented later and is a standard clinical procedure [4]. Antibiotics were added to cement to provide local antibiotic delivery in addition to intravenous doses [2-5]. This practice has improved implant survival and reduced reinfection rates. The non-porous PMMA bone cement

allows for release of only a portion of the antibiotics which are evenly distributed throughout the cement [6]. For example, current cement formulations release 75% of that released within the first 24 hours [7-9].

2.1.2 Calcium phosphate (CP) Bone Cement

Calcium phosphate (CP) bone cements and bone graft substitutes have become materials of choice for bone repair, because of their biocompatibility and osteoconductivity. Generally, a CP formulation contains calcium and phosphorous based ingredients in powder form, which on mixing with an aqueous medium, forms a workable, self-setting putty. The ingredients dissolve in the medium, making it supersaturated with the desired calcium phosphate which is re-precipitated inside the mass. The growth of the calcium phosphate phase as entangled crystallites helps the putty to retain its strength and shape. The design of a calcium phosphate cement is done on the basis of the calcium–phosphorous ratio of the final precipitate and the physicochemical characteristics of precipitation. We have chosen α and β-tricalcium phosphate as the bone cement material, which shows a desired setting time, hardness, chemical stability and biofunctionality [10].

2.1.3 Limitations of Antibiotics Mixed into Bone Cement

Prophylactic antibiotics are added while mixing the PMMA bone cement together. Gentamicin, ciprofloxacin and colistimethate are used to treat various types of bacterial infections, particularly gram-negative infections. All of these antibiotics are available in a powdered form that can be mixed into the cement base. Once pure PMMA is mixed with 0.5-1 wt% of antibiotics and used in a procedure, the antibiotics will leak

from the bone cement into surrounding areas [4,5]. The local concentration of antibiotics is usually sufficient to initially kill the bacteria left in the operative wound.

The surgical bone cement formulations face major challenges in meeting demands for more functional, bio-instructional and longer-lasting products. Current treatment modalities of mixing antibiotics in commercial bone cement have three significant limitations. First, the addition of antibiotics to bone cement leads to a weakening of PMMA and calcium phosphate bone cement, in particular, to a loss of mechanical strength. In addition, sustained releases of the antibiotics from the current bone cements are available for only a short time period, providing no long-term protection against infection [4,5]. Second, mixing-in the antibiotics uniformly is difficult, even with a sonicator. The non-porous nature of PMMA and other bone cements not only contributes to the limited release of the antibiotics, but also causes the antibiotics to be unevenly distributed throughout the cement. Mixing antibiotics intra-operatively into bone cement presents a certain risk of allergic reactions, cement mechanical failures, toxicity, and development of bacterial resistance. Third, many common antibiotics have carbonyl groups that react with PMMA monomers or decompose during free radical polymerization when added directly. This construct will allow separation of antibiotics from other components of the implants and hence provide a larger choice of antibiotics. During polymerization, the composite temperature could increase up to 80 °C, which is harmful to the adjacent tissues.

PMMA and CP material strength is also compromised by cement additives [11]. There is an essential drawback in direct loading of many antibiotics to pre-cement MMA mixtures because of the reaction with these monomers during free radical polymerization

(all antibiotics containing carboxyl groups are decomposed). The goal for bone cement halloysite composites is to achieve a more controlled, sustained release of antibiotics without compromising implant strength. Therefore, the composite will enable the use of a wider variety of antibiotics without their decomposition.

2.2 Microcapsules for Loading of Healing Agents into Polymeric Matrix

Microencapsulation of healing agents was under intensive development for polymer composites. The first example of capsule-based feedback bulk material was developed with the dicyclopentadiene (DCPD)-Grubbs' first-generation catalyst system by White, *et al.* [12]. In a series of papers describing autonomic feedback of DCPD healing agent and Grubbs' catalyst, Brown, *et al.* [13] reported high healing efficiencies for bulk polymers. Moll, *et al.* [14] developed a self-sealing composite by incorporating DCPD-filled capsules into epoxy. Rong, *et al.* [15] incorporated epoxy resin–filled capsules in an epoxy matrix containing a thermally-activated imidazole catalyst. Beiermann, *et al.* [16] extended the multicapsule PDMS system to a self-sealing laminated composite by dispersing encapsulated tin catalyst di-*n*-butyltindilaurate. A separate system with latent functionality was developed by incorporating thermally-polymerizable epoxy spheres into epoxy materials; these oxidize upon release, yielding a corrosion-preventing film [17]. Mesoporus SiO_2 nanoparticles were also used for encapsulated benzotriazole and other drugs, and incorporated them into a protective sol-gel matrix [18]. However, polymer microcapsules are soft and often ruptured by shear forces upon mixing with the polymers, causing premature release of their content. The state-of-the-art represents the application of large (>20 μm) capsules and requires mechanical opening which is not convenient for medical applications. We will use

smaller (<1 μm) tubule containers, endowed to provide effective long lasting drug release.

2.3 Halloysite Nanotubes

Halloysite occurs naturally as a hydrated mineral with the idealised chemical formula of $Al_2Si_2O_5(OH)_4 \cdot 2H_2O$. It is similar to kaolinite except for the presence of an additional water monolayer between adjacent layers. Morphologically, halloysite tubes are rolled aluminosilicate sheets with 15-20 adjacent layers in their walls. Heating halloysite to 120 °C results in evaporation of the interlayer water and in a smaller (0.7 nm) spacing in the multilayer tube walls of the dehydrated halloysite [11, 19-39].

The tubular structure with external diameters of 50-100 nm is clearly evident (Figure 2-1 a, b). The length of tubes ranges from 0.5 to 1.5 μm. Lumen diameter is 15 to 25 nm and its volume consists 15-30% of the tube volume (it may be adjusted with selective lumen etching) [37, 38]. In Figure 2-1b one can see the periodic multilayer nature of the halloysite wall as well as views of the internal aluminol (Al-OH) and external siloxane (Si-O-Si) surfaces. The periodicity in the individual layer packing, determined with X-ray analysis, was found to be 0.70±0.02 nm, which corresponds to dehydrated halloysite. Elemental composition (atomic %) of the halloysite is: Al, 18.5; Si, 19.1; O, 62.2. Brunauer-Emmett-Teller (BET) surface area of the halloysite sample was 65±10 m^2/g [23,24].

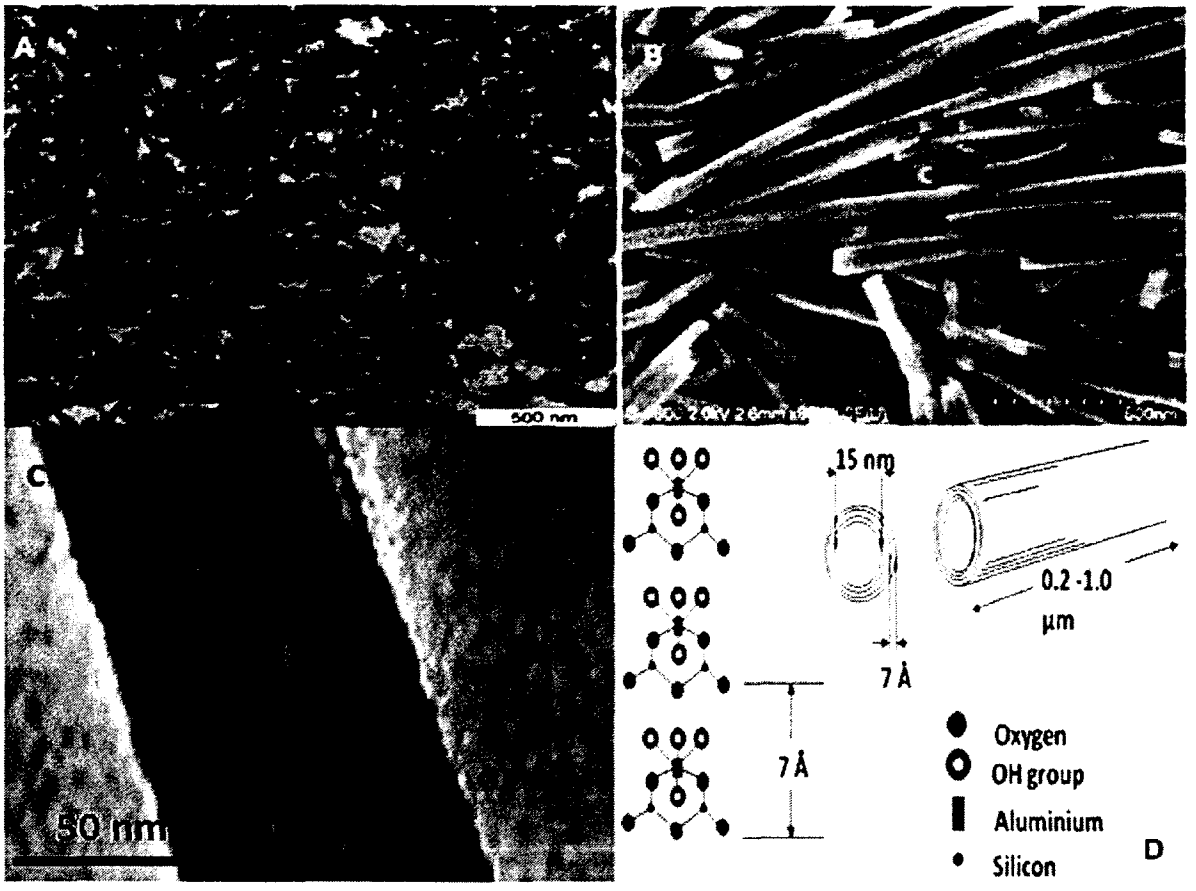

Figure 2-1: a-b TEM and SEM images of halloysite tubes with detailization (c) halloysite tube lumen (scale bar is 25 nm) (d) chemical structure of halloysite.

Figure 2-2 shows the zeta-potential for halloysite nanotubes, silica and alumina nanoparticles [34] at different pH. The zeta-potential of halloysite acts just like silica nanoparticles because the chemical on the external surface of halloysite is silica based. Halloysite has a negative charge at pH 7.

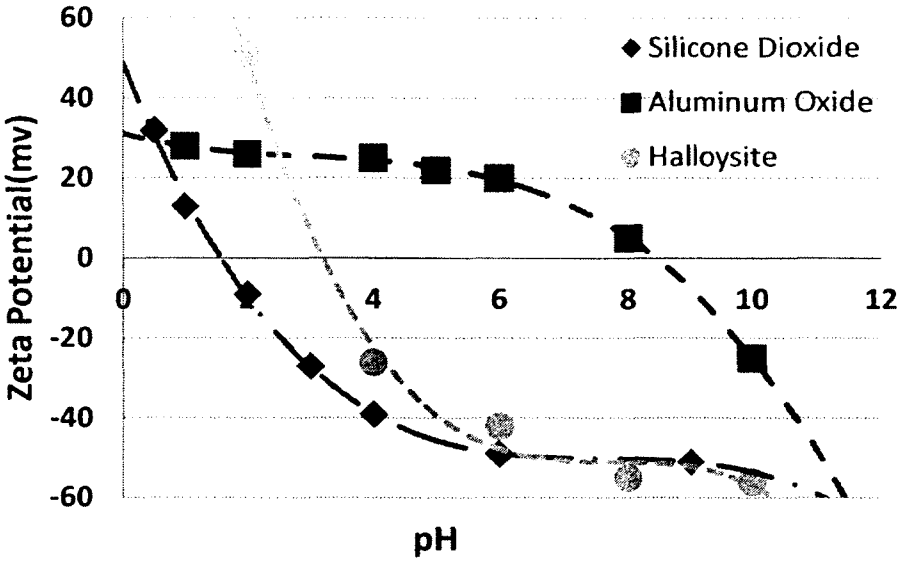

Figure 2-2: Zeta-potential for halloysite nanotubes, silica and alumina nanoparticles [34].

2.4 Halloysite Biocompatibility

Halloysite is a natural material and it does not add contamination risk to the environment. Kommireddy, *et al.*, used halloysite as a substrate for cell attachment and proliferation to test its biocompatibility [39]. *In vitro* cytotoxicity testing is one of the important biological test methods for checking the biocompatibility of a material, as per International Standard Organization (ISO) standards. The outside surface of halloysite nanotubes contains silica, which makes it negatively charged. However, for the cytotoxicity study, both negatively charged halloysite (raw halloysite) and positively charged halloysite (through coating with polycations like poly-L-lysine and protamine sulphate) were used to examine the surface interaction of the halloysite with the cells [40]. These tests were conducted on MCF-7 cells [34], and the results are shown in Figure 2-3. The percentage of live cells, as determined by Celltiter-96 reagent, was measured for various concentration of testing agents; raw halloysite, poly-L-lysine coated

halloysite, protamine sulphate coated halloysite and NaCl as a negative control. NaCl was not a good negative control because it is water soluble; however, halloysite is insoluble in water. In all cases, the halloysite was non-toxic to the cells, even with concentrations as high as 100 μg/ml. In addition, a more comprehensive study on halloysite toxicity showed that even after cells ingest halloysite into the cells cytoplasm, the cells remain alive [34].

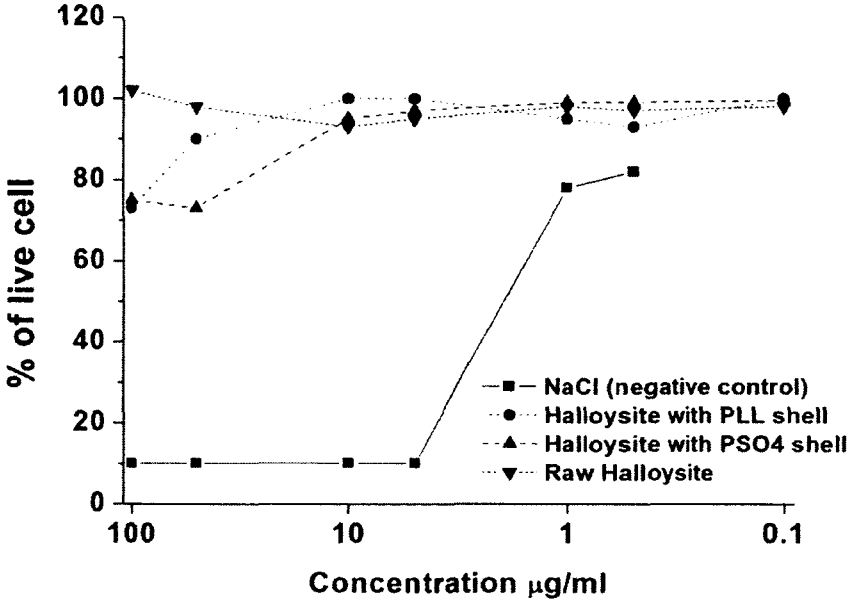

Figure 2-3: Viability assay of MCF-7 cells on halloysite nanotubes and halloysite coated with cationic polylysine (PLL) and protamine sulfate (PSO_4) (after 24 hrs) [34].

2.5 Halloysite Encapsulate and Sustain Release of Antibiotics

Based on the hollow structure of halloysite, halloysite nanotubes can be used as nanocontainers to load with a broad variety of substances for sustained and slow release. The substances can range from simple organic and inorganic molecules, to high molecular weight polymers, and biologically active substances including drugs, enzymes and DNA [19]. A typical method to load chemicals in halloysite is the vacuum method.

In the vacuum method, the first step is to add dry halloysite into a saturated solution of the chemical, and mix the suspension thoroughly by stirring or sonication. Second, place the suspension in a vacuum chamber for 10-30 minutes, which allows small air bubbles to be removed from the halloysite nanotubes. Third, vent the vacuum chamber to atmospheric pressure, during this process the chemical solution will enter into the lumen and load the chemical within the tube. Finally, repeat these steps 3-4 times to increase the loading efficiency. After loading, the halloysite is washed to remove the chemical remaining attached to the external wall. After drying, the chemical loaded into the halloysite will be remaining. Loaded halloysite will release under aqueous environment, with the release lasting approximately 10-50 hours [40-46]. The release kinetics of the chemical from the loaded halloysite follows first order kinetics with exponential function: $R = M_{\infty}(1 - e^{-kt})$, where $M_{\infty}$is the amount of active agent released at infinite time (*i.e.* amount loaded within lumen) and k is the release rate constant.

2.6 Formation of Tube Ending Stopper

Previous research has shown that halloysite nanotubes have a good ability to encapsulate chemicals and allow the slow release of these chemicals over long period time. The addition of stoppers on the end of the halloysite tubes can significantly extend the release time. Figure 2-4 shows halloysite tube endings coated with glucose complex, which is an ideal stopper for covering only the ends of the tubes. Stoppers can also be formed on loaded halloysite by coating the whole tube with nanoflims or nanoshells.

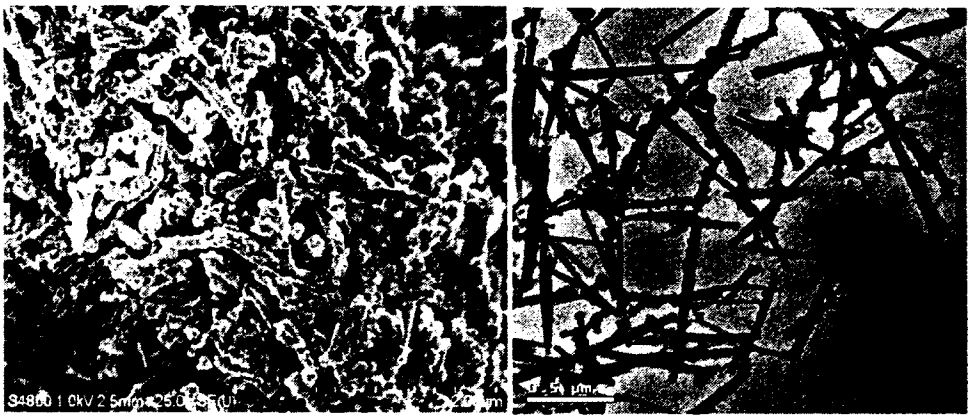

Figure 2-4: SEM and TEM of halloysite nanotubes ending with a glucose complex.

2.6.1 Use of the Layer-by-Layer Technique to Form a Stopper

The external surface of halloysite is silica based, so halloysite has a negative charge. Using the Layer-by-Layer (LbL) technique (Figure 2-5), halloysite can be effectively coated by sequential adsorption of positively and negatively charged polyelectrolytes. The multilayers of polyelectrolytes will form a shell encapsulated, loaded halloysite, working as a stopper to decrease the release of loaded substance [47].

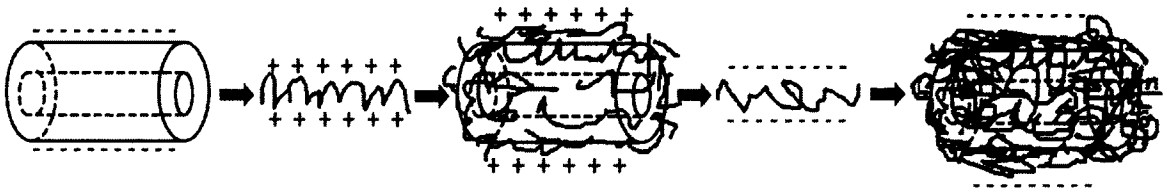

Figure 2-5: Scheme of halloysite LbL-modification with polycation and polyanion, (e.g., red PEI/ blue PSS).

2.6.2 Metal-imidazole and Metal-triazole Form Stopper

Metal ions can interact with imidazoles and triazoles to form a thin film complex (Figure 2-6). This film complex can be coated on the external halloysite surface by rinsing the halloysite with both compound solutions [23, 24, 26, 31]. The complex of

BTA-Cu is very strong and stable. Ammonia solution can be used to dissolve this complex.

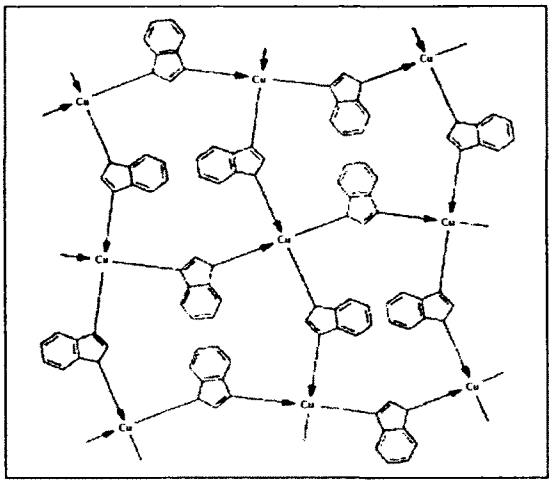

Figure 2-6: Chemical structure benzotriazole-copper complex.

2.7 Altering the Halloysite Lumen Property

To improve the loading efficiency of halloysite, we need to improve the lumen properties, such as lumen size, internal charge, hydrophobicity.

2.7.1 Increasing Lumen Size by Selective Etching

A disadvantage of halloysite is that the lumen volume is only 10-15% of the total volume, so the loading efficiency is limited by the lumen volume. To improve the loading efficiency of halloysite, the lumen volume can be increased. Because the external and interior chemistry of halloysite differ (inner: alumina; outer silicon oxide), we can selectively etch the inner alumina to enlarge the lumen size [37, 48-52]. Figure 2-7 a, b show the TEM images of sulfite acid etched halloysite, Figure 2-7 c shows the lumen diameter distribution of sulfite acid etched halloysite. At the same time, the loss of alumina leads to a larger negative charge, which can increase the inner loading efficiency of positively charged chemicals.

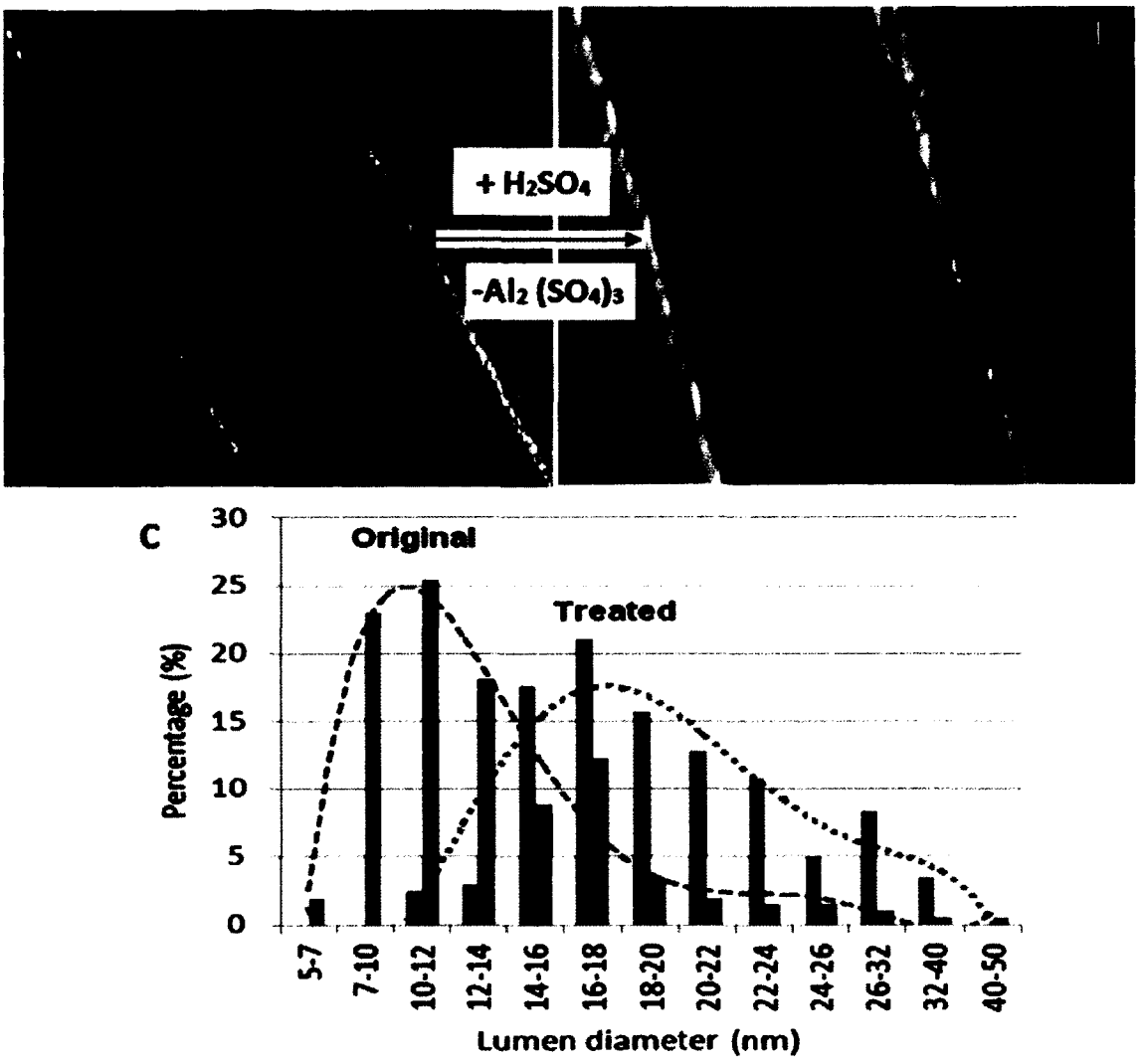

Figure 2-7: Sulfate acid etching increases the lumen diameter(a) before etching ,(b) after etching), (c) Lumen diameter distribution shows the average lumen diameter of halloysite is increased from 7-15 nm to 15-25 nm [37].

2.7.2 Modifying the Hydrophobicity of Halloysite

Natural halloysite is hydrophilic; therefore to load a hydrophobic substance inside of the halloysite lumen is very difficult, resulting a low loading efficiency. Selective modification of the halloysite inner lumen with octadecyl phosphonic acid (Figure 2-8), dopamine, or ionic surfactants will cause the inner lumen to become hydrophobic [34, 38, 53-63]. Figure 2-9 shows the release profile of ferrocene from halloysite and

halloysite-ODP over 48 hours [38]. The ODP-modified halloysite can absorb about twice as much hydrophobic ferrocene than unmodified halloysite. This result suggests that the ODP can successfully change the inner lumen to a hydrophobic state and, in turn, increase the loading efficiency for hydrophobic chemicals.

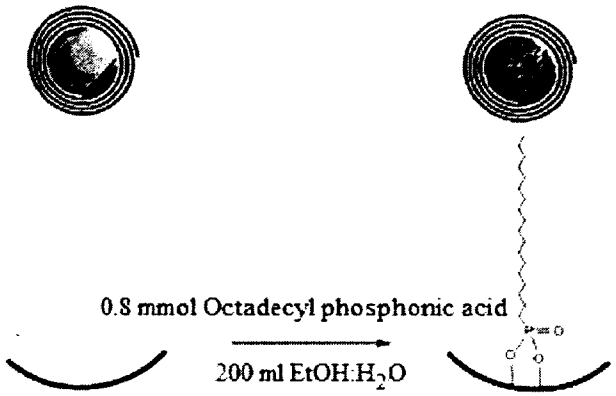

Figure 2-8: Schematic of modified halloysite inner lumen with octadecyl phosphonic acid [38].

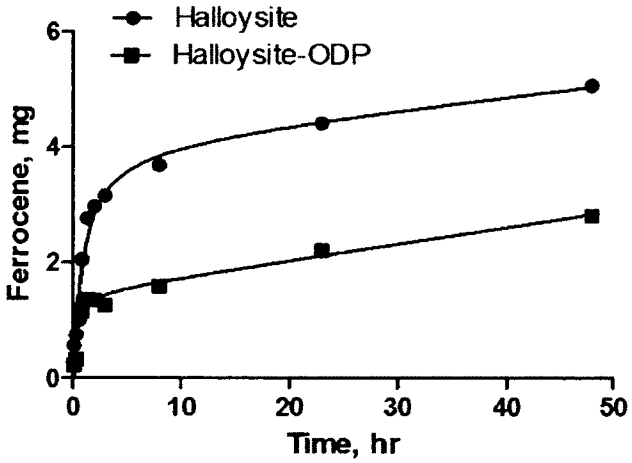

Figure 2-9: Release profile of the ferrocene from halloysite and halloysite-ODP over 48 hr [38].

2.8 Biopolymer Halloysite Nanocomposite

Halloysite nanotubes already have been proven to be biocompatible, dope loaded bioactive substances halloysite into biopolymers (amylose, DNA, pectin) can make biocomposites with functional release of loaded substances from the halloysite [64-71]. The additional halloysite added can improve mechanical strength and also provide functional properties by release of bioactive substances from halloysite. These "green" nanocomposites with sustained release of bioactive agents may find applications in cosmetics, bone implants, dentistry, for animal medicine formulation, plant nutrition, marine antifouling and other antimicrobial coatings.

2.8.1 Layer-by-Layer of Halloysite-Polycation Multilayers

The halloysite external shell has high negative charge. Thus, halloysite particles can be used as ions for thin film synthesis using the LbL-technique combined with positive charged biocompatible polycation or proteins (similar to Figure 2-5) [72,73].

2.8.2 Cast Halloysite-Biopolymer Composite from Solution

Most of the natural polymers decompose at high temperature without melting, thus, cast halloysite-biopolymer composite from polymer solution become the most common preparation method [74, 75]. Many researchers have already demonstrated that adding 10-50 wt% halloysite into biopolymers, such as starch, chitosan, gelatin, pectin, cellulose, and humic acid [71, 76-81], the mechanical and thermal properties of the composite significantly improved. For example, 4-5 wt% halloysite added in halloysite-gelatin composite, the tensile strength and elastic modulus increased to 13 and 300 MPa, respectively, compared with gelatin at 9 and 130 MPa, respectively. Figures 2-10 and Figure 2-11 show SEM images of Low-density polyethylene (LDPE) halloysite

composites and Ethylene vinyl acetate (EVA) halloysite composites. Halloysite has very good dispersion in the polymer matrix at 5-10 wt%. However, if the ratio of halloysite is up to 50 wt%, some halloysite aggregation will appear which will cause weak points and the composite will become easy to break at these points.

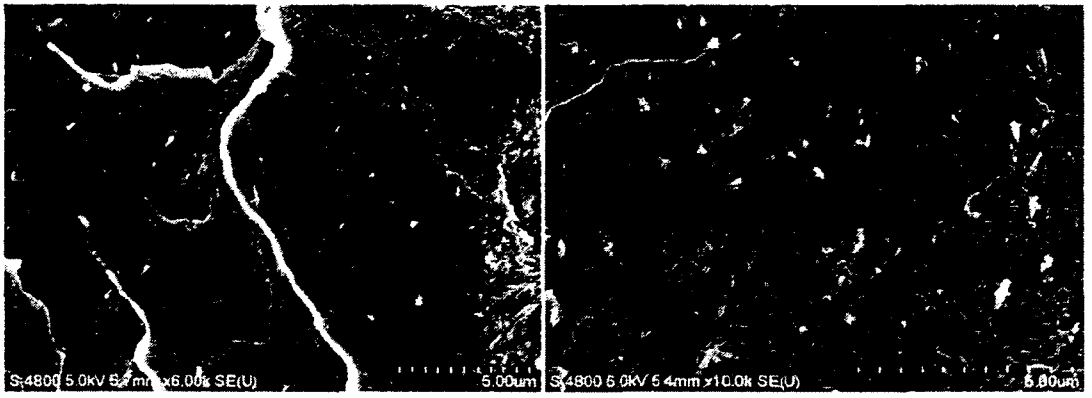

Figure 2-10: SEM image of Low-density polyethylene (LDPE) with 5 wt% (left) and 10 wt% (right) halloysite.

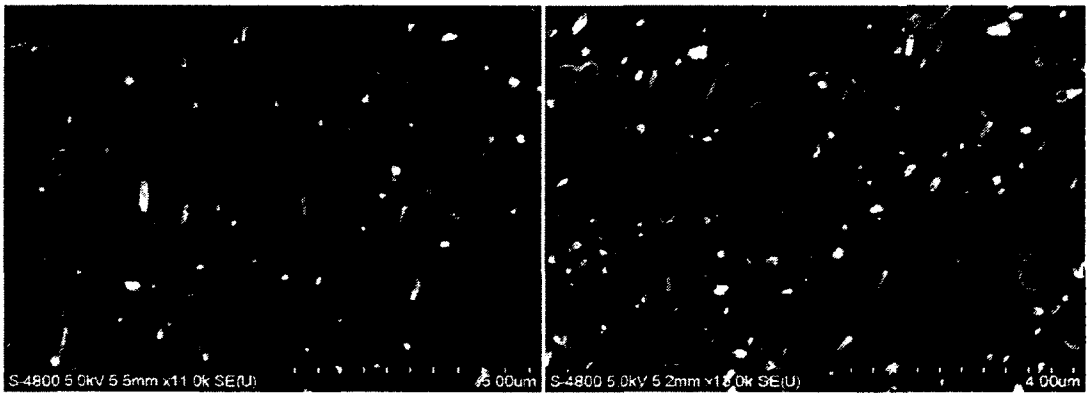

Figure 2-11: SEM image of Ethylene vinyl acetate (EVA) with 5 wt% (left) and 10 wt% (right) halloysite.

2.9 Halloysite-biopolymer composite for drug delivery

A typical loading efficiency of drug in halloysite nanotubes is 5-15 wt%, and release is within 10-50 hours. After adding loaded halloysite into biopolymer to form the

composite, the release rate will decrease and last for months, or even years. First, the loaded halloysite tubes need an aqueous environment to start the release process. In the well dispersed polymer/halloysite composite, most of halloysite tubes are located in the matrix, which makes them delay to start the release. Only the halloysite tubes near the outside surface of the composite can start the release process fast. Second, after the inside halloysite tubes release the drugs, these drugs have to go through the matrix in order to release from the composite. For example, a tetracycline loaded halloysite chitosan poloxamer composite drug delivery system was studied. This composite was capable of delivering antibiotic for up to 2.5 months and retained its sterilants over 9 months [82].

2.10 Halloysite Bone Cement Composite

What is desired is bone cement that has been augmented with material that can add strength to prevent mechanical failure, significantly increase adhesion, decrease heat effects, and provide a sustained release of loaded drugs. The material used to augment the bone cement must be biocompatible, without causing deleterious tissue changes or having toxic or injurious effects. In this study, halloysite nanotubes are used as an additional additive mix with polymethylmethacrylate (PMMA) and tricalcium phosphate (CP) bone cement to make a composite to solve the problems above.

CHAPTER 3

METHODS AND INSTRUMENTATION FOR EXPERIMENTATION AND ANALYSIS

This chapter describes the instruments and methods used in these projects.

3.1 Benchtop Vacuum Station

The method used to load a substance into halloysite nanotube in this dissertation is a vacuum method. Add powdered halloysite into a concentrated drug solution, mixed well by using stirring or sonication, then apply vacuum using a benchtop vacuum pump (Figure 3-1). Keep vacuum for 15-30 minutes, allowing air bubbles to be removed from the halloysite lumen. During the breaking of the vacuum, the drug solution will replace into the halloysite lumen and be sustained. Repeat these steps three times, followed by twice rinsing with DI water to remove the drugs adsorbed on the external surface of the halloysite. Finally, dry the samples. The dry samples will sustain the loaded substance.

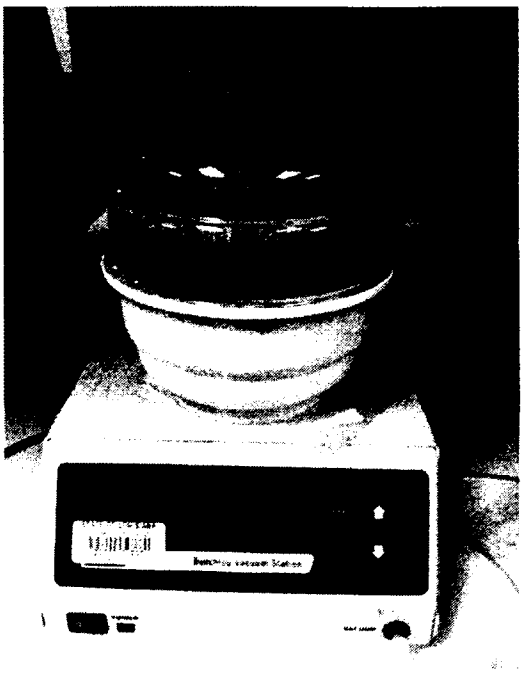

Figure 3-1: Benchtop Vacuum Station

3.2 Ultraviolet Visible Spectroscopy

In order to study the release kinetics of the substance from the halloysite, an ultraviolet visible spectrophotometer (Figure 3-2) is used to determine the amount of drugs released from the halloysite and halloysite/polymer composites. The ultraviolet-visible spectrophotometer is used for examine samples in the visible and ultraviolet regions of the electromagnetic spectrum. In UV-Vis spectroscopy, the wavelength and maximum absorbance of compounds are determined by examining electronic transitions.

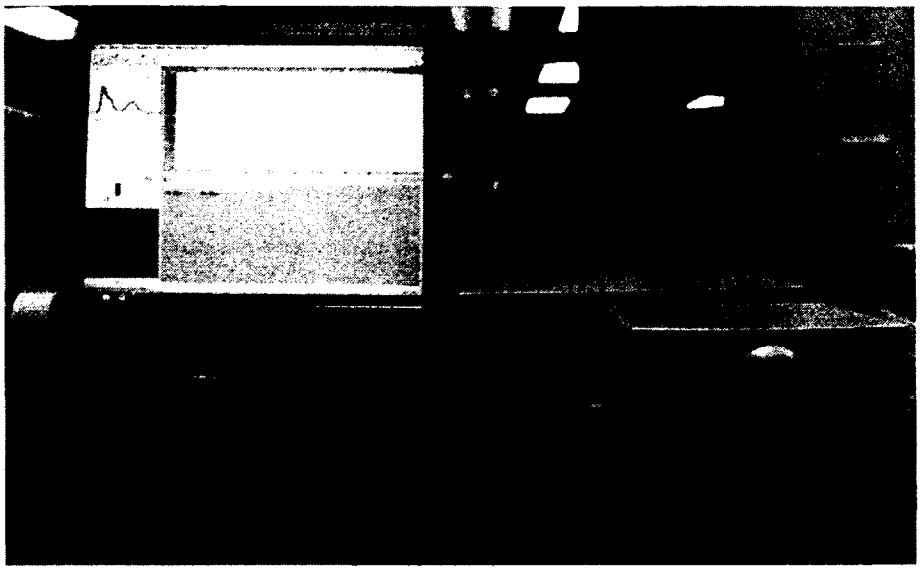

Figure 3-2: UV-vis Spectrophotometer (Agilent Technology, 2012).

3.3 Tensile Strength Meter

Figure 3-3 shows the tensile strength meter (ADMIT Corp, 2008) used in this study. The tensile strength meter is used to examine the mechanical properties of the halloysite/bone cement composites. The maximum loaded force of this machine is 2000 lb. The basic function of the tensile strength meter is to apply tension and compression to a material. There are also attachments to allow measurement of adhesive strength.

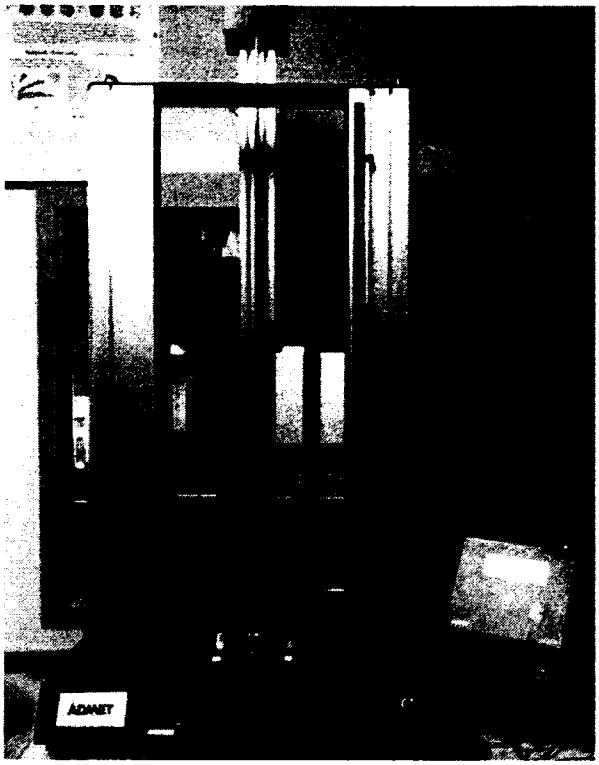

Figure 3-3: Tensile Strength Meter (ADMIT Corp, 2008).

3.4 Contact-Angle Measurement System

Figure 3-4 shows the contact-angle measurement system used in this study. This instrument is used to measure the water contact angle of the halloysite/bone cement composite surface to determine hydrophobicity. The water drop size is controlled by the system and the water drop size range is 0.5-5 μl.

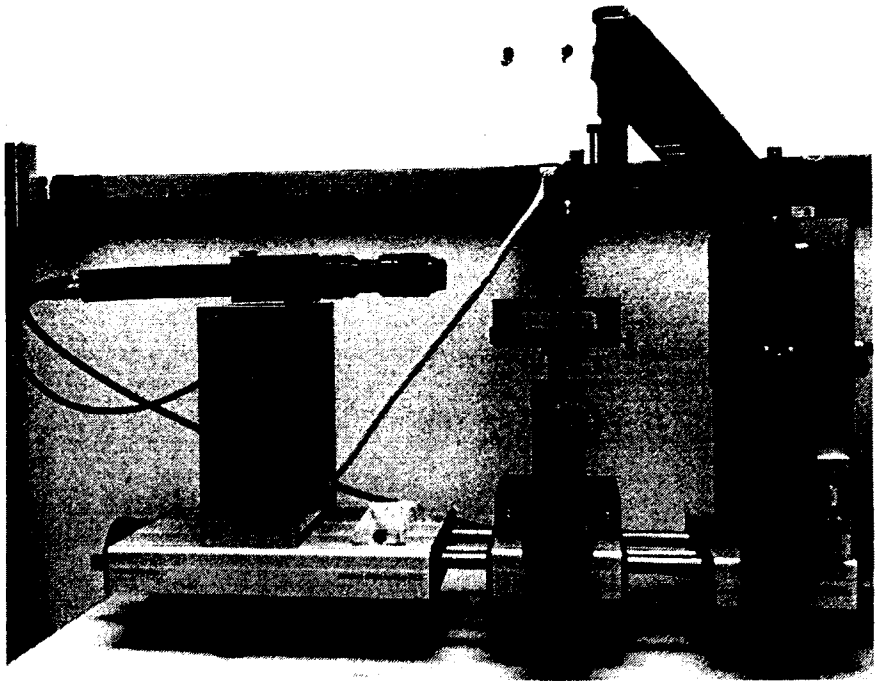

Figure 3-4: Contact-Angle Measurement System (Data Physics, Future Digital Scientific Corp, 2005).

3.5 Nitrogen & Helium Porosity Meter

Figure 3-5 shows the nitrogen & helium porosimeter used in this study. The nitrogen & helium porosimeter is used to measure the surface area and pore size. In this study, a Nova 2012, Quatachrome Instrument is used to measure the halloysite nanotube's surface area and average pore size.

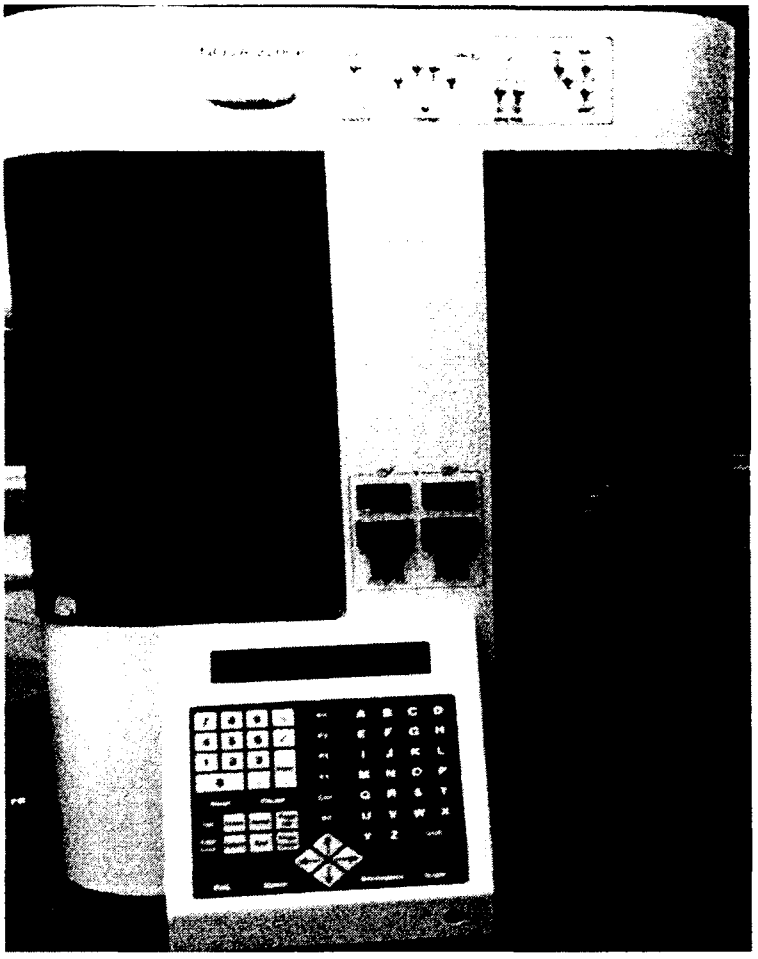

Figure 3-5: Nitrogen & Helium Porosimeter (Nova 2012, Quatachrome Instrument)

3.6 Scanning Electron Microscope Hitachi S-4800

Figure 3-6 shows the scanning electron microscope (SEM) Hitachi S-4800 used in this project. The SEM uses an electron beam as an alternative to light to form images. The electron beam, which is produced by an electron gun at the top of the microscope, passes through electromagnetic fields and lenses to focus on the sample. When the sample is scanned by the electron beam it will emit X-rays and electrons, and the X-rays and electrons are collected by suitable detectors as signals. These signals are used to form images on a monitor screen. In this study, the SEM is used to examine morphology of halloysite nanotubes and halloysite/bone cement composites.

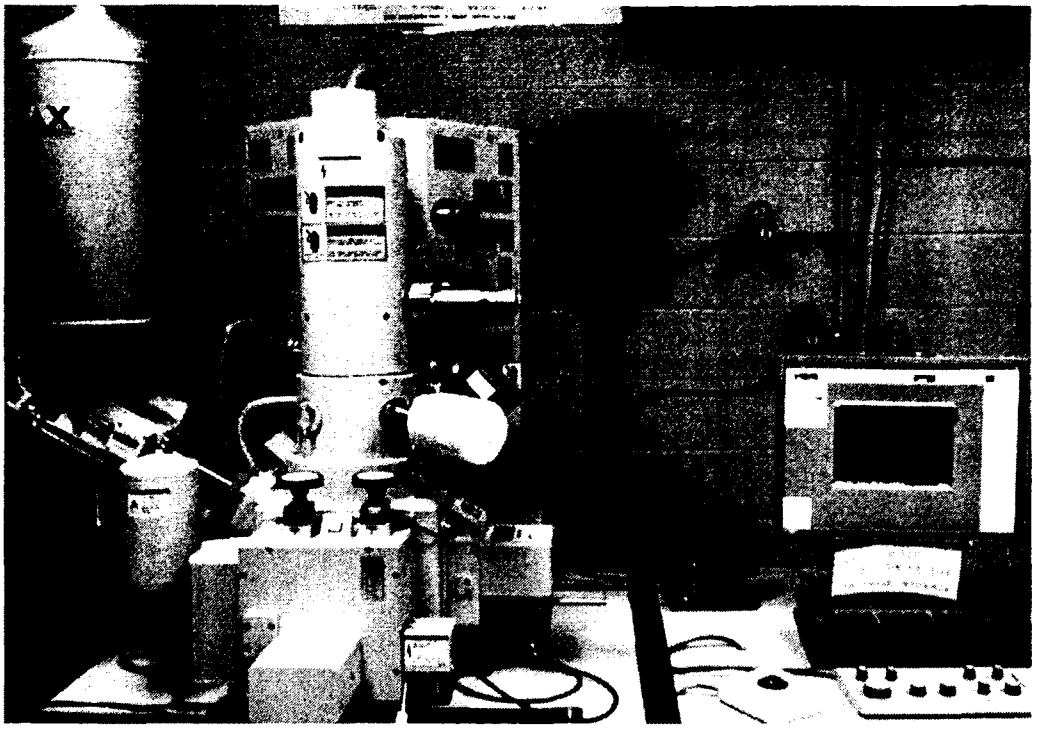

Figure 3-6: Scanning Electron Microscope (Hitachi S-4800).

3.7 Transmission Electron Microscopy Libra-120

Figure 3-7 shows the transmission electron microscopy (TEM) Libra-120 used in this project. The TEM is another electron microscope, in which the electron beam is transmitted through the sample, interacting with the sample as it passes through. The interaction of the electrons transmitted through the sample forms an image. In this project, the TEM is used to examine the morphology of halloysite nanotubes.

Figure 3-7: Transmission electron microscopy (Libra-120).

3.8 X-ray Diffraction XRD (Bruker-D8)

Figure 3-8 shows the X-ray diffraction system (Bruker-D8) used in this research. X-ray diffraction uses x-ray scattering techniques for materials characterization and quality control of crystalline or non-crystalline material. In this study, we used XRD to characterize halloysite nanotubes, and modified halloysite nanotubes.

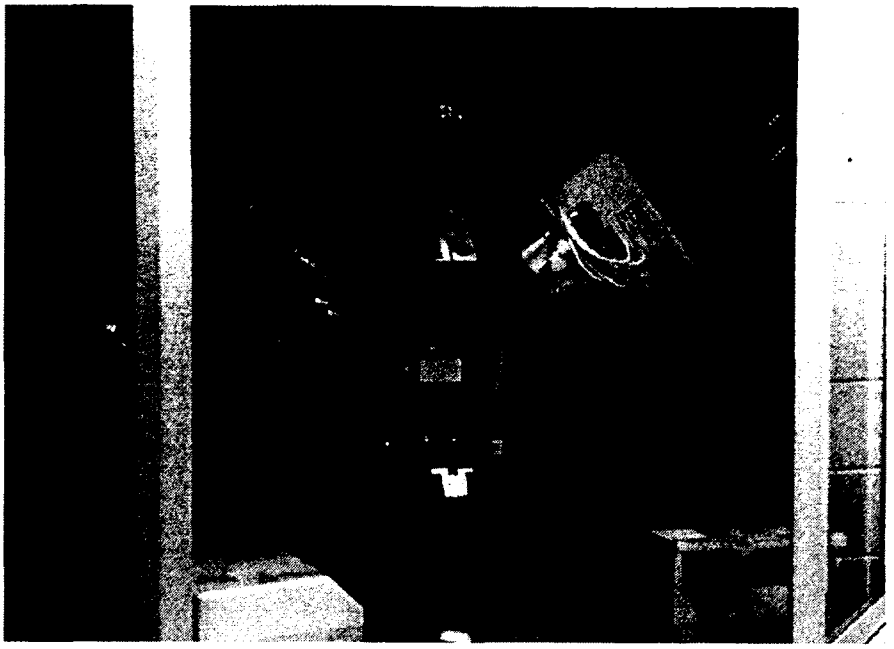

Figure 3-8: X-ray diffraction instrument (Bruker-D8).

CHAPTER 4

SUSTAINED RELEASE OF ANTISEPTICS FROM HALLOYSITE NANOTUBES

4.1 Introduction

Halloysite nanotubes are naturally occurring clay nanotubes found in several deposits worldwide [19, 34, 43]. The Dragon mine in Utah, alone, has over 2 billion tons of halloysite deposits making it economically viable for large scale production. Among other templates studied for biomineralization, drug release, and tissue engineering, halloysite has been undeservedly forgotten. Halloysite is a two-layered aluminosilicate, chemically similar to kaolin, and has a predominantly hollow tubular structure in the submicron range [11,34]. Halloysite nanotubes typically display an inner diameter ranging from 15–50 nm, an outer diameter from 10–30 nm and a length between 500–2000 nm [11,19-36].

Halloysite lumen provides a large capillary force for polar liquids (e.g. for water, capillary pressure is in the range of 100 – 500 atm) to aid in loading aqueous chemicals inside the tubes. At pH above 2.0, it has a negative surface charge characterized by electrical zeta-potential of ca.−40 mV, which allows good dispersibility in water, polar polymers and other media. Halloysite nanotubes have a large surface area of 60-70 m^2/g. These clay nanotubes can be loaded with different chemicals at 10-30 wt% and can be used for sustained and release [19,34,47,83,84]. Tube loading efficiency can further be increased with lumen enlargement using acid etching of alumina layers [37]. Halloysite

tubes are biocompatible as was checked on different cell cultures [39] and worms [34]. Surface chemistry, morphology and biocompatibility makes this nanomaterial an excellent candidate for nanopore controlled release of drugs, proteins and DNA with release time exceeding 50 hours [47,83,84]. Controlled release has been achieved using several methods such as, silanization of lumen to alter inner wall hydrophobicity or synthesis of artificial caps at tube ends [38,54].

In this study, we investigated halloysite as potential nanocontainers for loading with brilliant green to provide slow release for extended antimicrobial activity. Metal-benzotriazole nanofilms have been studied as tube end stoppers to provide controlled release reaching 200 – 300 hours. Such extended release allowed drastically increased antimicrobial efficiency of antiseptics.

4.2 Materials and Methods

4.2.1 Materials:

Halloysite has been obtained from Applied Minerals. Brilliant green, aspirin, amoxicillin, ciprofloxacin, gentamicin, Iodine, benzotriazole, copper sulfate, tryptic soy broth (TSB), and fluoresceine diacetate (FDA) were obtained from Sigma Aldrich. Propidium iodide (PI) was obtained from Fluka. NaCl (SmartSpec™ 3000) was obtained from BioRad. Plate reader: FluostarOptima (BMG Latch), and FLx800 was used for checking bacterial cell viability. Cells were imaged with Nikon Eclipse TE 2000-U inverted fluorescent microscope (Japan) equipped with CCD OI-17-EM monochrome digital camera. Halloysite has been characterized with SEM (Hitachi 4800 FESEM) at 5 kV acceleration voltage.

4.2.2 Loading Procedures

Brilliant green (200 mg) was dissolved in 10 ml acetone. 500 mg of halloysite was then added to the solution and thoroughly mixed followed by sonication for 30 minutes. The solution was placed in a vacuum chamber at 100 torr for 30 minutes. Air bubbles were removed from the halloysite pores causing the drug solution to enter within the lumen. After 30 minutes the vacuum was released and the suspension was taken out from the vacuum chamber to be kept at standard atmosphere for 15 minutes. This vacuum cycle was repeated three times followed by washing with DI water to remove any unloaded antibiotic. Samples were placed in an oven at 50 °C for drying. The dried sample was milled to a fine powder. Figure 4-1 shows a typical procedure of load active agents into halloysite nanotube.

Figure 4-1: Loading procedure of active agents into halloysite nanotube.

4.2.3 Tube Encapsulation Benzotriazole-Copper Complexation

Halloysite was additionally encapsulated with benzotriazole-copper film to provide controlled release (Figure 4-2). Nanotubes loaded with antiseptics were washed with benzotriazole solution in acetone and followed by aqueous $CuSO_4$. Nanoporous film has been formed by the interaction of adsorbed benzotriazole with copper ions (Cu^{2+}). Antibiotic release is achieved through the pores existing in the film. The structure of this

film has been described in [26]. Pore size (*i.e.* release rate) has been controlled by varying the concentrations of the benzotriazole and Cu (II).

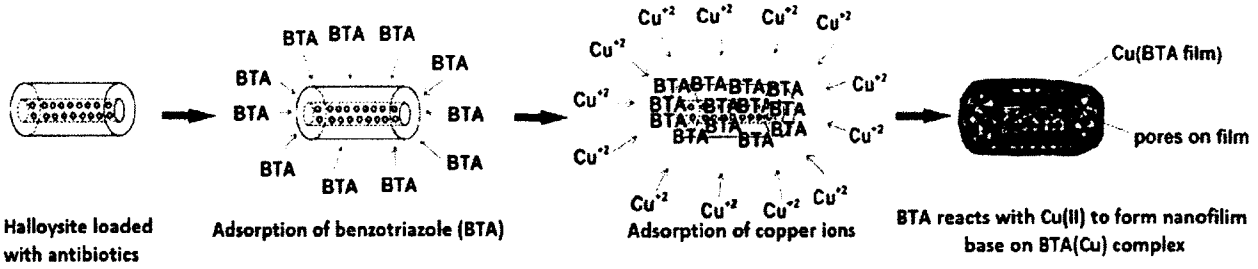

Figure 4-2: Formation of caps on antibiotic loaded halloysite tubes.

4.2.4 Drug Release from Halloysite

Drug release experiments were conducted by stirring 50 mg of antibiotic loaded halloysite in1 ml of deionized water (DI). At each reading, the supernatant was removed by centrifugation at 7000 rpm and fresh DI water added. The collected supernatant was analyzed by UV-Vis spectroscopy (Agilent 8453) at 625 nm wavelength for the amount of brilliant green released.

After 72 hours of release, nanotubes were dispersed in 50 ml of DI water and sonicated in ultrasonic bath for 30 minutes. Then the supernatant was collected by centrifugation at 5000 rpm. This process was repeated one more time to normalized 100% release.

4.2.5 Cultivation of Staphylococcusaureus

Bacteria were cultivated in tryptic soy broth (TSB, Sigma) at 37 ° C according to manufacturer protocol. 30 g of rehydrated media was dissolved in 1L of DI water and sterilized at 121 ° C for 1h. A day before the experiment, bacteria was inoculated into fresh broth and grown overnight. Concentration of cells was determined by UV spectrophotometric measurement at 600 nm (SmartSpec™ 3000, BioRad) with

conventional coefficient of 1 o.u. being equal to 10^8 CFU/ml. Purity of culture was checked by standard Gram-staining technique.

4.2.6 Kinetic Viability Assay

A 5 ml aliquot of cells at a concentration of 10^4 CFU/ml was used for each experiment. Dried loaded tubes were placed into tubes containing 10^4 CFU/ml and cultivated at 37° C in shaker-incubator during 24-72 h. After every 24 hours 1 ml aliquots were collected and the replacement of the old media aseptically by fresh nutrient media followed. The remaining 4 ml of sample was centrifuged for 5 min at 8000 rpm. The supernatant was removed and aseptically replaced by 5 ml fresh TSB, vortexed, and incubated.

4.2.7 Live/Dead Assay

Live/dead cell ratio was monitored by fluoresceine diacetate/propidium iodide (FDA/PI) double staining. FDA is a non-fluorescent ester which is able to pass through cell membranes and become fluorescent after intracellular esterase cleavage. PI stains only membrane compromised cells. First, 0.5 ml of each sample was washed by 0.85% NaCl twice followed by centrifugation at 7000 rpm. Then, 2.5 µl of FDA was added to each sample from a stock-solution of 10 mg/ml in acetone (final amount of FDA 50 µg) and incubated for 20 min at room temperature. After that, 2.5 µl of PI stock-solution (1 mg/ml in water) was added to each tube and incubated for 10 min. Finally, 100 µl of each sample were dispensed in 96-well black plate in three replicates and fluorescence intensity was measured at 540 nm for FDA (excited at 485 nm) and at 600 nm for PI (excited at 548 nm). Live/dead cell ratio was represented as the relative ratio of green/red fluorescence units.

4.2.8 Fluorescent Microscopy

Nikon Eclipse TE 2000-U (Japan) inverted fluorescent microscope equipped with Cool Snap ES Photometric monochrome digital camera was used to visualize treated cells using FDA/PI double staining of *S. aureus* cells. Before microscopic observation, cells of 10^8 CFU/ml concentration were incubated in TSB nutrient media supplemented with free brilliant green (BG), BG loaded halloysite, and BG loaded halloysite capped with benzotriazole-copper stoppers for 3 hours. Weights of these additives were adjusted so that each sample contain663 μM of BG, assuming that loading efficiency of sample without stopper is 5% while loading efficiency of sample with stopper is 15% (values for loading efficiencies were obtained from BG release studies). Following this, cells were washed twice with sterile 0.85% NaCl and centrifuged at 7000 rpm for 2 min. Then precipitated cells were resuspended in 0.5 ml 0.85% NaCl sterile solution. To this solution 0.75 μl of PI (stock solution in DMSO 20 mM) and 0.5 μl of FDA (stock solution in acetone 10 mg/ml) were added, vortexed and incubated for 20 min at room temperature. Samples were analyzed using fluoresce microscopy using broadband blue filter (λ_{ex} = 480 nm, λ_{em} = 535 nm) for viable cells and green filter (λ_{ex} = 540 nm, λ_{em} = 620 nm) for dead cells. Pictures were colored using MetaMorph software. As a control sample, we used *S. aureus* cells at a concentration of 10^8 CFU/ml incubated at room temperature for 3 hrs without the addition of halloysite and BG.

4.3 Results and Discussion

Preliminary results on brilliant green were obtained by Shraddha Parshottambhai Patel in our IfM nanoassembly lab-L7, co-advised by Dr. Mills and Dr. Lvov. According to Patel's dissertation tilted "Nanotechnology In Regenerative Medicine," it was shown

the release profiles of pristine halloysite loaded with brilliant green, chlorhexidine, iodine curcuma longa, povidone iodine, amoxycillin and doxycyclin. In my dissertation work, we extended and improved this technique with encapsulating loaded halloysite nanotubes with additional end-stoppers to slow-down antiseptics release time and to increase loading efficiency by selective lumen etching. All drugs release results presented in this Chapter are obtained by myself.

4.3.1 Release of Active Agents

In this study, several drugs were used to load in the halloysite. The release results show loaded halloysite can slow the release of the loaded substance for 5-48 hours, as compared to free drugs release in water within only 15 minutes. Figure 4-3 shows all the drug formulas used in this study.

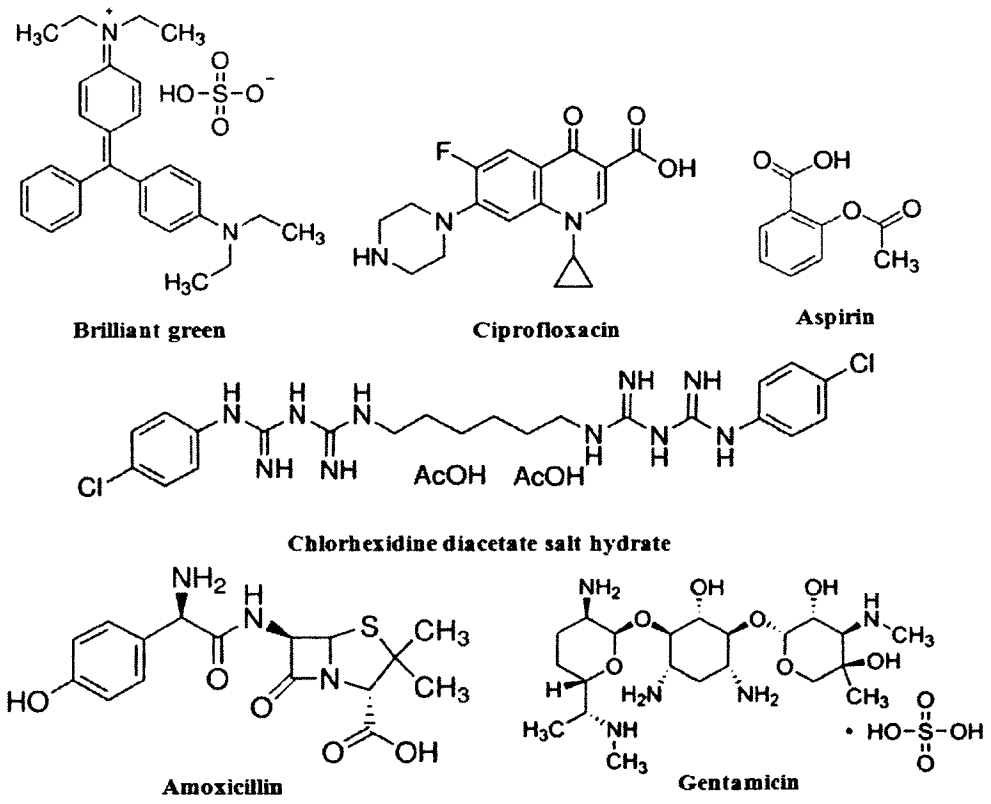

Figure 4-3: Molecular structures of the drugs used in this study.

4.3.2 Brilliant Green Release from Halloysite with BTA-Cu Stopper

A commonly used antiseptic agent - brilliant green (BG) was studied in three different forms; free microcrystals, loaded within halloysite lumen, and loaded within halloysite followed by sealing with BTA-Cu nanofilms as nanotube end caps. As one can imagine, the level of encapsulation increases in the above mentioned order. Free microcrystals have no shells for sustained release, while halloysite and BTA-Cu films provide tight control over the brilliant green release rate (Figure 4-4). Crystals of brilliant green reached 100% release within 15 minutes; however, release from halloysite lumen was about 70% in 3 hours. BTA-Cu stoppers allowed only 4% of brilliant green release within 3 hours.

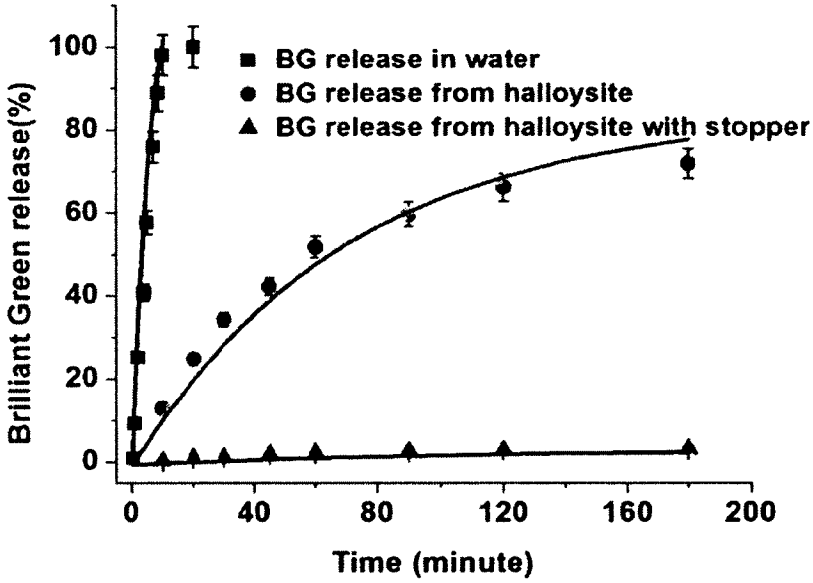

Figure 4-4: Brilliant green releases in water, from loaded halloysite, from loaded halloysite with BTA-Cu stopper.

Factors affecting BTA-Cu film formation, i.e. the concentrations of the BTA and Cu (II), were studied in detail. Concentrations of BTA and $CuSO_4$ were varied from 40–170 mM and 4–80 mM ranges, respectively. Figure 4-5 a, b present BG release

curves from halloysite treated with these films. The release rate gradually decreases at a fixed Cu (II) concentration of 4 mM upon increasing the BTA concentration (Figure 4-5 a), as expected. A tighter film forms at higher BTA concentrations leading to smaller pores, retarding the release rates. Surprisingly, an opposite phenomenon was observed at high Cu (II) concentration of 80 mM. In this case BG release rate is slowest at 41mM BTA concentration and gradually increases with the increasing of its concentration. This might be explained by the variation of BG loading efficiency upon formation of the caps. As one would expect, faster film formation occurs upon using higher concentrations of BTA, which results in lesser amounts of leaked BG during film formation. Higher loading efficiency causes a higher concentration gradient between the inner pores and the external solution, which is the major driving force for drug release. Indeed, loading efficiencies of the samples capped with 41mM, 82 mM and 165 mM BTA and 80 mM $CuSO_4$ solutions increase from 6.5 wt% to 15.8 wt%. Compared with loaded halloysite without stopper, the loading efficiency was only 3wt%. From here we conclude that two main factors affect the BG release rate; loading efficiency and BTA-Cu film porosity. Loading efficiency dominates at higher Cu (II) concentrations, while film porosity dominates at lower concentrations. These effects allow for long lasting release of active agents loaded within the halloysite lumen, and they can be generalized to all the bioactive agents.

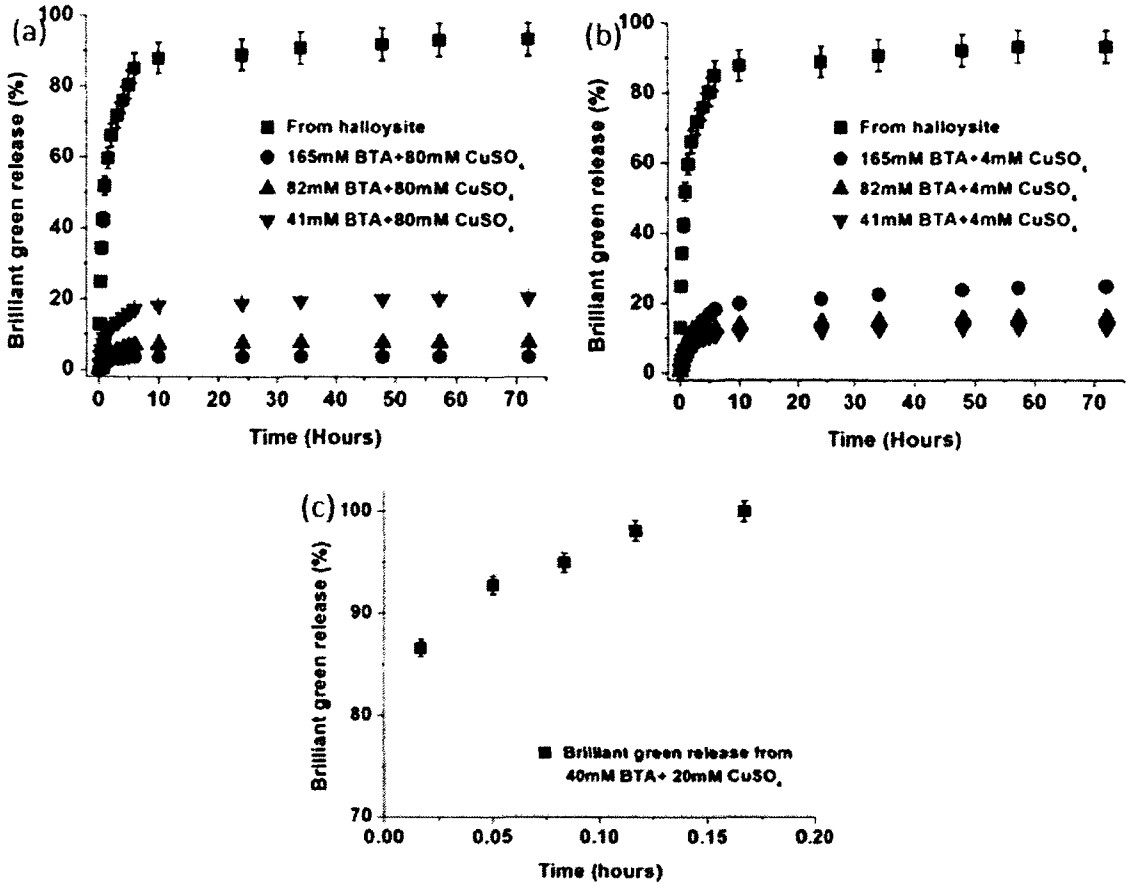

Figure 4-5: (a) BTA-Cu stopper which has various concentrations of BTA and 80 mM $CuSO_4$. (b) halloysite with BTA-Cu stoppers which have various concentrations of BTA and 4 mM $CuSO_4$.(c) Brilliant green release from microcrystals BTA-Cu encapsulated without halloysite tubes.

Release curves in Figure 4-4 and Figure 4-5 can be described by using first order kinetics: $R = M_\infty(1 - e^{-kt})$, where M_∞ is the amount of active agent released at infinite time (*i.e.* amount loaded within the lumen) and k is the release rate constant. Release profiles are composed of two parts: Rapid release in the initial 6 hours and slow release in the remaining time. Different constants of the reaction rate were used to describe these two parts of the release profiles. They are presented in Table 4-1. Initial release is associated with brilliant green that is deposited close to tube endings or external pockets

of the tubes. These molecules are loosely attached to the halloysite surface and release quickly in water.

Table 4-1: First order release parameters M_∞-k of different brilliant green release samples.

Sample	M_∞ (6hours)	K (6hours)	M_∞(remain)	k2(remain)	LE(wt%)
BG release in water	122	10.4	-	-	-
BG release from halloysite	83	0.84	93	0.37	2.8%
165 mM BTA+80 mM Cu	3.5	0.65	3.8	0.40	15.8%
82 mM BTA+80 mM Cu	7.0	0.59	7.75	0.39	11.5%
41 mM BTA+80 mM Cu	17	0.53	20.2	0.27	6.5%
165 mM BTA+4 mM Cu	18	0.55	24	0.21	10.8%
82 mM BTA+4 mM Cu	12.5	0.55	15.5	0.27	8.6%
41 mM BTA+4 mM Cu	11	0.65	12.7	0.33	7.8%

4.3.3 Antibacterial Effect of Brilliant Green Loaded Halloysite

Figure 4-6 shows live/dead ratio of *Staphylococcusaureus* cells with different BG loaded halloysite samples with and without stopper and free brilliant green. We used fluoresceine diacetate and propidium iodide double staining to assess the value of the live/dead cell ratio using plate reader assay. Kinetic experiments include centrifugation and discarding of old media steps, which leads to an unavoidable loss of cells causing by turn change in relative fluorescence intensity of the living cells. According to the results of the fluorescent plate reader assay, both brilliant green loaded halloysite with and without stopper suppress the growth of *S. aureus*, as compared with untreated cells. In addition, free brilliant green only suppress the growth of *S. aureus* within approximately

5 to 10 hours; after that, *S. aureus* cells grow similar to the untreated sample. Kinetic viability test data has shown that capped BG-loaded tubes significantly inhibit bacteria growth, as compared to both untreated control (165 mM BTA 80 mM Cu) and uncapped sample (BG HNTs). Bacteria growing in nutrient media supplemented by equal amount of free BG continue growing after 1st media replacement. Moreover, it has been observed that *S. aureus* decolorize free brilliant green for 5 hours, whereas media containing loaded halloysite tubes remains green within 72 hrs. Previous studies have shown that the inhibitory effect of brilliant green is connected with the colored form of the dye [85].

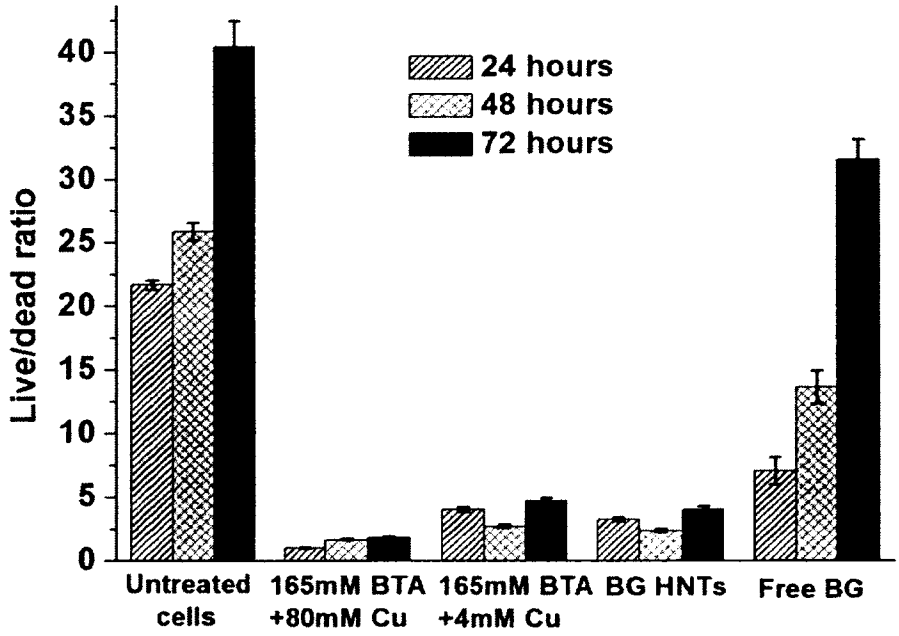

Figure 4-6: Kinetic of live/dead *S. aureus* cells ratio treated with brilliant green loaded halloysite with and without stopper and free brilliant green. Data are represented as Average±2SE. Control – untreated cells.

Samples were visualized using Fluorescence microscopy with broadband blue filter ((λ_{ex}= 480 nm, λ_{em} = 535 nm) for live cells and green filter (λ_{ex} = 540 nm, λ_{em} = 620 nm) for dead cells. In the images presented in Figure 4-7, green dots represent live cells while red dots indicate dead ones.

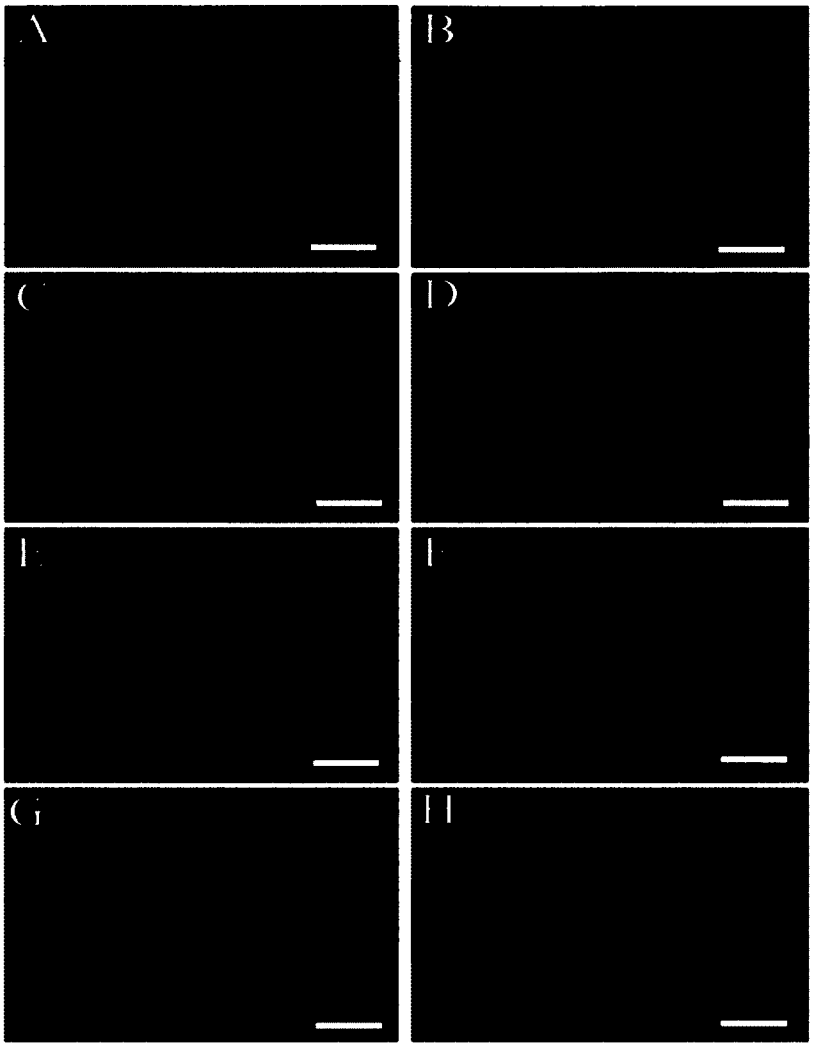

Figure 4-7: Fluorescent micrographs of samples untreated (A, B) and treated *S. aureus* cells with 663 μM of free brilliant green (C, D), loaded halloysite nanotubes without stopper (E, F) and loaded halloysite nanotubes with stoppers (G, H). Scale bar – 10 μm. Pseudo-colors.

According to fluorescence microscopy data, one can clearly see that the samples treated with loaded halloysite (capped and uncapped) and free brilliant green contain dead membrane compromised cells as compared with the control sample. The control contained 3±1% dead cells whereas the free BG treated sample, BG-HNTs treated and 165 mM BTA 80 mM Cu loaded capped HNTs treated cells, contained 80±5%, 65±3% and 68±4% dead cells, respectively. The significantly large amount of dead cells in the

sample treated free BG can be explained by immediate action of BG, but, according to the kinetic viability assay, bactericide action of BG lasts less than 24 h and is eliminated after the 1st media replacement (Figure 4-6). It was also noticed that some cells have double green/red emission. This phenomenon can be explained in that brilliant green partially damages the cell membrane and enables propidium iodide to penetrate through the formed gaps and stain the nucleic acids inside the cells.

Other commonly used antiseptics, such as tetracycline and benzotriazole, were also loaded into halloysite nanotubes at 5-6 wt% and have shown 6-10 hours release time even without additional encapsulation. This proves that, for a number of simple antiseptics, we may drastically increase their antibacterial activity over many tens to and hundreds of hours. This is especially important for hospital-acquired infections (with the well-known nosocomial infections) which drives even further the use of antimicrobials in medical applications.

4.3.4 Other Loaded Drugs into Halloysite

In this study, some other drugs (aspirin, amoxicillin, ciprofloxacin, gentamicin, Iodine) also were used. All drugs used the vacuum method (section 2.5) in order to be loaded into halloysite.

Figure 4-8 shows the release of aspirin from loaded halloysite. About 90% of aspirin released within the first hour.

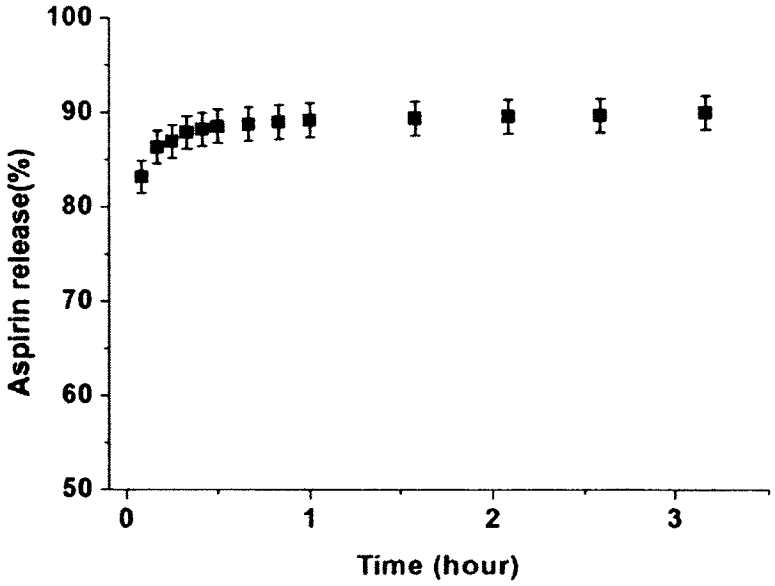

Figure 4-8: Release of aspirin from halloysite.

Figure 4-9 shows the release of amoxicillin from halloysite. Compared with free amoxicillin release in water in only 15 minutes, the loaded amoxicillin releases 90% in three hours.

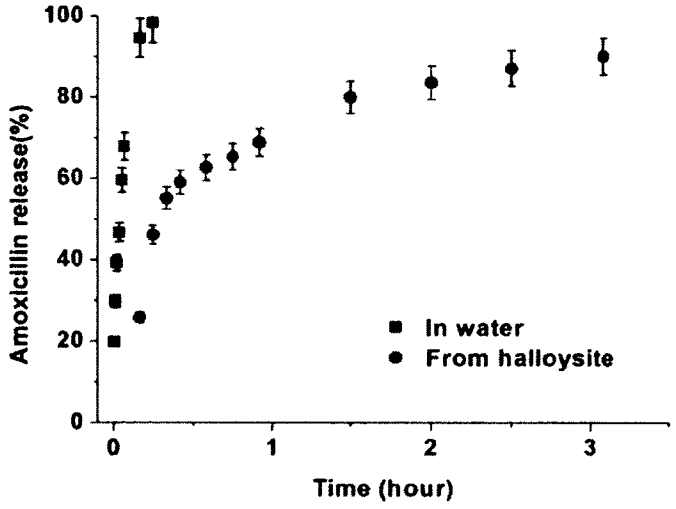

Figure 4-9: Release of amoxicillin from halloysite and in water (W. Wenbo results extending Dr. Patel's approach).

Figure 4-10 shows the release of iodine. Free iodine is released in water within about 5 minutes, whereas iodine loaded halloysite release 90% in 1 hour. However, loaded iodine with an additional stopper significantly reduced the release to 30% in 1 hour.

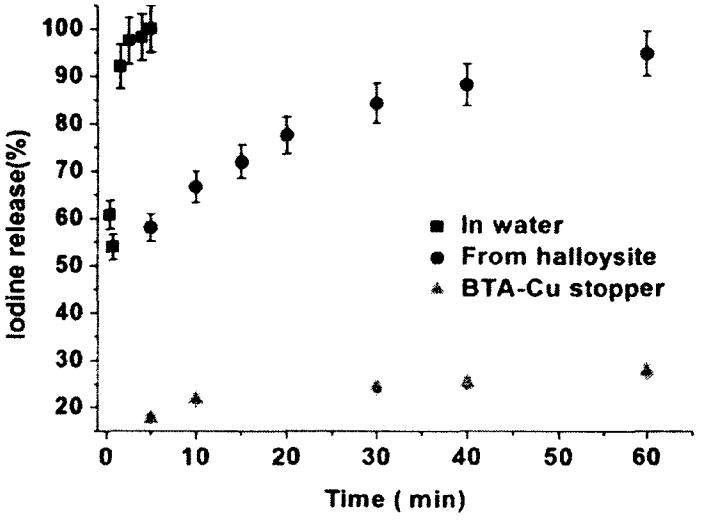

Figure 4-10: Release of iodine from water, halloysite, and halloysite with BTA-Cu stopper (W. Wenbo results extending Dr. Patel's approach with new formulation).

Two dyes, bromocresol purple, and bromothymol blue (Figure 4-11) were also used to study stoppers. Figure 4-12 shows that the BTA-Cu stopper significantly reduced the release of both dyes.

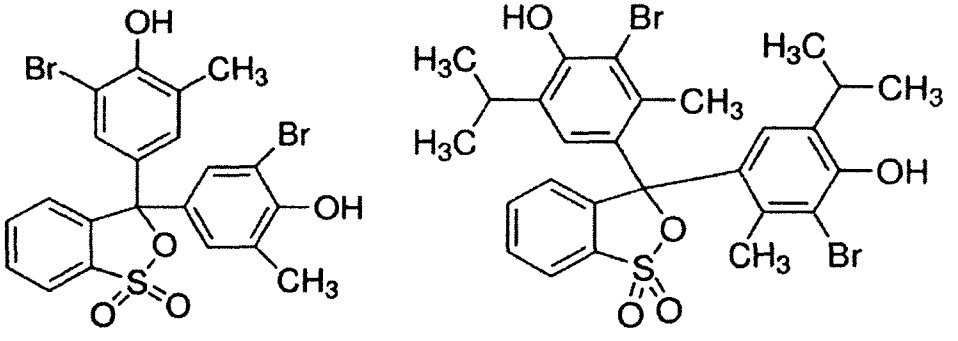

Bromocresol purple **Bromothymol blue**

Figure 4-11: Formula of bromocresol purple, and bromothymol blue.

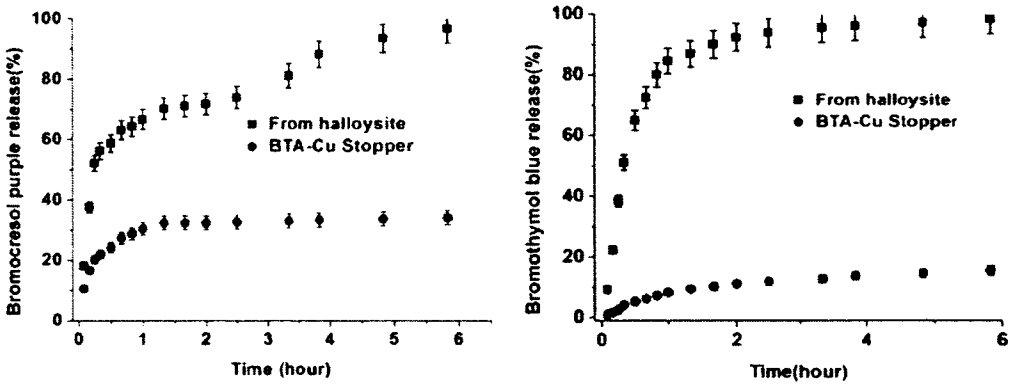

Figure 4-12: Release of bromocresol purple, and bromothymol blue from halloysite with BTA-Cu stopper.

Next, sulfate acid was used to etch the halloysite and determine the impact on loading and release [37]. Based on how much aluminum oxide has been etched, the processed samples were grouped as 10, 35, 45, and 60% etching. These modified nanotubes were tested for drug loading and compared the release and loading efficiency with untreated halloysite. Figure 4-13 shows chlorhexidinediacetate salt hydrate release from halloysite, with 10% etching, 35% etching, and 45% etching of the halloysite. For the higher etched halloysite, a higher loading efficiency was obtained. 10% etched halloysite did not show a big difference from untreated halloysite.

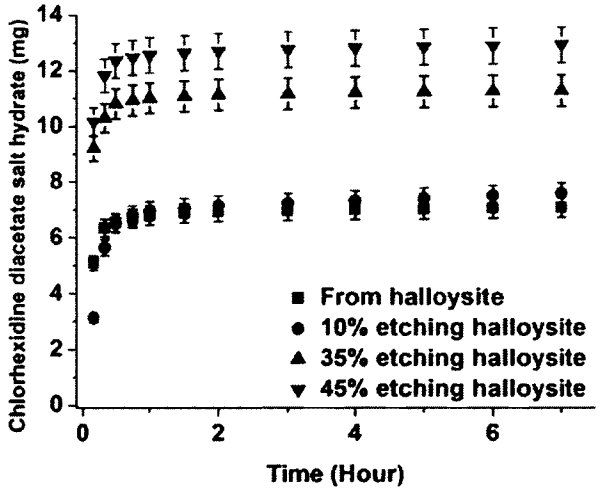

Figure 4-13: Chlorhexidinediacetate salt hydrate release from etched halloysite.

According to the results of drugs release from acid etched halloysite, increasing lumen size lead to a higher loading efficiency, however the larger lumen diameter will also cause faster leakage of loaded substance. The fast release at a high etching percentage also can be explained as when most of the aluminum was reacted with acid, the structure of halloysite will only leave the silica base, there will be some holes obtained on the surface of halloysite, and the tube will become more like porous silica.

Another advantage of acid etching halloysite is that after removing some aluminum from the inner lumen, it can decrease the positive charge. In other words, etched halloysite may have negative charge inside the lumen. Most drugs have positive charge, so the negative charged lumen will provide stronger absorption which will lead to slow release.

4.3.5 Antibiotics Release from Halloysite

Antibiotics are another more specific antibacterial compounds studied for extended efficiency due to clay nanotube encapsulation. We optimized loading and release for two antibiotics widely used in medicine: ciprofloxacin and gentamicin. To increase the antibiotics loading efficiency we enlarged the lumen diameter of clay nanotubes using acid to etch the internal aluminum layers [37].

Figure 4-14 shows loaded gentamicin release from halloysite. After 12 hours, about 1.3 mg of gentamicin were released from loaded halloysite, on the other hand, loaded halloysite with stopper released 1.1 mg gentamicin in the same time.

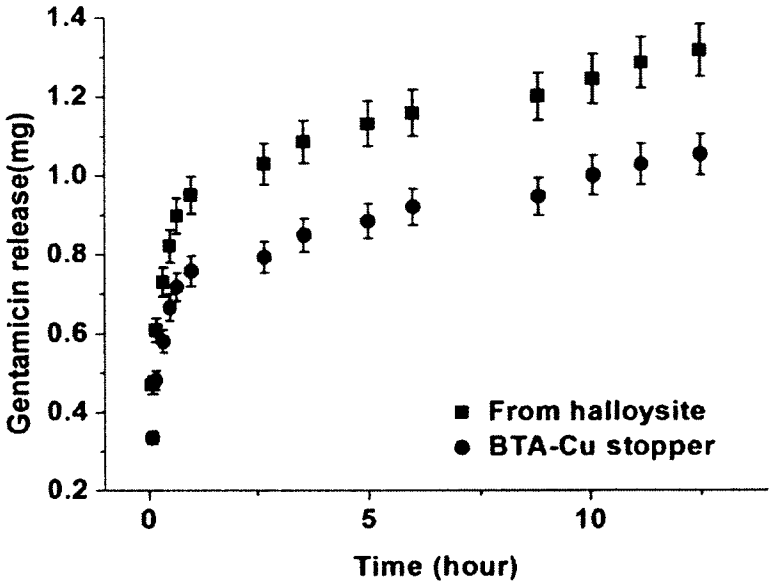

Figure 4-14: Release of gentamicin from halloysite with BTA-Cu stopper.

Figure 4-15 shows ciprofloxacin release from 35% etched halloysite and 60% etched halloysite. The loading efficiency of 60% etching halloysite shows 6 times higher than in untreated halloysite. However the release of 60% etching halloysite is faster compare with 35% etching halloysite.

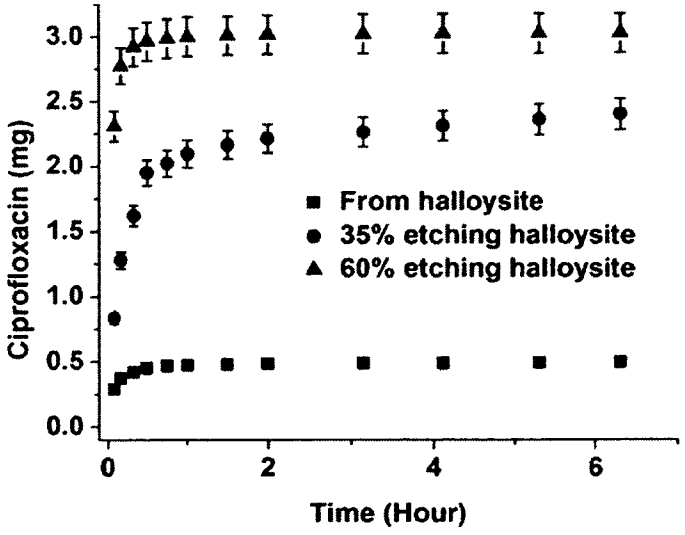

Figure 4-15: Ciprofloxacin release from halloysite etched at different rate.

Figure 4-16 shows ciprofloxacin release from halloysite and with BTA-Cu stopper. Loaded ciprofloxacin released about 60% in 24 hours, and with additional stopper, the release significantly reduced to 30% release in 24 hours.

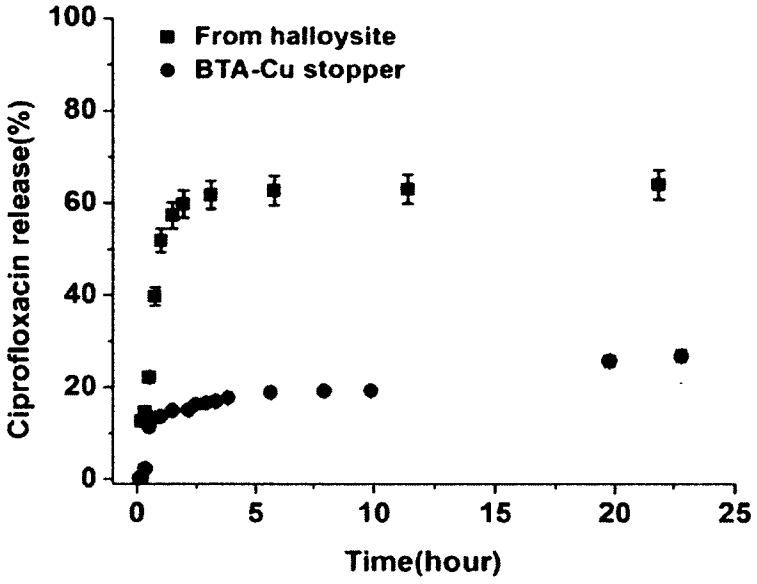

Figure 4-16: Release of ciprofloxacin from halloysite with BTA-Cu stopper.

4.3.6 Antibacterial Effect of Ciprofloxacin Loaded Halloysite

Halloysite loaded with ciprofloxacin and Halloysite loaded with ciprofloxacin with stopper, were compared to ciprofloxacin alone in a disc diffusion assay. Total amount of ciprofloxacin loaded onto each disc was 5μg in all cases. Halloysite was weighed out and diluted with sterile water for distribution onto disc. The same discs were transferred from one plate to a fresh spread plate every 24 hours. The inhibition of ciprofloxacin was longer when loaded into halloysite crystals. The formulation without end stopper appeared to have a longer effect. Loaded halloysite sample still showed a weak zone on two of the discs at 72 hours. Both halloysite formulations beat ciprofloxacin alone in this simple test of prolonged release and inhibition of growth.

Loaded halloysite with stopper lost inhibition zone after 72 hours can be explained the release amount was too less to kill bacteria.

Table 4-2: Antibacterial efficiency of ciprofloxacin loaded halloysite (24, 48, 72 hours).In collaboration with Dr. K Lewis, Pharmacy Dep., Northeastern University.

Sample	Inhibition zone 24h	Inhibition zone 48h	Inhibition zone 72h
Halloysite	No inhibition	No inhibition	No inhibition
5μg ciprofloxacin	30-32 mm	No inhibition	No inhibition
Halloysite/ciprofloxacin	30-32 mm	20-22 mm	8-10 mm
Halloysite/ciprofloxacin/stopper	26-28 mm	16-20 mm	No inhibition

4.4 Conclusions

Release study and antibacterial effect of common antiseptic agent brilliant green, iodine, amoxicillin and antibiotics ciprofloxacin and gentamicin have been studied using halloysite clay as nanocontainers for loading and controlled release. Complete release of non-encapsulated brilliant green occurred within 10 minutes while 70% of this antiseptic was released from halloysite tube lumen within 3 hours and 90% within 5 hours. Tunable controlled release was achieved by synthesizing copper-benzotriazole complexation on the tube surface (predominantly - at tube ends). Factors affecting release rate from such formulations *i.e.* concentrations of copper and benzotriazole used for cap formation, were analyzed in details and optimized for the best release profile. Release rate reduces with increased benzotriazole concentration at lower copper concentrations, which is associated with formation of tighter films with less porosity. However, opposite phenomenon was observed at high Cu^{2+} concentrations, which is associated with increased loading

efficiency of the drugs. *S. aureus* bacterial viability assay revealed that antiseptics loaded within halloysite lumen provided much longer activity compared to the free microcrystals.

CHAPTER 5

SYNTHESIS OF SILVER NANORODS CORE-SHELL STRUCTURES FOR ANTIBACTERIAL COMPOSITES

5.1 Introduction

This chapter is based on my contribution to the publication titled "Natural Tubule Clay Template Synthesis of Silver Nanorods for Antibacterial Composite Coating", *ACS Appl. Mater. Interfaces,* 2011 [46]. I am the author of this paper, and its content is used only in my dissertation. In this chapter a method for loading silver nanorods in halloysite is presented. Loaded halloysite with silver nanorods have unique antibacterial properties that can be used to functionalize the nanocomposites. Also in collaboration with LSU Dental School in New Orleans joint work will begin on artificial halloysite (loaded with silver and antibiotics) composites for adhesive and antibacterial teeth fillings. In addition, the synthesis metal in halloysite lumen also present potential to assisted X-ray detection of the composites.

Metallic nanomaterials (nanoparticles, nanowires, and nanorods) have gained a large interest in industry due to their unique physico-chemical properties resulting from nano-confinement effects [86, 87]. Different template structures (micro- and nano-containers) have been utilized for synthesizing these nanomaterials: carbon nanotubes [88-90], porous alumina templates [91], liposomes [92], micelles [92], and DNA [93]. The tubular templates allow for the synthesis of internal metal nanorods

protected against surrounding environmental effects, such as oxidation or light degradation, and provide better admixing with polymers. For instance, silver nanorods enclosed in alumosilicate tubes may have enhanced catalytic and antimicrobial properties.

Among other nanotemplates, halloysite, naturally available aluminosilicate clay with ca. 15 nm diameter lumen and of 600 - 1500 nm length, can become a promising candidate for nano-confined reactions because of its well-defined hollow tubular structure, abundance in nature as a raw material, and the increasing demand for environmentally friendly products. So far, it has been used for encapsulation and sustained-release of different chemical agents, such as proteins, drugs, antiseptics, antimicrobial agents, and corrosion inhibitors for metal protection [19,23,26,31,84,94-96]. The usage of the hollow lumen of the nanotubes for nanoconfined enzymatic synthesis of $CaCO_3$ was also demonstrated [43,97]. Clay nanotubes, therefore, offer great benefits as a template for synthesizing metallic nanomaterials due to their appropriate lumen diameter and low cost.

In this work, we report on the selective formation of silver nanorods within the inner lumen of halloysite. Our technique requires loading of silver acetate into the tube lumen under reduced pressure, washing, separation, and heating without any harsh conditions or complicated steps. High-resolution transmission electron microscopy (HR-TEM) and field-emission scanning electron microscopy (FE-SEM) images reveal the formation of silver nanorods inside the lumen as well as within some void spaces in the tube multilayered walls. These in situ syntheses offer a simple method for fabricating metallic nanorods and core-shell ceramic nanocomposites which can be used as well dispersible antimicrobial additives in plastic composites [98-100], nanoelectronics [101]

and optical materials [102-105] with additional biocompatibility and environmentally friendliness.

5.2 Materials and Methods

5.2.1 Materials

Dehydrated halloysite clay (halloysite-7Å) was obtained from Applied Minerals Inc, NY. Silver acetate was purchased from Sigma-Aldrich, USA. Industrial oil based blue paint on the basis of PDS-33 powder was purchased from GPM (Cary, IL). *Escherichia coli*, *Staphylococcusaureus* Rosenbach and Lysogeny broth were purchased from Fischer Scientific.

5.2.2 Characterization of Halloysite

FE-SEM images were acquired using a Hitachi S-4800 FE-SEM (accelerating voltage, 5 kV) to observe nanotube external surface morphologies. Halloysite samples were coated with 1.6 nm thick platinum by Cressington Sputter coater (208HR) before each SEM experiment. TEM images were acquired using JEM-2000EX (JEOL) microscopy (accelerating voltage, 200 kV) equipped with a CCD camera. HAADF-STEM (High Angle Annular Dark Field - Scanning Transmission Electron Microscopy) and EDS-STEM (Energy-Dispersive X-ray Spectroscopy - STEM) analyses were carried out using JEM-2100 (JEOL) microscopy (accelerating voltage, 200 kV). A suspension of halloysite samples in distilled water (0.2 wt%) was sonicated for 2 hrs and the solution was settled for 4 hrs. The supernatant of the halloysite solution (2 µl) was spotted on a copper TEM grid covered by an elastic carbon-support film with a filter paper underneath, and excess solution was blotted immediately with filter paper. The TEM grid was dried under a reduced pressure overnight before observation. No coating or staining

was applied for TEM observation. Nitrogen BET adsorption isotherms were obtained with Nova 2000, Quantochrome Instruments. Halloysite samples were degassed in a vacuum at 300 °C before each BET absorption measurement. An X-ray powder diffractometer (Bruker-D8 Discover, Cu K_α radiation 0.154 nm) was used for the crystal analysis. Light microscope (Olympus, Japan) with video camera (Sony SSC DC 80) was used to analyze paint samples.

5.2.3 Synthesis of Silver Nanorods

Halloysite (5 mg) and silver acetate (10 mg) were added into deionized water (10 ml) and the suspension was immersed into a vacuum for 30 min. Loading of silver acetate was achieved by pulling and breaking vacuum three times. After the loading procedure, halloysite was washed, separated by centrifugation, dried at 80 °C for about 3 hrs, and heated at 300 °C for 1.5 hrs to decompose silver acetate into silver nanorods.

5.2.4 Kinetics of Silver Acetate Decomposition

Dried and grinded halloysite loaded with silver acetate was placed on an Isotemp hot plate at 300 °C. Samples were collected at certain time intervals, dispersed in DI water and sonicated for 10 min (water was bubbled with nitrogen for 20 minutes to remove dissolved oxygen). Then copper strips were inserted into the solution causing reduction of non-decomposed Ag^+ salt (or Ag_2O) present in the sample. The quantity of silver ions were calculated by measuring the concentration of Cu(I) ions released into water due to the oxidation of metallic copper with Ag^+ ions. Cu(I) were further oxidized to Cu(II) ions by hydrogen peroxide and detected with UV-Vis spectrophotometry using sodium diethyldithiocarbamate.

5.2.5 Halloysite Based Antimicrobial Paint

Antimicrobial paint was prepared by the addition of 10% of halloysite silver composite into blue oil based paint and mixed by means of simple mechanical mixing. A sample was applied to thin aluminum foil and dried for 4 days. Then the paint was released by etching the foil in 0.5 M NaOH solution and dried 1 more day. The original paint was released in a similar way.

In order to test antimicrobial properties, 15 g/L solutions of Lysogeny broth (LB) and LB agar in DI water was prepared and sterilized at 121 °C for 15 minutes. LB agar was poured into Petri plates after sterilization and cooled down. Two kinds of bacteria, gram-negative *Escherichia coli* and gram-positive *Staphylococcusaureus* Rosenbach, were cultured at 37 °C overnight and dissolved separately in 3 ml of LB solution and again stored at 37 °C overnight. 100 microliters of this solution was spread over the plates by using glass beads and dry pieces of paint samples were carefully placed in the bacteria culture. Samples were stored at 37 °C. After one week samples were analyzed with Light Microscope to observe bacteria growth around the paint.

5.2.6 Halloysite/Paint Mechanical Property Test

Stress-strain curves of the paint samples were obtained by using an ADMET tensile tester (EP-0801161-M-48VAC). Dimensions of the paint film samples were 5.5±0.5 mm in width, 13.0±0.5 mm in length, and of 0.25±0.04 mm thicknesses. Samples were pulled with the speed of 0.3 mm/min for obtaining a stress – strain curve. Impact strength of the paint was tested by applying it onto 1 mm thick iron plates (A366 Iron alloy). Samples were dried for 1 week and then subjected to the rapid deformation by

dropping 0.2 kg iron bar on the back sides of the paint. Paint was analyzed with a light microscope for the formation of cracks.

5.3 Results and Discussion

5.3.1 Silver Nanorods

Silver nanorods were selectively synthesized within the halloysite inner lumen via the loading of silver acetate from aqueous solution. In this one-step facile method, the aqueous suspension of halloysite containing silver acetate was first degassed under vacuum, followed by loading of silver acetate, which was carried out by pulling and breaking vacuum. After washing and drying, the silver nanorods in the halloysite nanotubes were formed on heating at 300 °C for 1.5 hrs to reduce the silver ions (Figure5-1).

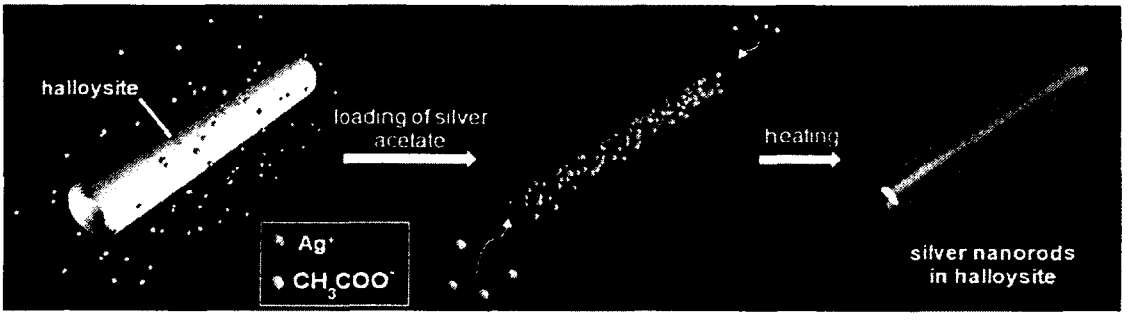

Figure 5-1: Schematic illustration of the synthesis of silver nanorods within the halloysite inner lumen: suspension of halloysite and silver acetate in water; loading of silver acetate; formation of silver nanorods within halloysite templates on heating [46].

Formation of silver nanorods takes place in two steps; decomposition of silver acetate into tiny silver nanocrystals within halloysite pores, and growth of these nanocrystals into nanorods. The first process takes place at lower temperature (~ 280 °C) followed by the second process (~ 290-300 °C). Figure 5-2 a shows STEM images of silver nanorods within halloysite tubular templates, exhibiting unbroken silver nanorods

extended along the tube lumen. Its diameter corresponds to the lumen diameter of 15±2 nm and the length is of several hundred nanometers. Sizes of the silver nanoparticles and nanorods are smaller than the data observed by Logvinenko, *et al.* [106] during thermal decomposition of free silver acetate. We assume that crystalline defects on halloysite facilitate formation of smaller silver nanocrystals and their growth is limited by the tube lumen size. Silver nanorods were effectively encapsulated by the halloysite tubes allowing the formation of a metal core with insulating alumosilicate shell. This insulation protects the silver nanorods from the effects of the external environment containing oxygen and light.

Besides the nanorods synthesized in the tube lumen, minor quantities of silver were deposited into the interlayer space and in external tube defects. One can see the linear arrangements of such silver nanoparticles and the parallel orientation of smaller silver rods (Figure 5-2 b-d).

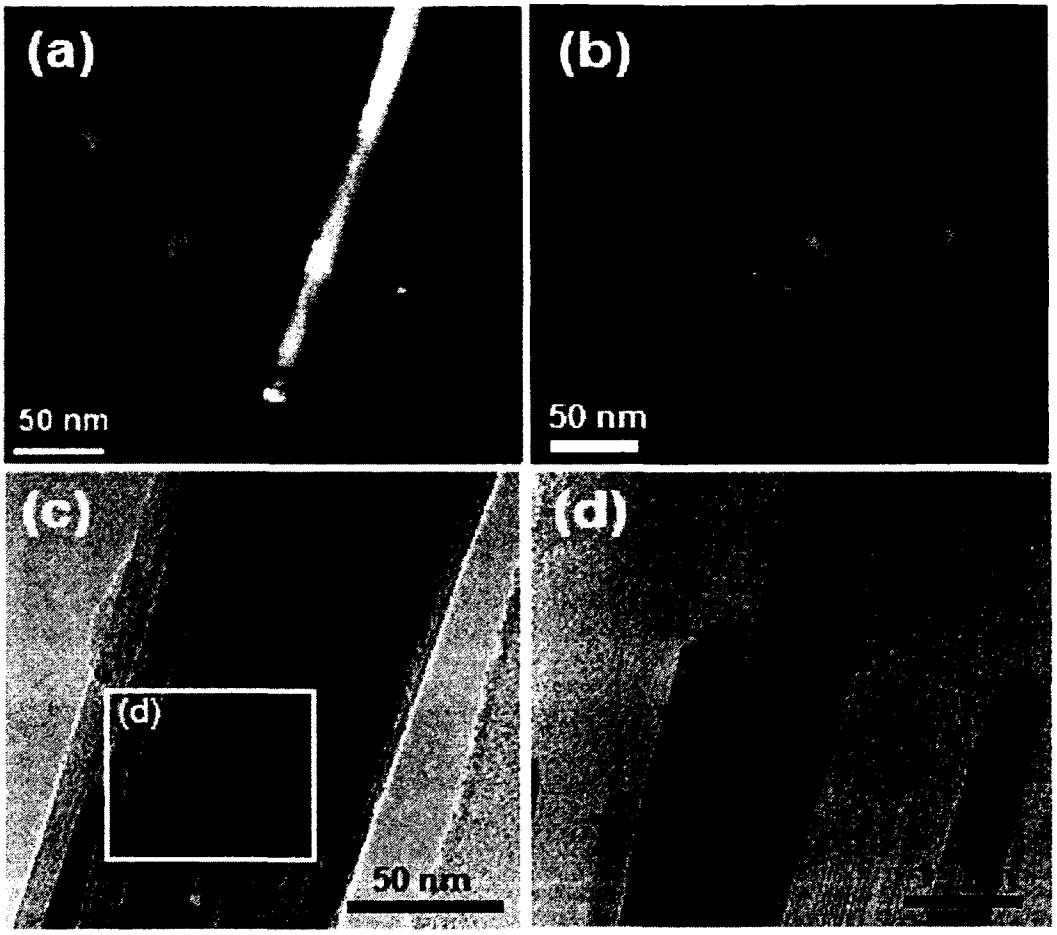

Figure 5-2: (a, b) HAADF-STEM and (c, d) HR-TEM images of silver nanorods within halloysite tubular templates [46].

The arrangement of the silver nanoparticles along the tubes clearly indicates the presence of linear defects on the halloysite external surface. This observation is in accordance with the expectation that the vacancies on the layers may produce localized negative charges resulting from the missing of Si^{IV}, which attract positively charged Ag^{+} ions and their reduction to the silver nanoparticles and nanorods along the defect. The presence of localized linear defects on the surface of the halloysite tubes was also suggested by Kirkman [108]. Using the crystal dislocations theory, he assumed that the linear arrangement of the vacancies on the halloysite external surface is responsible for the rolling of aluminosilicate layers, and this was supported by the presence of kinks on

the halloysite outermost layers. Despite the formation of silver nanoparticles in the halloysite voids, their coagulation to larger particles was hindered because of the confined internal space.

5.3.2 Spectral Analysis of Elemental Composition and Crystalline Structure

Figure 5-3 (a) gives the results for the energy dispersive X-ray spectroscopy (EDS) elemental analysis of the silver-halloysite nanocomposites. Signals from silver (Ag) are clearly visible for L-α (3.0 keV) and L-β (3.2 keV) spectral lines. Concentration of silver is 6±3 atomic %. Signals from copper (Cu) arises from the TEM grid. Signals from oxygen, aluminum and silicon, the main constituents of the halloysite nanotubes, are also presented. Small amounts of Na are present in the halloysite sample as an impurity. Na and Ca based impurities increase the cation exchange capacity (CEC) of the halloysite which is related with the quantity of the vacancies [107].

Figure 5-3 b gives the XRD profile of the silver nanorods formed in the halloysite clay tubes. Picks corresponding to the (111), (200), (220), and (311) planes of Ag are clearly visible, which proves silver is in crystalline form. Reflections at the scattering angles below 38° are from halloysite clay and overlapped with (100) Ag peak. Peaks at 45 - 65° range are from clay impurities (quartz, alunite). Smaller intensity of the silver peaks in the XRD spectra is associated with a smaller concentration of the metallic silver present in the sample. Partial oxidation of silver to Ag_2O is also probable.

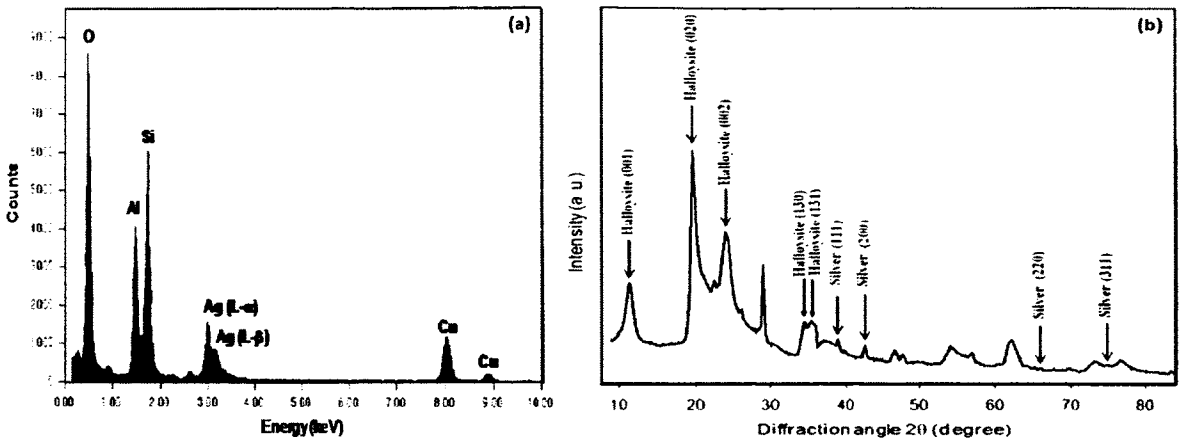

Figure 5-3: (a) EDS elemental analysis of the silver nanorods loaded in the halloysite nanotubes, (b)XRD profile of silver nanorods encased in halloysite tubes [46].

5.3.3 Kinetics of Silver Acetate Thermal Decomposition

Silver nanorods and nanoparticles are synthesized in the halloysite lumen by thermal decomposition of loaded silver acetate. The original white sample was gradually turning into a dark silvery color during the reaction. Figure 5-4 a, b gives the UV spectra of the reaction mixtures taken at different time intervals and the decomposition kinetics. The absorption at 445 nm is constantly decreasing with time indicating the thermal decomposition of the silver acetate into metallic silver.

Decomposition took ca 30 min and follows the first order reaction kinetics with the rate constant of 0.183 min^{-1} at 300 °C.

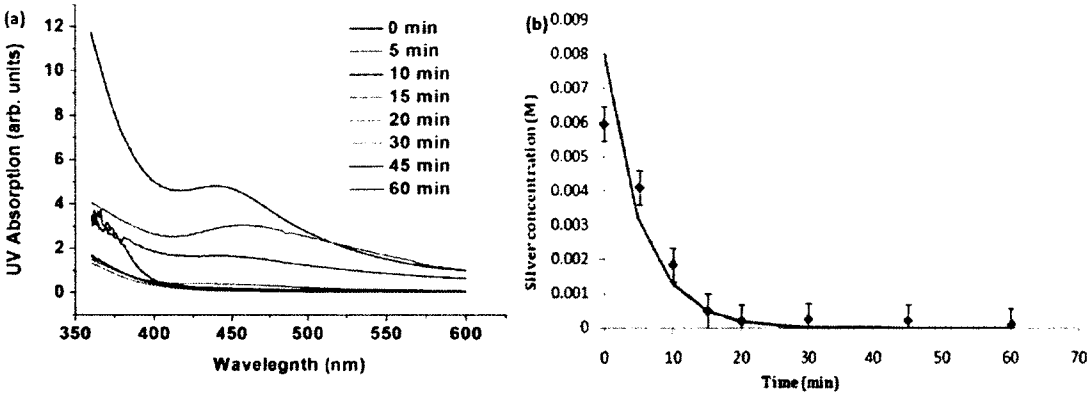

Figure 5-4: (a) UV spectra of the silver acetate decomposition on halloysite nanotubes taken at different time intervals, (b) silver acetate decomposition kinetics [46].

5.3.4 Elemental Mapping

To study the elemental composition throughout the core-shell nanostructures, a detailed chemical analysis was carried out using EDS mapping. The elemental maps displayed in Figure 5-5 give the distribution of the constituent elements, that is, Si, Al, and Ag. Signals from silver are located in the tube interior whereas silicon and aluminum mappings show their elemental distribution along the entire tube body. The halloysite empty lumen confined the volume available for the crystallization of silver leading to nanorod formation. The diameter of the rods coincides with the diameter of the inner lumen which is 15±2 nm.

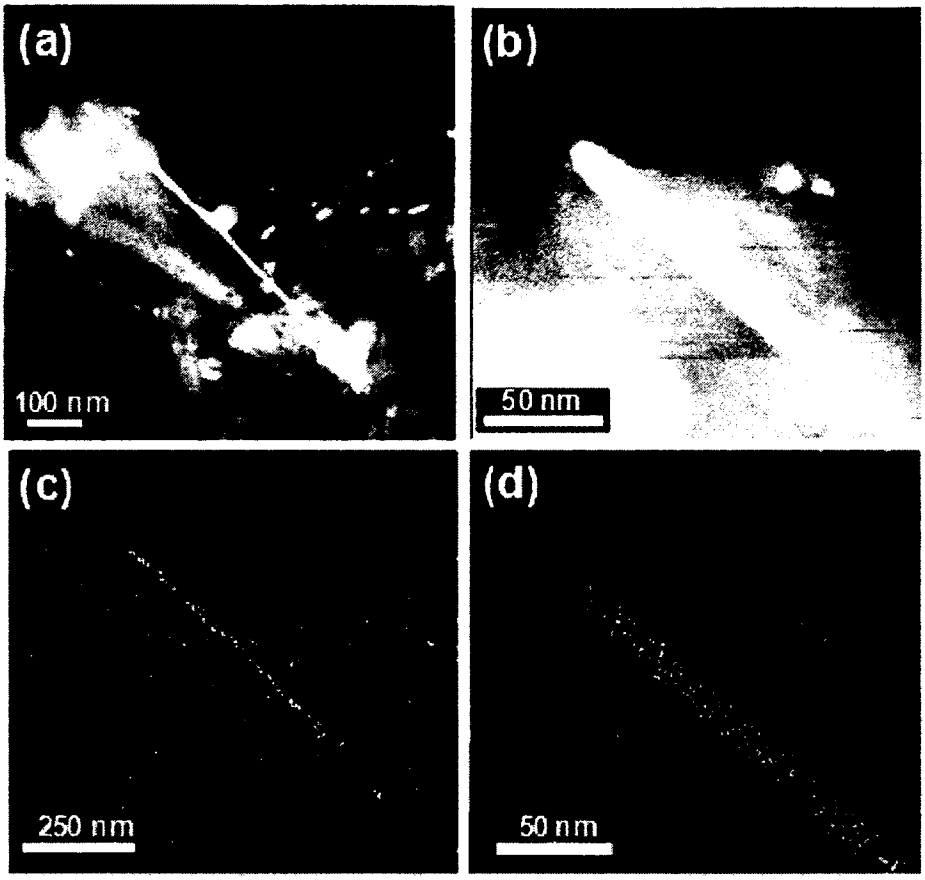

Figure 5-5: STEM images of silver nanorods loaded in the halloysite nanotubes (a, b) and corresponding EDX mapping of Ag (c, d) [46].

5.3.5 TEM Observations of Silver Crystalline Structure

To further describe the crystalline structure of the silver nanorods, samples were analyzed with High Resolution Transmission Electron Microscope. Figure 5-6 shows HR-TEM images of silver nanorods in the halloysite nanotubes. The lattice fringes are clearly visible in the magnified image (Figure 5-6 b), indicating the monocrystalline silver nanorods. Periodicity of the lattice is approximately 0.32±0.02 nm which coincides with (111) *d*-spacing of the silver crystal. Interestingly, the lattice plane is oriented at 68±3° toward the halloysite tubule axis which corresponds to the orientation of (111)

plane toward the (100) plane alined along the tube. The crystal structure of silver in the halloysite nanotubes was also verified by powder X-ray diffraction analysis (Figure 5-3).

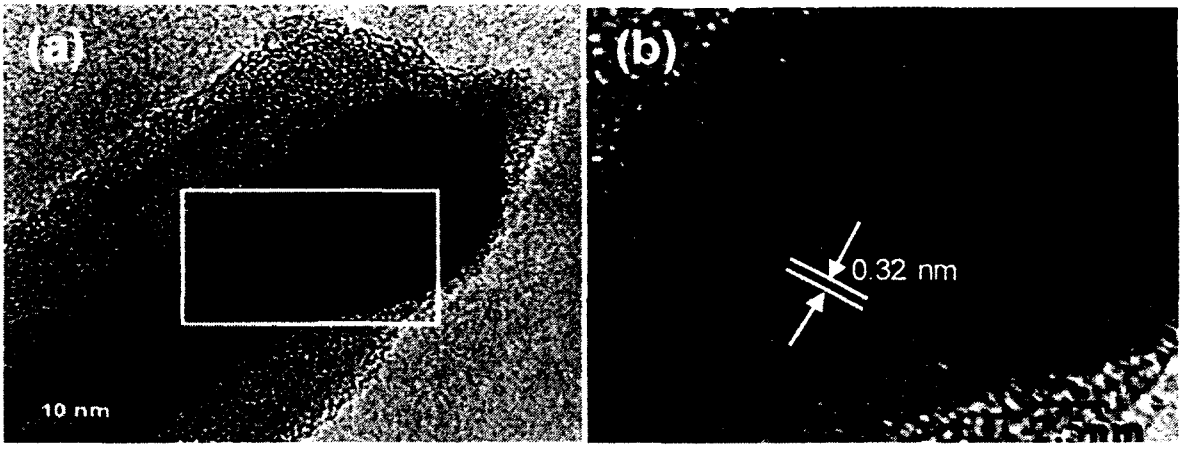

Figure 5-6: HR-TEM images of silver nanorods synthesized by thermal reduction of silver acetate loaded in the halloysite lumen [46].

5.3.6 Sliver Nanoparticle on Halloysite External Surface

We also can get many silver nanoparticles synthesized on the external surface of halloysite by skipping the wash step. Since Ag ion is positively charged, it will be attracted by the negatively charged halloysite external surface (Si). After the vacuum loading method, if we skip the wash step, some Ag ions absorb on the external surface of the halloysite. After heating at 300 °C, these Ag ions will form silver nanoparticles on the halloysite external surface (Figure 5-7).

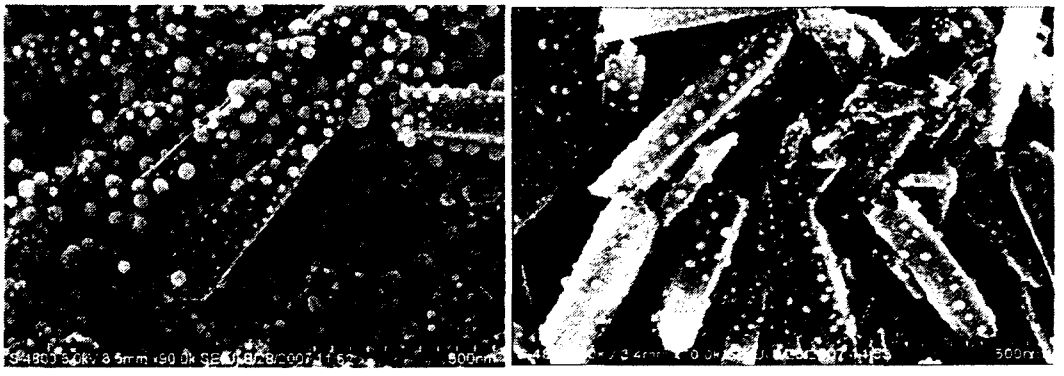

Figure 5-7: Sliver nanoparticle on halloysite external surface.

5.3.7 Antimicrobial Coatings with Silver Loaded Halloysite Nanotubes

Nowadays paint products contain a lot of additives including nanoparticles, such as titanium dioxide, silica, clay, mica, and latex. Silver based composite particles can be applied as an antimicrobial additive to prevent bacterial corrosion [105,109-112]. A direct addition of the silver compounds to the paint has some disadvantages. Paint samples with silver based additives acquire a characteristic yellow – brown color due to the decomposition of silver compounds into silver nanoparticles, which is not desirable (Figure 5-8 and Figure 5-9). Besides, silver nanoparticles absorb UV light and emit plasmons which enhance polymer degradation. In our core-shell structures, encased silver nanorods are better mixable with polymers than individual silver nanoparticles. As demonstrated in Figure 5-8 and Figure 5-9, the color of our coating doped with core-shell silver nanorods was preserved.

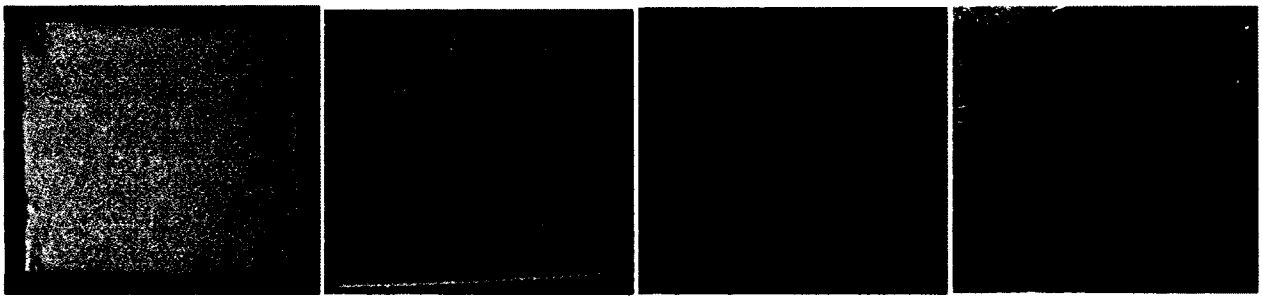

Figure 5-8: Images of acrylic latex paint after one week light exposure: (a)-original paint, (b) doped with 5 wt% halloysite-silver composite, (c) with 5 wt% silver oxide and (d) with 5 wt% silver nitrate 20-40 nm diameter nanoparticles.

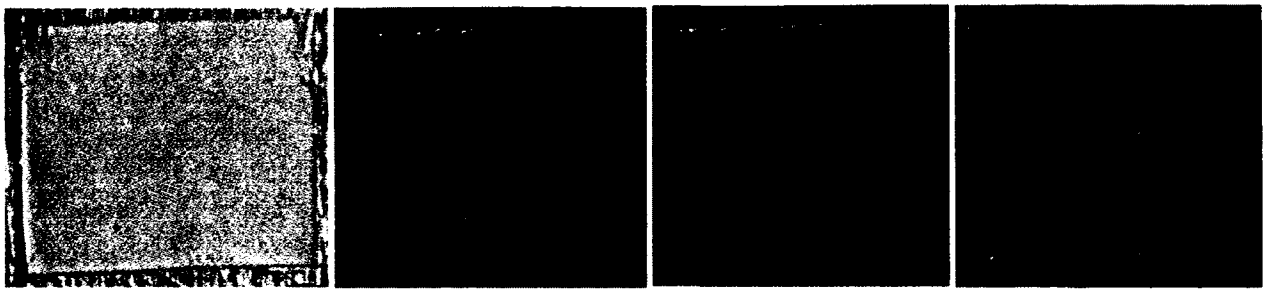

Figure 5-9: Images of epoxy paint after one week light exposure: (a)-original paint (b) doped with 5 wt% halloysite-silver composite, (c) with 5 wt% silver oxide and (d) with 5 wt% silver nitrate 20-40 nm diameter nanoparticles.

An incorporation of silver nanoparticles into halloysite tubes also extended lifetime of the antimicrobial effect. In Figure 5-10, images of the polymer based metal coatings and their composites with halloysite tubes are shown after one week of exposure to *E. coli* and *S. aureus* bacterial cultures. Bacteria grow rapidly in the regions around the original paint without halloysite-silver additives. The edges of the paint samples are not clear in Figure 5-10 (a), (c) indicating that some bacteria was growing on the surface of the paint. A significant amount of bacteria was growing underneath the paint, also indicating bacterial inhibition. Silver nanorod loaded halloysite doped in the paint significantly inhibited bacterial growth. Ag^{+} ions slowly leak from the tubes and inhibit bacterial growth on the paint surface, and additionally a clear zone of inhibition at the paint edge, were observed in both the cases (Figure 5-10 (b), (d)).

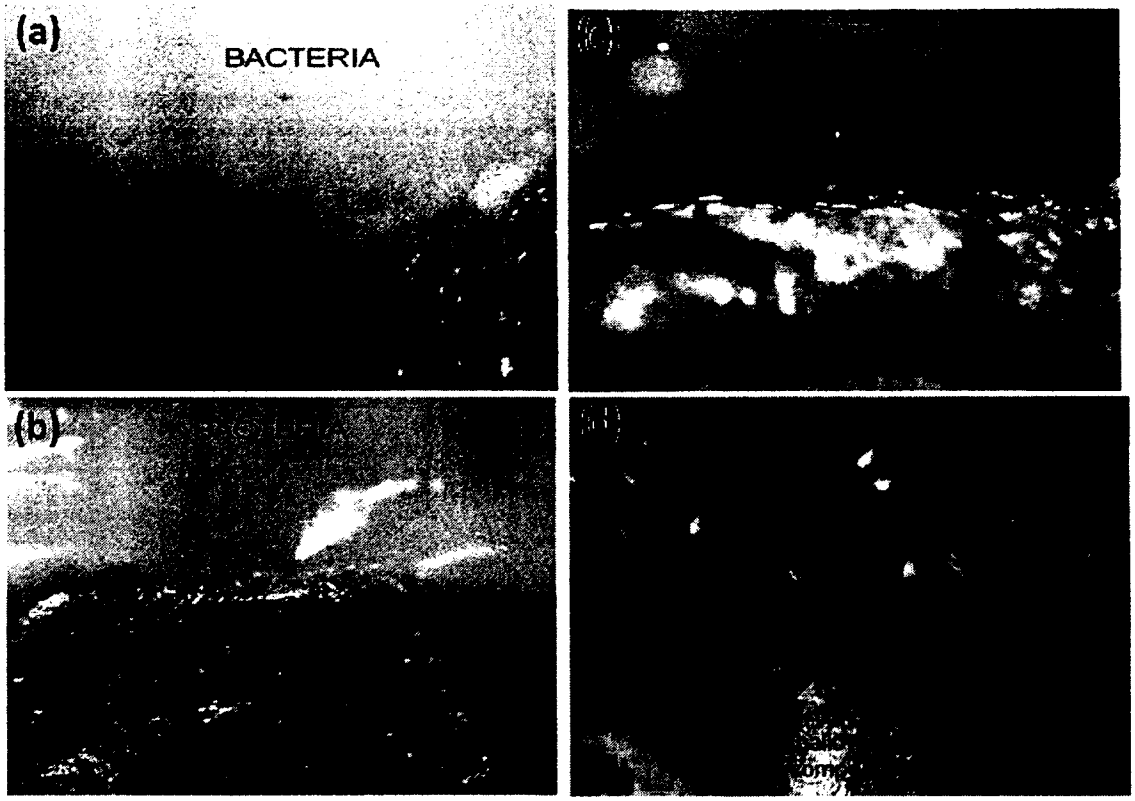

Figure 5-10: Images of the original paint samples (left) and paint prepared by addition of 5 wt% halloysite nanotubes with silver nanorods (right) after one week of exposure to *E. coli* (a, b) and *S. aureus* (c, d) [46].

Antimicrobial activities of silver-halloysite composites are related with the amount of silver ions released: 10 mg/ml of halloysite-silver nanocomposites releases approximately 1 mM of silver ions to the aqueous environment (Figure 5-11). It is 5 times more than the corresponding data for the silver oxide doped bioactive glass nanoparticles [113] and 20 times more than the corresponding data for silver doped carbon nanotubes [109]. Higher release of silver ions is related with the higher concentration of silver in the nanocomposite (Ag : Si ratio is 0.30 in our case vs 0.023 reported by Kawashita, *et al.* [110-111] for silver-containing silica particles).

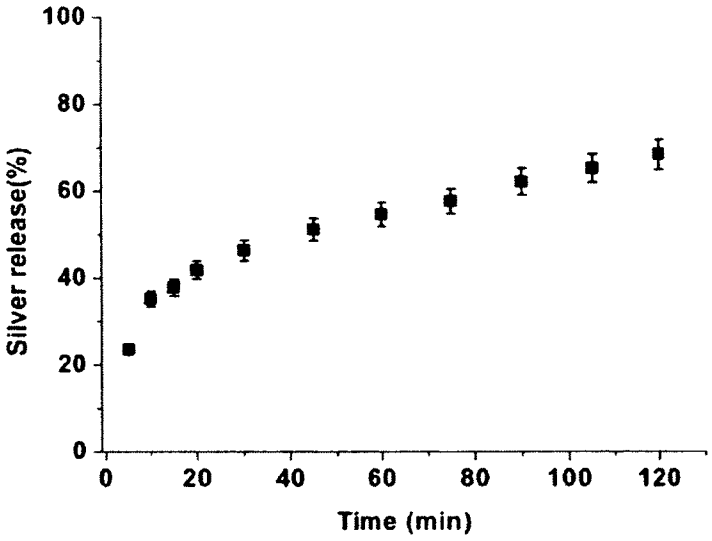

Figure 5-11: Silver ion release kinetics from halloysite-silver composites.

Larger zone of inhibition was observed around the cracks in the paint (Figure 5-12 a). This is assumed to be an indication of halloysite nanotube openings in the cracks. Tubes are exposed to the external environment in the cracks thus enhancing the leakage of Ag^{+} ions, which kills bacteria and preventing biocorrosion.

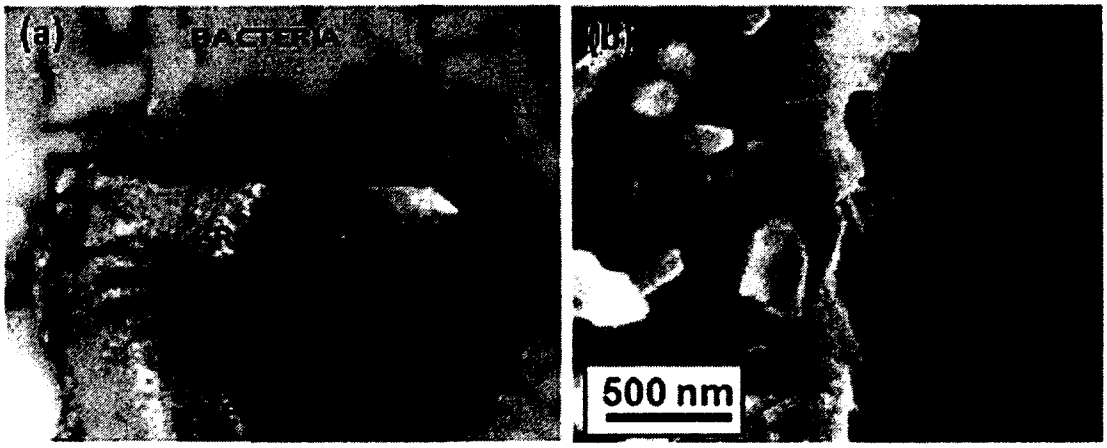

Figure 5-12: Inhibition area around the cracks in the paint (a) and a representative SEM image of the halloysite tubes at the paint cracked surface (b) [46].

5.3.8 Halloysite/Paint Composite Mechanical Property

In Figure 5-13(a), the stress-strain relationship of the oil based blue paint and halloysite - paint composite is shown. Addition of 5-10 wt% of the halloysite significantly increased the tensile strength of the paint. The halloysite - paint composite also shows better performance towards rapid deformation, as demonstrated in Figure 5-13(b), (c). A 0.2 kg metal bar was dropped on the painted iron plates (on the basis of A366 alloy) from the height of 1 m in order to subject the plates to rapid deformations. The thickness of the metal plate was 1 mm in both cases. As indicated in the picture, the metal coated with pure paint has a lot of cracks in it due to the rapid deformation of the plate, while the same paint containing 10 wt% halloysite did not show any evidence of the cracking.

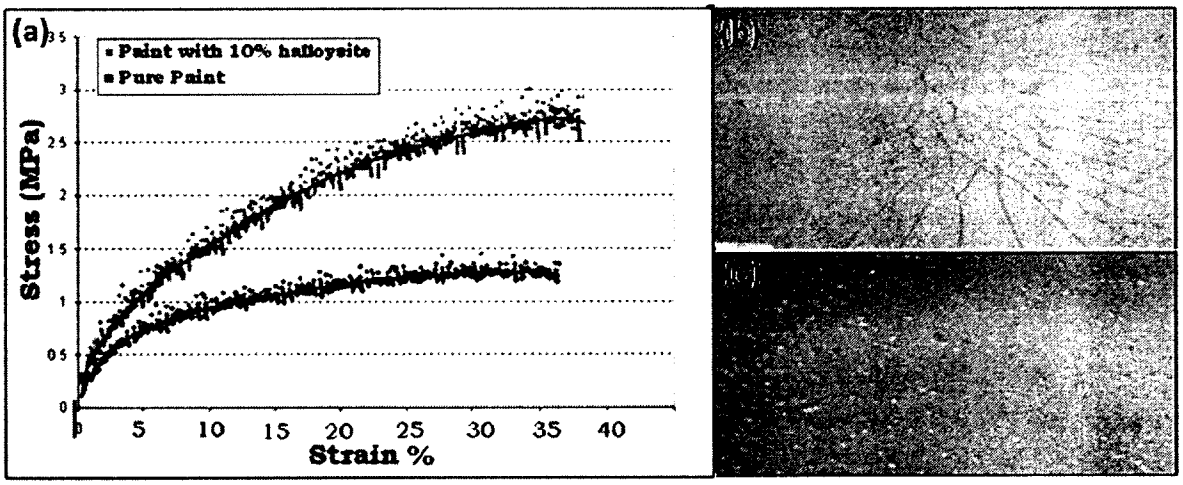

Figure 5-13: Mechanical properties of pure paint and halloysite paint nanocomposite (a). Stress-strain relationship and images of the pure paint (b) and 10 wt% halloysite-paint composite (c) after rapid deformation test [46].

5.4 Conclusions

We reported syntheses of silver nanorods using halloysite nanotubes as a template created by this metal-ceramic core-shell nanocomposite. The growth of single crystal

silver nanorods with 15 nm diameter in the clay tube lumens has been demonstrated. Some nanoparticles were also formed in the nanotube defects caused by the presence of vacancies in the tubes (voids within the multilayer walls). An addition into the paint of 5 wt% of such silver nanorods encased in clay tubular shells resulted in the composite antimicrobial properties with synergistic enhancement of the coatings tensile strength and preservation of the coating color even after strong light exposure. These core-shell silver nanorods can be used as antimicrobial additives for polymer composites and paints. Halloysite is a cheap natural tubule nanomaterial which has a good potential for scalable manufacturing of metal nanorods.

CHAPTER 6

HALLOYSITE NANOTUBES COMPOSITES FOR BONE CEMENT WITH CONTROLLED RELEASE OF ANTIBIOTICS

6.1 Introduction

This chapter is based on my contribution to the publication titled "Clay Nanotube/Polymethylmethacrylate Bone Cement Composites with Sustained Antibiotic Release." *Macromol Mater Engineering,* 2012 [83]. I am the first author of this paper and its content is used in the following Chapter six with proper referencing. This material is not used in any other PhD or MS theses produced in our research group. In this research we expanded our results for drug loading and sustained release with clay nanotubes by doping drug loaded tubes into bone cements. With this method, we improved the polymethylmethacrylate (PMMA) and calcium phosphate bone cements traditionally used in orthopedic surgery with new properties (enhanced strength, adhesivity and antimicrobial efficiency).

Polymethylmethacrylate (PMMA) bone cement has been used in orthopedic surgeries since 1958 [3]. Its biocompatibility and mechanical properties have made it a remarkable and indispensable tool in orthopedic repair, specifically in joint replacement arthroplasty. The two-stage knee arthroplasty revision for infection, with implant removal and interval of antibiotic therapy before implant replacement, was invented later and is a standard clinical procedure [4]. Antibiotics were added to bone cement to improve local

antibiotic delivery in addition to intravenous doses [3, 7]. This practice has improved implant survival and reduced reinfection rates. The non-porous PMMA bone cement allows for release of only a portion of the antibiotics evenly distributed throughout the cement [8]. Current cement formulations release less than 3% of the total loaded gentamicin sulfate during the first ten days, with at least 70% of that released within the first 24 hours [5,6,9]. PMMA's material strength is also compromised by cement additives, though there has been recent development of PMMA – montmorillonite composites that promote greater antibiotic elution and enhanced material strength [114]. The development goals of these PMMA composites are increased efficient and sustained release of antibiotics without compromising implant strength.

Encapsulation of antibiotics, particularly within micro- and nano-scale containers, has the potential for prolonged and more evenly distributed release. One such container is halloysite clay nanotubes which are described in Chapter 2. Halloysite nanotubes loaded with tetracycline were also incorporated in dental fillings in a canine model [82]. In addition to the potential for sustained release, admixed halloysite also enhances polymer and epoxy physical properties [117]. An attractive aspect of halloysite nanotubes is that it is economically viable. Halloysite's particle size is not in the range where silicosis or asbestosis related complications would occur [34].

In this study, we used clay tubule nanocontainers to produce PMMA cement/halloysite nanocomposites with the properties of sustained drug release and without compromising bone cement strength. Enhancement of the composite adhesiveness to bone over PMMA alone was also shown.

6.2 Materials and Methods

6.2.1 Materials

Polymethylmethacrylate (PMMA) bone cement, Orthoset-3, was kindly provided by Wright Medical Technologies (Arlington, TN). Halloysite nanotubes were provided by Applied Minerals, Inc. (New York, NY). Gentamicin sulfate was purchased from Cellgro by Mediatech, Inc. (Manassas, VA).

6.2.2 Loading Antibiotics in Halloysite Lumen

Powdered halloysite was added to a concentrated aqueous solution of gentamicin sulfate (50 mg/ml). The suspension was then sonicated for 2 hours, followed by 20 minutes in a vacuum at 100 torr to draw the drug into the tubes. Vacuuming was done in three intervals with 20 min at atmospheric pressure between each vacuum processing step. Samples were then briefly washed to remove gentamicin associated with the outside surface of halloysite. After centrifugation, the supernatant was removed and the remaining samples were placed in an oven to dry at 55 °C for two hours. Typically, 10 to15 wt% loading of halloysite with gentamicin was achieved. For some experiments, loaded halloysite was used without washing for testing with gentamicin also bound to the outside of the tube.

6.2.3 Gentamicin Release

Drug release experiments were conducted by putting samples in deionized water (DI). At each reading, the DI water was removed and replaced with fresh DI water. Because gentamicin does not have UV signal, equal parts liquid sample, isopropanol, and o-phthaldialdehyde solution were mix together and allowed to sit at room temperature for 30 minutes. With an Agilent-8453 UV-vis spectrophotometer, the mixture absorbency

was monitored at the 331 nm wavelength. O-phthaldialdehyde solution was made by adding 2.5 g o-phthaldialdehyde, 62.5 ml methanol, 3 ml β-mercaptoethanol (Sigma-Aldrich, St. Louis), and 560 ml 0.04 M sodium borate. The solution was then allowed to sit at room temperature for 24 hrs before usage (solution was then used within 72 hrs).

6.2.4 Tensile, Flexural and Adhesion Tests

A tensile tester (ADMET Corp., EP-0801161-M-48VAC) was used to test the samples' tensile and flexural strength. All the samples were made in a standard bone shape (the center section is 3 cm×1 cm×0.5 cm) and kept in DI water to allow the leakage of gentamicin. This treatment with water allows the consideration of the effect of surrounding body fluids to the mechanical properties of the implants after long time exposure.

Adhesion of bone to cement was assessed using cow femurs (obtained from Louisiana Tech's Meat Processing Plant). Adhesion was tested using two standard methods (ASTM D5178 and D4541 standards). The surfaces of the bones were cleaned before every test with ethanol. In the first test, cement was applied to two pieces of flat bone with grooves on the surface to combine perpendicular and tangential adhesion properties (interface area was 0.8 cm×0.8 cm). Then the bones were pulled apart, and the force required to break the sample was registered. The fractured interface was analyzed with a light microscope (Olympus, Japan). For the second adhesion test, cement was coated on the surface of the bone (area 1.0 cm×1.0 cm). The maximum peel force required to remove the cement layer from the bone was measured.

Adhesion strength on a titanium implant was assessed by cutting the titanium implant and choosing the top part which has a cylindrical geometry. Glue

PMMA/halloysite bone cement on the cylinder titanium implant as a ring structure (width of the ring composite is 15 mm; the thickness of the ring composite is 3 mm). We drill a hole on the metal plate, the diameter of the hole is equal to the diameter of the cylindrical titanium implant in which the implant can go through the hole but the cement ring cannot. Then, using the tensile strength machine to pull the implant through the hole of the metal plate to separate the implant and the bone cement, we measure the maximum force needed.

Halloysite/glue composite flexural strength was assessed by mixing thoroughly a certain amount of halloysite with glues for making composites. Using the composite glue to connect two pieces of ceramic, and using pure glues to connect another two pieces to be the control. Let all samples dry at room temperature for 24 hours. The ADMET tensile strength machine will be used to measure the flexural strength of all samples.

6.2.5 Structural Analysis

SEM images of the broken sample sections coated with 0.5 nm of gold were obtained with a Hitachi Field Emission Scanning Electron Microscope. Transmission electron microscopy (TEM) was done with the help of JEM-2000EX instrument, Japan. Halloysite X-ray diffraction analysis was performed with XRD, Bruker-D8 Discover instrument, Cu K_α radiation $\lambda = 0.154$ nm. Brunauer-Emmett-Teller (BET) surface area of the samples was measured with the nitrogen Quantochrome Inst., NOVA 2200.

6.2.6 Statistical Analysis

Statistical evaluation was performed by using Student's *t* test:

$t = |\bar{x} - \mu_0|/(s/\sqrt{n})$, where *t* is the Student's *t*-functional and corresponds to 2.92 in our

case (degree of freedom=2 and 90% probability), $\bar{x}$ is the sample mean, μ_0 the true mean, s the standard deviation of the sample, and n is the sample size.

6.2.7 Antibacterial Tests

Escherichia coli and *Staphylococcus aureus* were used for the antibacterial test of PMMA/halloysite/gentamicin composites. We used four samples: pure PMMA cement, PMMA cement with 1 wt% free gentamicin, PMMA with 7.5 wt% unloaded empty halloysite and PMMA with 7.5 wt% gentamicin loaded halloysite. Each sample was placed in *E. coli* and *S. aureus* cell cultures for 7 days, and digital images of the bacterial colony development were then taken.

6.3 Results and Discussion

6.3.1 Halloysite-PMMA Composite Structure

Bone cement samples were prepared by free radical polymerization of methylmethacrylate (MMA) with benzoyl peroxide following a standard procedure recommended by the manufacturer. A dry mass containing the benzoyl peroxide and partially polymerized MMA was thoroughly mixed with liquid MMA (2:1 mass ratio) and left for 10 minutes for complete polymerization.

Halloysite-PMMA composites were prepared using halloysite admixed dry powder instead of the original commercial sample. Figure 6-1 shows images of the PMMA/halloysite samples. Original PMMA cement has a white color that turns creamy yellow upon the addition of halloysite. Addition of free gentamicin did not have an effect on the color of the cement composite.

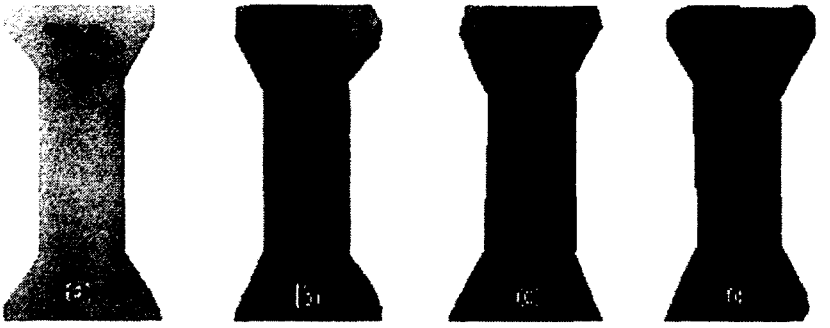

Figure 6-1: Images of PMMA bone cement (a) and PMMA/halloysite composites with 5 wt% (b), 7.5 wt% (c) and 10 wt% (d) halloysite [83].

Figure 6-2 shows the SEM images of PMMA bone cement/halloysite composites. The addition of 5 wt% halloysite into PMMA cement gives a good distribution of clay nanotubes within the polymer matrix (Figure 6-2 b). However, particles were significantly aggregated in the PMMA samples with 10 wt% halloysite (Figure 6-2 d).

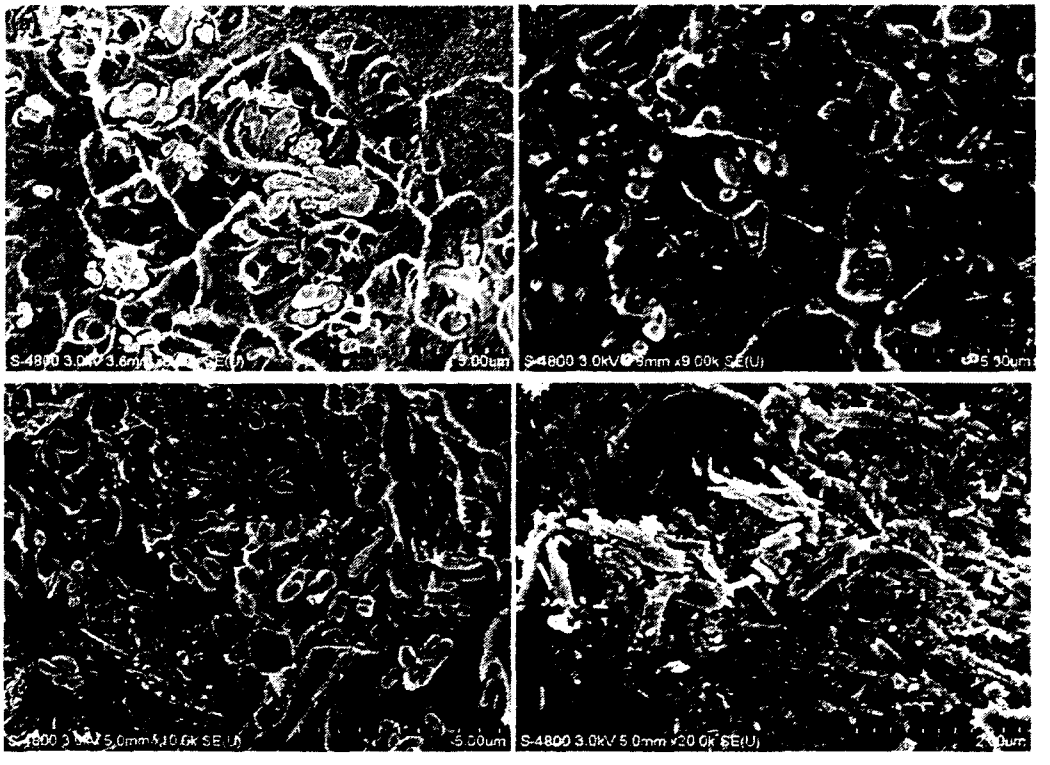

Figure 6-2: Cross-sectional SEM image of PMMA (a) PMMA/halloysite composites doped with 5 wt% halloysite (b), 7.5 wt% halloysite (c) 10 wt% halloysite (d).

6.3.2 Mechanical Properties of Halloysite-PMMA Composites

The mechanical strength and adhesion of bone cement are crucial for the success of joint replacements as bone cement is the weakest mechanical link in such a construction, and this is likely to be a factor in the loosening of the prosthetic device [118]. Therefore, it is important to assess the influence of the additives to PMMA on the mechanical and adhesive properties of the final composite material. We used seven samples with different percent combinations of halloysite and gentamicin in order to analyze the influence of these combinations individually. Halloysite nanotubes were loaded with gentamicin in all cases. Samples were kept in water for 50 days and wetted before tests in order to mimic the effect of the surrounding *in-vivo* interstitial fluid environment on the mechanical properties of the cement.

6.3.3 Tensile Strength of PMMA/Halloysite Composite

The ADMET tensile tester was used to determine the strength of the dog bone shaped PMMA/halloysite composites. Samples were prepared according to ISO-527 standard and pulled with the speed of 0.02 mm/sec until their failure. Stress and strain generated in the samples are calculated from the formula [26]:

$$\text{Strain}(\sigma) = \Delta L/L_0 \times 100;\ \text{Stress}(\epsilon) = F/(w \times t) \qquad (1)$$

Where, L_0 is the original length of the sample, F is the force loaded on the sample, w is the width of the sample, and t is the thickness of the sample.

Figure 6-3 shows tensile strength results of the PMMA / halloysite composite samples. Tensile strength of the composites increased from 18.0 MPa to 26.1 MPa when 5 wt% halloysite was added (ends of the blue and pink lines). Tensile strength slightly decreased when the amount of the halloysite exceeded 10 wt% but it was still higher than

original PMMA cement. The tensile modulus of the composite did not change significantly.

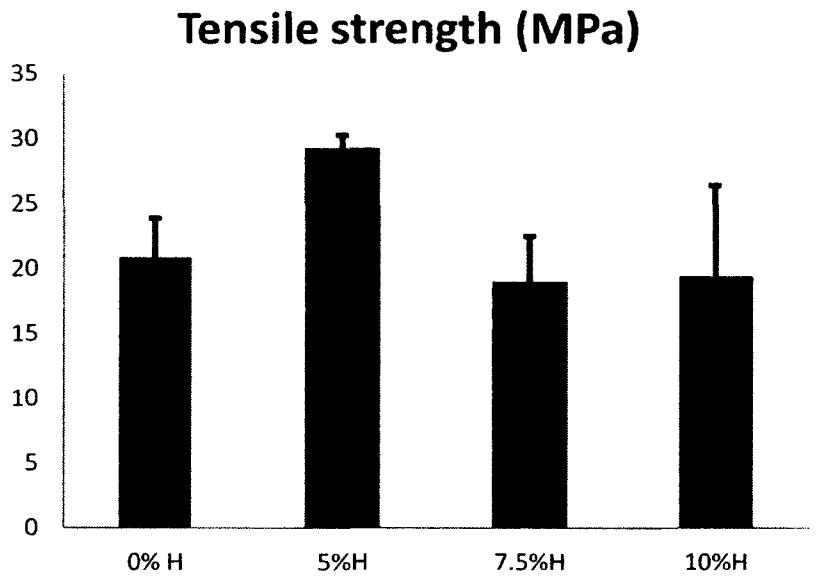

Figure 6-3: Tensile strength of the PMMA / halloysite composites.

Table 6-1 shows the results of the tensile testing based on the average of three experiments. We compared the results for original PMMA cement, PMMA cement doped with gentamicin loaded halloysite nanotubes, and PMMA cement loaded with both halloysite nanotubes and the addition of traditional 1.5 wt% admixing of free gentamicin into the cement monomers before polymerization. Samples containing 5 wt% halloysite had the maximum strength and exceeded the strength of pure PMMA cement and PMMA cement loaded with free gentamicin (addition of 1.5 wt% of free gentamicin reduced the strength of the samples).

Table 6-1 Mechanical and adhesive properties of PMMA / halloysite composites.

	Peak stress (MPa)	Tensile Modulus (GPa)	Flexural Strength (MPa)	Max force at balanced beam adhesion test (N)
Original PMMA	21±3	0.25±0.03	39±2	28±13
Samples doped with loaded halloysite, without free gentamicin				
PMMA + 5% halloysite	29±1	0.24±0.02	35±2	103±15
PMMA + 7.5% halloysite	20±4	0.23±0.02	31±1	123±22
PMMA + 10% halloysite	19±7	0.26±0.03	24±2	187±23
Samples doped with loaded halloysite + added 1.5% of free gentamicin				
PMMA + 5% halloysite	26±1	0.21±0.02	32±1	99±16
PMMA + 7.5% halloysite	24±4	0.23±0.02	27±1	159±46
PMMA + 10% halloysite	20±7	0.26±0.03	28±2	222±27

6.3.4 Flexural Strength of PMMA/Halloysite Composite

A three point bending model was used to measure the flexural strength. All PMMA/halloysite composites were made into a rectangular shape with dimensions of 3 cm×1 cm×0.5 cm. Flexural stress and strain was calculated from the formula:

$$\text{Stress}(\sigma) = 3PL/2wt^2\,;\ \text{Strain}(\epsilon) = 6td/L^2 \qquad (2)$$

Where, P is the load at a given point on the load deflection curve, L is the length of support span, w is the width, t is the thickness of the sample, and d is the beam deflection at the center.

Maximum flexural strength was observed for the original PMMA sample and was decreasing from 41 MPa to 27 MPa upon addition of 10 wt% of halloysite suggesting that samples become more brittle with the addition of halloysite. Results presented in

Table 6-1 also support this conclusion. The addition of 1.5 wt% of free gentamicin slightly reduced the strength of the samples.

Considering the mechanical properties of the PMMA/halloysite composites, optimal doping of the halloysite is 5 wt% which gives both higher tensile strength and good flexural properties. Halloysite was loaded with ca 15 wt% of gentamicin, which means that 5 wt% halloysite doping provides 0.75 wt% gentamicin concentration in the composite. In some cases, it is reasonable to have a combination of traditional 1.5 wt% gentamicin admixing in MMA monomers before cement solidification plus doping with gentamicin loaded halloysite, which provides for combined release of the antibiotic in the bone implant. Strength parameters of such composites were also improved and are shown in the bottom section of Table 6-1.

It is interesting to compare our results with other PMMA bone cement composites with added nano and microparticles. Gomoll, *et al.* [119] showed that the addition of 1-3 μm diameter barium sulfate microparticles decreased by 40% the composite tensile strength. However, a smaller 100 nm particle diameter allowed restoration of the initial PMMA cement strength and increasing its fatigue life. Our halloysite nanofiller increases the tensile strength of the composite and, as it will be shown below also increased its adhesivity.

6.3.5 Adhesion of PMMA/Halloysite Composites to Bone Surface

The adhesive force between PMMA/halloysite composites and bone surfaces was tested in bovine femoral bone, since most of the failures occur at the PMMA/bone interface. There are many different methods for the testing of adhesion and all of them have certain limitations. In this study, we used a tensile tester to demonstrate the effect of

the addition of halloysite on PMMA adhesion to a bone surface. For this test, we glued two pieces of bone samples to each other with the PMMA sample and pulled them apart to determine the maximum force.

In Figure 6-4, images of the bone-PMMA interface, after being pulled apart with the tensile tester, are shown. An SEM image of the bovine femoral bone surface is also shown. The bone has pores with a diameter of ca 200 nm. Three samples of PMMA cement: original (without additives), with 1.5 wt% of free gentamicin and with 7.5 wt% of halloysite loaded with gentamicin were used as connecting glue (total amount of gentamicin available for release from both cement samples was equal to 1.5 wt%). The purpose of this test was to show the efficiency of using gentamicin loaded halloysite instead of free gentamicin as an additive in PMMA to get the equivalent antibacterial properties without loss of structural integrity. These images clearly indicate that the PMMA composite with 7.5 wt% halloysite loaded with gentamicin has significantly increased adhesion to the bone surface compared with the original PMMA sample and the sample with 1.5 wt% of free gentamicin. For the PMMA/halloysite composite connector, failures occurred within the bone whereas it occurred at the cement-bone interface with the other two samples. These data suggest that the PMMA / halloysite nanocomposite provides greater adhesion to bone compared with the original PMMA sample and the 1.5 wt% free gentamicin sample. The force required to break nanocomposite samples was 500±20 N, original PMMA cement sample was290±20 N,and the sample with free gentamicin loaded was 280±80 N (average of three experiments). This result suggests that using gentamicin loaded halloysite instead of

free gentamicin as a filler in PMMA bone cement has a major advantage in terms of its adhesive properties.

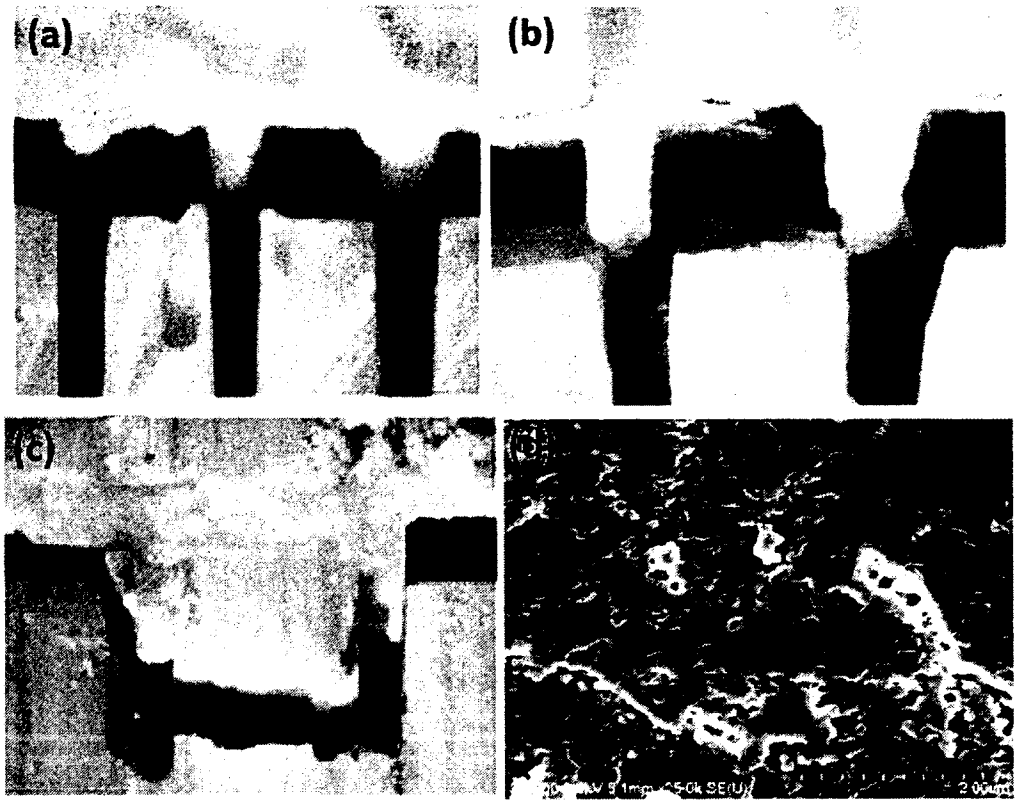

Figure 6-4: Images at PMMA composites – bone interface after fracturing with tensile tester. Original PMMA (a) 1.5 wt% gentamicin-PMMA (b) 7.5 wt% halloysite-PMMA, and (c) SEM of cow femur bone structure (d) [83].

In order to characterize the increase in adhesive properties with the addition of halloysite into bone cement, we used the balanced beam adhesion test (ASTM D5178 standard method), since it provides the best method for analyzing the adhesion between two hard (non-deformable) solid materials [120]. In Figure 6-5, a simplified sketch of the apparatus used for testing the adhesive force between PMMA and the bone samples is shown. The device contains a beam with a movable cantilever that pushes the samples attached to the surface once a load is applied to the end of the beam. In order to get more precise results, we slightly modified the industrially available balanced beam adhesion

tester and attached it to the tensile tester to measure the load applied to the end of the beam. With simple calculations, we found the relation between the force applied to the PMMA sample and the load applied to the beam as follows:

$$F = (P + b)L/a \times (ctg(\beta) - \mu) \quad (3)$$

Where, F is the force applied to the PMMA sample; P is the load on the end of the beam; a and L are dimensions of the apparatus; b is the weight of the beam; $ctg(\beta)$ is the cotangent of the beam inclination angle (β) and μ is the friction force between the cantilever tip and the bone surface. For simplicity we considered $\mu = 0$ since the friction force was negligible compared to the adhesion force between PMMA and the bone surface. One can see that an almost six times larger force is needed to detach the cement composite doped with 10 wt% halloysite as compared to the original PMMA cement (Figure 6-5 b).

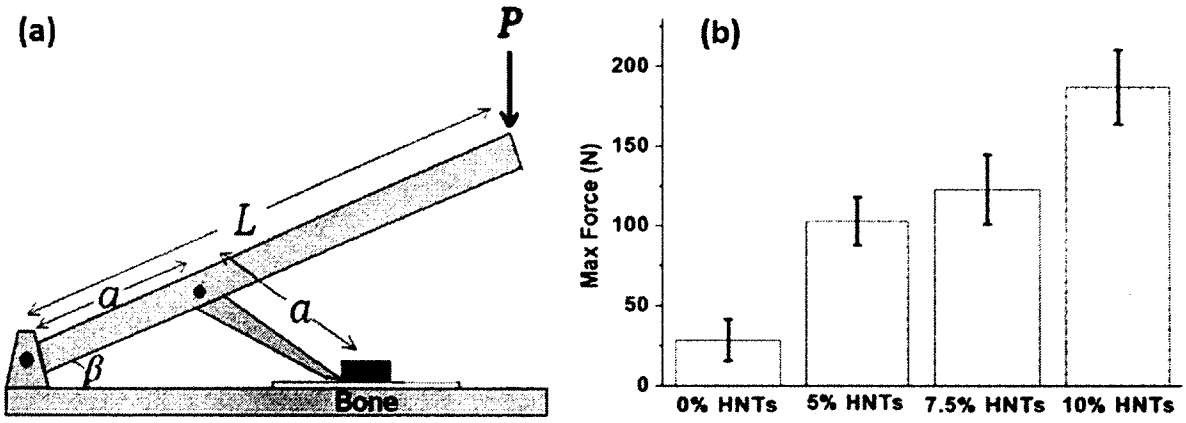

Figure 6-5: Simplified sketch of the apparatus for testing the adhesive forces between the PMMA bone cement and cow femur bone (a), and the maximal force needed to detach the cement depending on the halloysite doping ratio(b) [83].

The maximum force required to remove the PMMA cement layer from the cow femur bone is shown in Table 6-1 for PMMA bone cements with different amounts of added halloysite. The force increased five times when PMMA doped with 7.5 wt%

halloysite (which is considered as the optimal in view of different strength parameters), and continues to increase monotonically with the increase of the halloysite concentration. The addition of free gentamicin did not significantly affect the adhesion between the PMMA cement and bone surface.

6.3.6 Adhesion of PMMA/Halloysite Composites to Titanium Implant

Based on our previous research on PMMA/halloysite composite results, the composites shows improved adhesive ability on the bone surface. The next step is to find out if the PMMA/halloysite composite can also improve adhesive ability on the implant surface. In this research we choose a titanium implant (Figure 6-6).

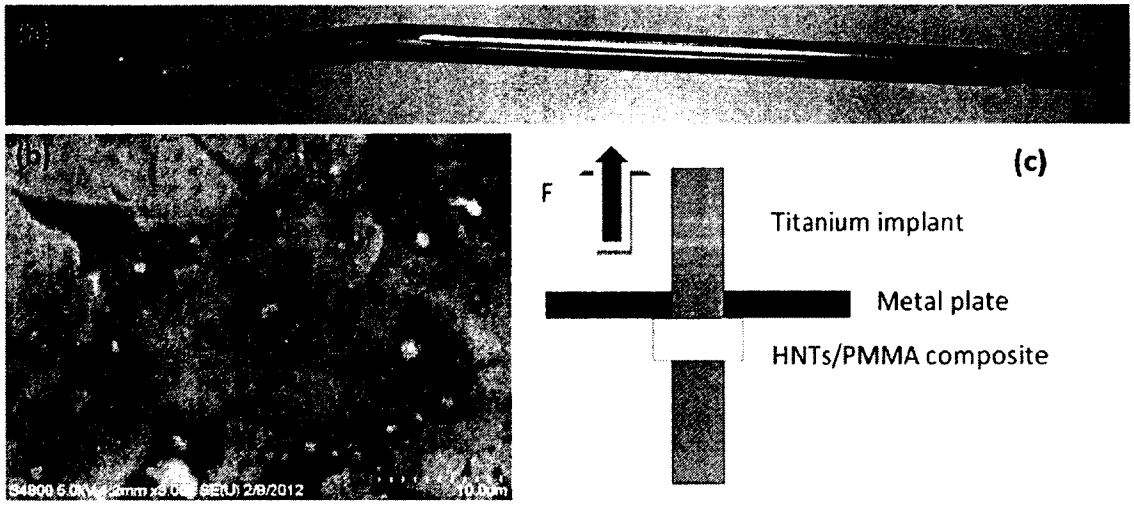

Figure 6-6: (a) Titanium implant (b) SEM of titanium implant surface (c) Simplified sketch of the apparatus for testing the adhesive forces between the PMMA bone cement and titanium implant.

5 samples are made: PMMA with 0 wt% halloysite, PMMA with 5 wt% halloysite, PMMA with 7.5 wt% halloysite, PMMA with 10 wt% halloysite, and PMMA with 1.5 wt% gentamicin.

Figure 6-7 shows that after halloysite is added into the PMMA bone cement, the maximum force needed to remove the PMMA/halloysite composite decreases from

640±20 N (0 wt% HNTs) to 600±20 N (5 wt% HNTs) and 610±20 N (7.5 wt% HNTs), respectively. However, the maximum force of the composite with 10 wt% HNTs increased to 760 ±20 N. On the other hand, PMMA bone cement mixed with 1.5wt % gentamicin also shows that the gentamicin has almost no influence on PMMA bone cement adhesion on a titanium implant.

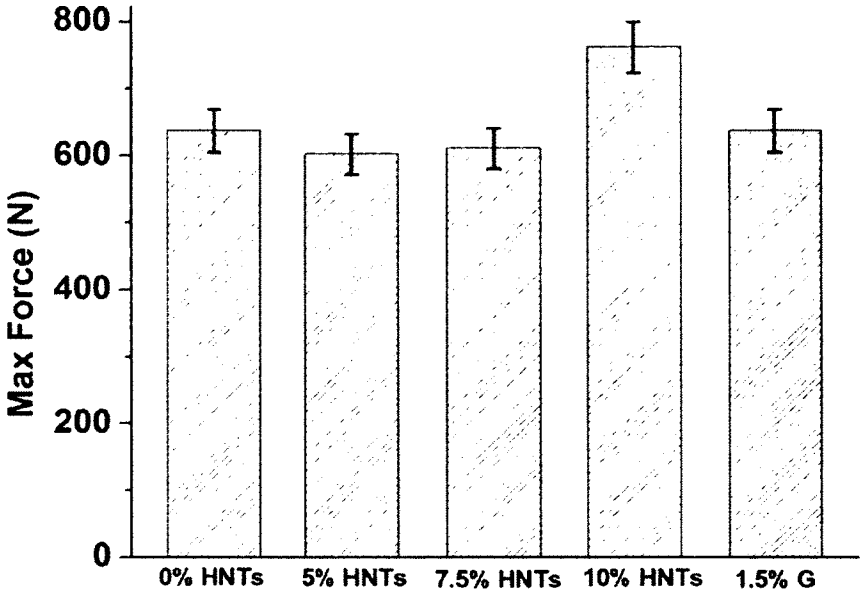

Figure 6-7: The maximal force needed to detach the cement from titanium implant depending on the halloysite doping ratio.

6.3.7 PMMA/Halloysite Composite Hydrophobicity

In Figure 6-8, the water contact angle measurements for the PMMA bone cement samples are presented. One can see that the contact angle is slightly reduced upon the addition of halloysite into PMMA (from 64.3° to 54.9°). This suggests that the moderate increase of the hydrophilic forces between PMMA and bone surface upon addition of halloysite is only partially responsible for the observed large increase in adhesion force. The second reason for the drastic increase of halloysite composite adhesiveness may be related to the intercalation of the needle-like clay nanotubes into the porous bone surface

(Figure 6-4 d). Halloysite nanotubes of 50-100 nm in diameter can easily penetrate into 100-300 nm size pores at the bone surface and cause anchoring which increases the resistance towards the external shear forces.

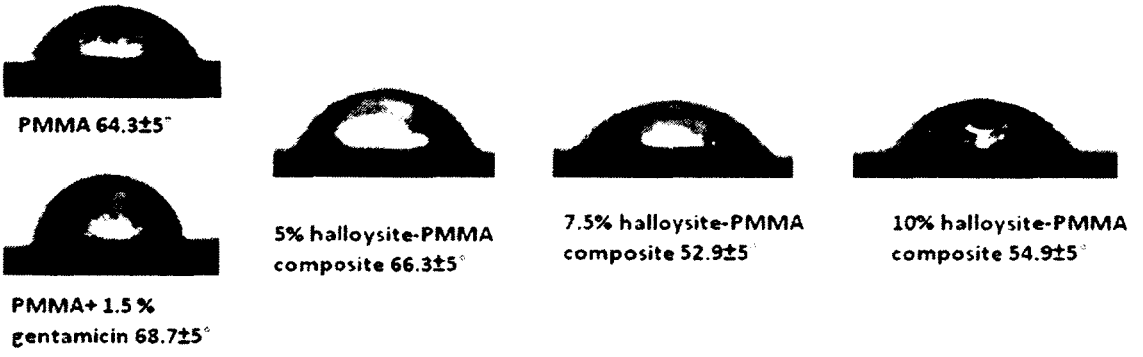

Figure 6-8: Water contact angle changes after halloysite is added into the PMMA bone cement [83].

6.3.8 Adding Halloysite into Glue to Enhance Adhesive Property

Based on our PMMA/halloysite composite results on adhesive property on bone surface and titanium implant, when adding halloysite into PMMA bone cement the adhesive property shows a significant increase of 5 times when 7.5 wt% halloysite is added. According to this result, we propose to add halloysite into any kind of glue to find out if additional halloysite can enhance the adhesive property on a porous surface. In this study, ceramic is used as the porous surface; epoxy glue and silicon glue are used to examine the flexural strength of halloysite glue composites (Figure 6-9).

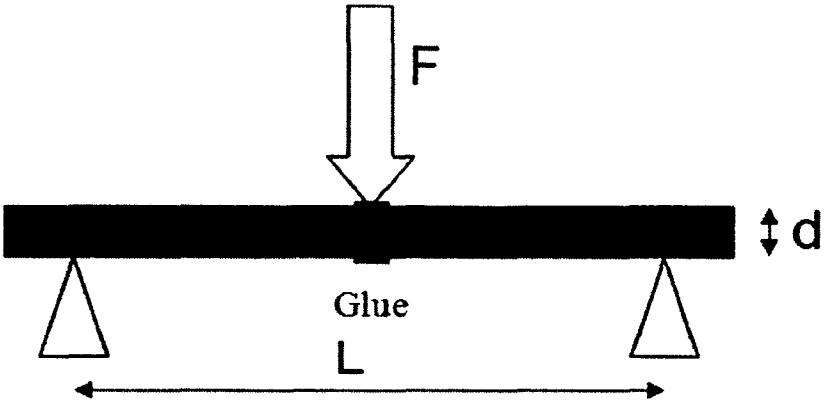

Figure 6-9: Glue composite three-point bending setup.

Figure 6-10 shows the strain-strain of 2 wt% halloysite/epoxy glue composite. Adding 2 wt% halloysite into epoxy glue, the stress increases about 4 times, and the max force to break two pieces of ceramic increase about 8 times. The water contact angle increases from 40±5° for epoxy glue to 70±5° for the halloysite epoxy glue composite.

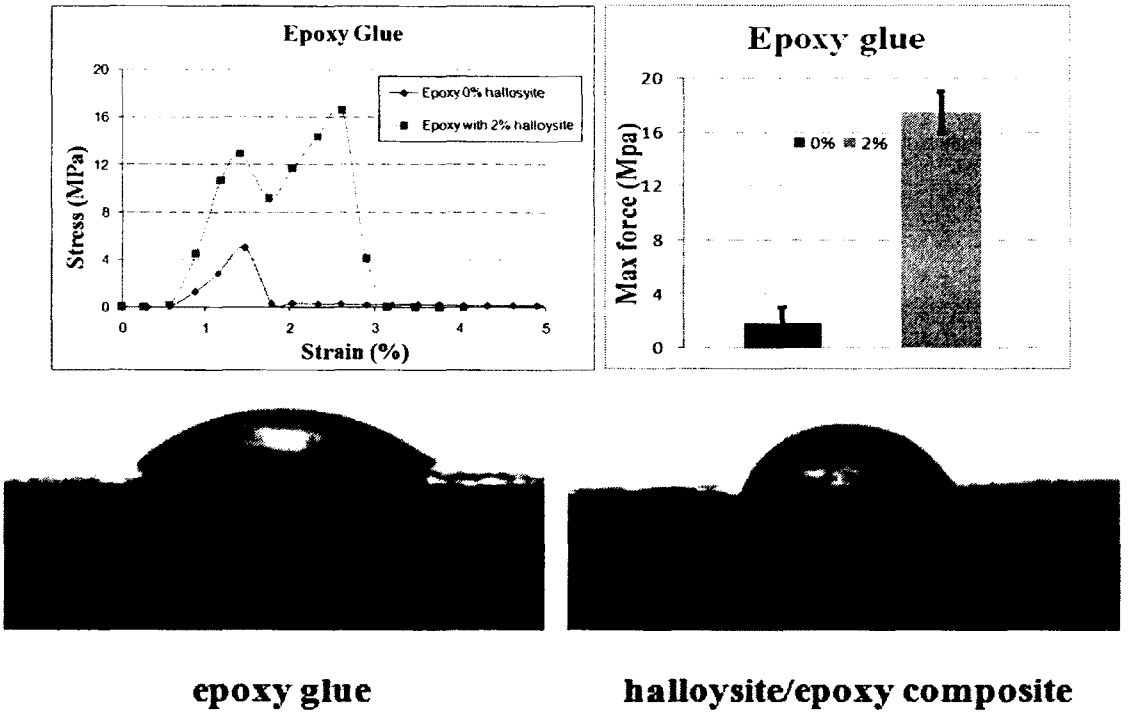

Figure 6-10: Halloysite/epoxy glue composite adhesive strength and water contact angle for halloysite/epoxy glue composite (40±5°to 70±5°).

Figure 6-11 shows the strain-strain of 4.4 wt% halloysite/silicone glue composite. Adding 4.4 wt% halloysite into the silicone glue, the stress increases about 3 times, and the max force to break two pieces of ceramic increases from 1.6 MPa to 2.3 MPa. The water contact angle decreases from 110±5° for epoxy glue to 90±5° for halloysite epoxy composite.

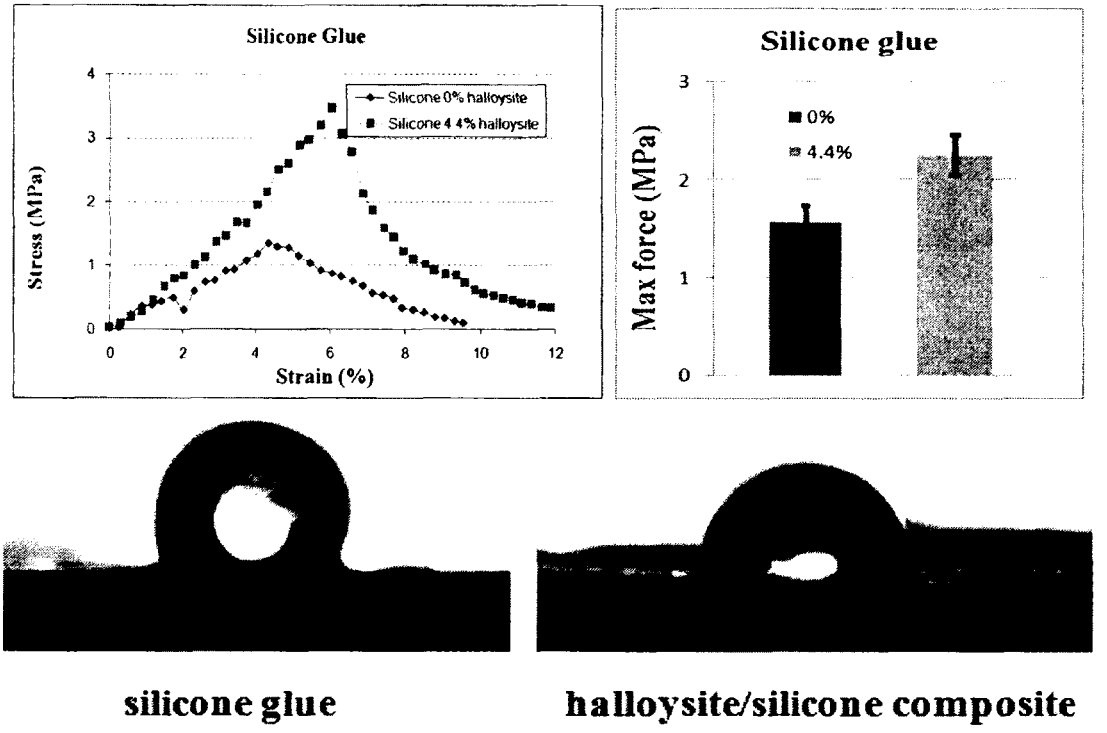

Figure 6-11: Halloysite/silicone glue composite adhesive strength and water contact angle for halloysite/epoxy glue composite (110±5°to 90±5°).

6.3.9 PMMA/Halloysite Composite Thermal Effects

PMMA polymerization is an exothermic process with the heat effect of 55 kJ/mole which causes heating as high as 70 °C, and causing thermal necrosis of the surrounding tissue. The addition of 10 wt% halloysite by weight effectively reduced the temperature peak down to 50 °C (Figure 6-12), which is safe for surrounding tissue, if we consider that the duration of this state is less than 90 sec.

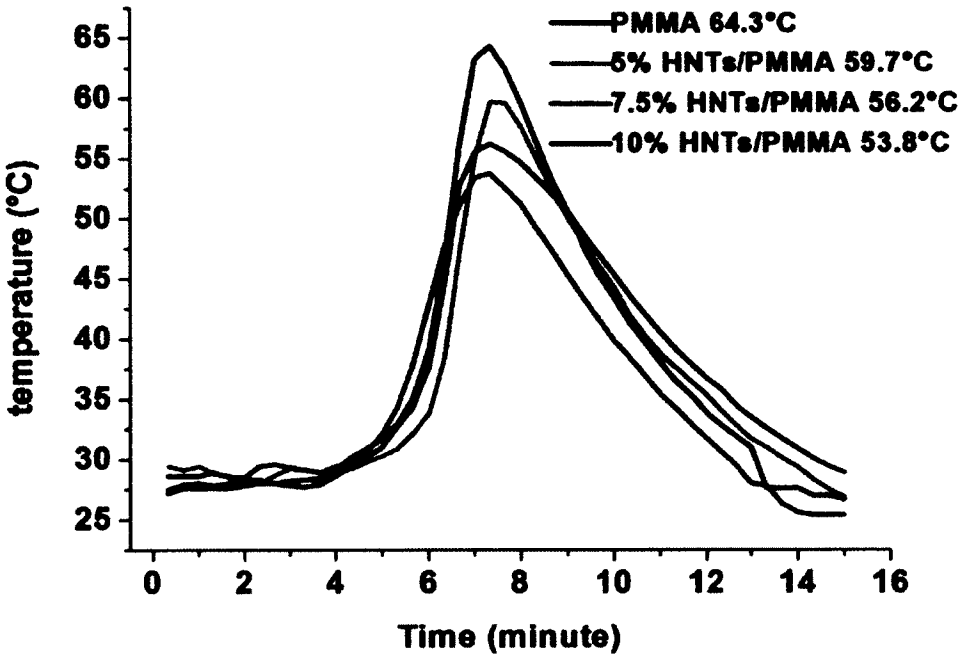

Figure 6-12: Temperature of PMMA cement composites during polymerization process for pure PMMA and cement doped with halloysite.

6.3.10 Antibiotics Release from Bone Cement

Gentamicin was loaded into halloysite using vacuum cycling, as described earlier. Before washing the sample, gentamicin comprised ca. 15% of the total mass of the nanotubes. After two brief rinses, the gentamicin amount was reduced to 11% and was probably located within the tube (lumen volume is ca. 10% of the halloysite tube). The lost gentamicin may be associated with the outer surface of the tubes. The outer surface of halloysite is primarily silica-based and has a negative charge. Gentamicin, having an isoelectric point of over 8.0, will have a small positive charge at pH 7 and may adsorb on the outer surface of halloysite. To observe the drug release from the tube interior, we removed any bound gentamicin to the halloysite outer surface, through repeated washings in DI water, leaving mostly gentamicin internalized in the halloysite lumen. For the halloysite powder (without PMMA) 94% of loaded gentamicin was released within 48

hours. However, gentamicin release was drastically extended with the halloysite incorporated in the PMMA.

For the PMMA bone cement composite doped with clay nanotubes, gentamicin loaded halloysite was admixed to MMA monomer. During PMMA solidification, additional encasing of the antibiotic inside the tube occurred. Release from PMMA composites became much slower and reached ca. 60% in 250 hours. Figure 6-13 presents the gentamicin release profiles from the PMMA bone cements admixed with different quantities of loaded halloysite. There are two groups of results presented: in Figure 6-13 a cement doped with gentamicin is encapsulated in the tubes, and in Figure 6-13 b samples with combined 1.5 wt% free gentamicin admixing and doping with loaded halloysite. The data clearly show that more gentamicin is released from the samples with a larger halloysite percentage.

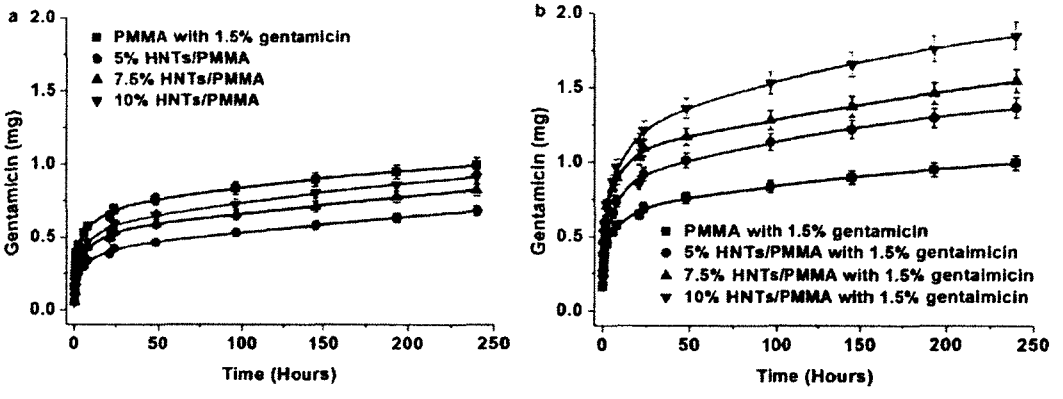

Figure 6-13: Gentamicin release from PMMA / halloysite composites: a) corresponds to the samples doped with only loaded halloysite (halloysite was loaded with gentamicin prior to mixing with PMMA). b) Corresponds to the samples with 1.5 wt% of free gentamicin in addition to loaded halloysite. Weight of the samples is 150±10 mg [83].

The amount of gentamicin leakage from bone cement samples modified with halloysite nanotubes is lower than the ones containing both free gentamicin and halloysite. This is due to the partial blocking of the halloysite tube endings by the PMMA

polymer matrix. Admixing 1.5 wt% of additional free gentamicin allowed for double antibiotic release. The combination of free gentamicin and loaded halloysite tubes as additives allowed for higher antibiotic loading with faster initial release without compromising the mechanical strength (Figure 6-13 b) the bottom curve corresponds to the samples with only 1.5 wt% of free gentamicin and the higher curves demonstrate the addition of loaded halloysite).

There is an interesting feature of induced gentamicin release in the PMMA/loaded halloysite composite in implant defects (such as cracks) (Figure 6-14). Additional gentamicin leakage was observed after the cracking of the composite sample, which was due to the additional exposure of the internal halloysite tubules. This result also demonstrated that the total amount of gentamicin release from the composite was equal to the release from the halloysite. When cracks appear on the composite after surgery, the jump in release will provide a fast release of antibiotics to protect against infection.

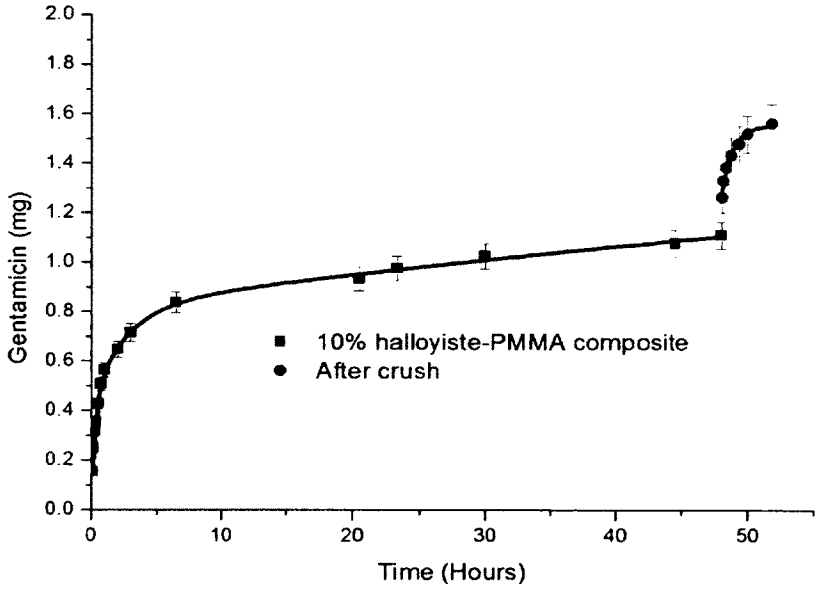

Figure 6-14: Gentamicin release for 48 hours. Red line shows gentamicin release from 150 mg of PMMA composite containing 15 mg of halloysite. After 48 hours, the PMMA sample was crushed; this resulted in additional release [83].

Figure 6-15 presents the ciprofloxacin release profiles from the PMMA bone cements admixed with different quantities of loaded halloysite for 2 weeks. There was about 70% of ciprofloxacin released from each sample over two weeks.

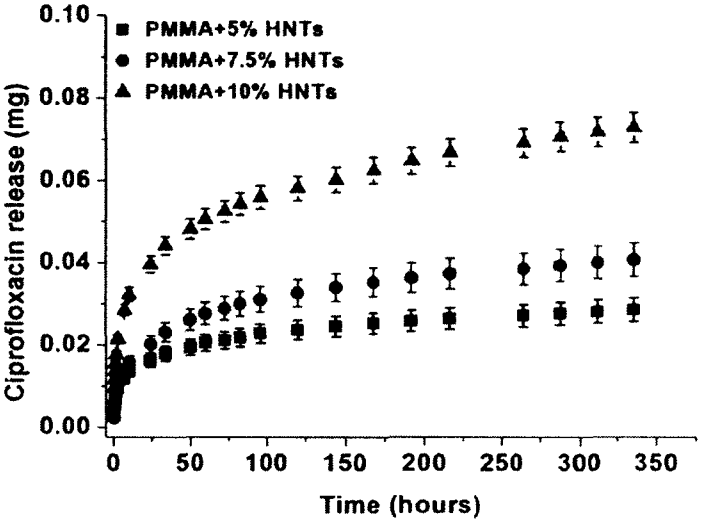

Figure 6-15: Ciprofloxacin release from PMMA / halloysite composites.

The reason antibiotics released slower from the PMMA/halloysite composites than from the halloysite nanotube was that the release from composites has two steps, first, antibiotics release from halloysite nanotube to the composite matrix, second, the antibiotics in the composite matrix release to the outside environment. The composite of PMMA and antibiotics loaded halloysite demonstrated a longer and slow release of antibiotics, and the potential for additional fast release when a crack appears.

6.3.11 Antibacterial Effect of Gentamicin Loaded Halloysite Doped in PMMA

Preventing infection is an important aspect of implant surgery. Gentamicin is bactericidal on proliferating and resting pathogens and often is used for bone cement. With its broad therapeutic spectrum, gentamicin covers a variety of gram-positive and gram-negative bacteria. We used the antibiotic gentamicin to demonstrate its efficiency after encapsulating it in halloysite nanotubes doped into bone cement. Encapsulation in

halloysite tubes allowed for sustained release of gentamicin, giving a prolonged antibacterial effect.

In Figure 6-16, images of the bacterial growth of *E. Coli* (a, b) and *S. aureus* (c, d) cultures around PMMA cement and PMMA + 7.5 wt% gentamicin loaded halloysite are presented. Unloaded cement and gentamicin loaded halloysite/PMMA bone cement squares were placed onto bacterial streak cultures. Bacteria readily grew around unloaded PMMA composites (Figure 6-16 a, c). The cement composite with gentamicin-loaded halloysite inhibited bacterial growth (Figure 6-16 b, d). These results show that the release of antibiotics, such as gentamicin from the PMMA/halloysite composite can help solve the infection problem without compromising the implant mechanical strength for halloysite doped PMMA composites.

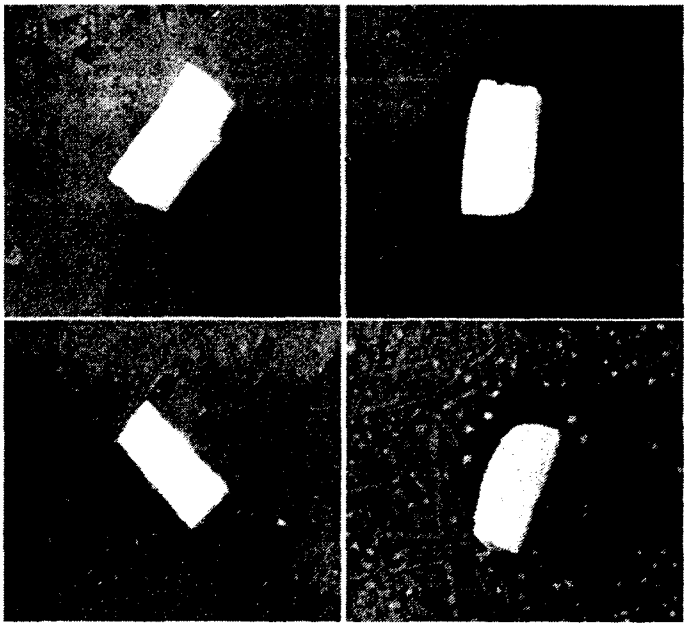

Figure 6-16: Images of *E. coli* (a, b) and *S. aureus* (c, d) around original PMMA cement (left images), and PMMA + 7.5 wt% halloysite loaded with gentamicin (right images) after one week of the bacterial culture growth [83].

6.3.12 Tricalcium Phosphate Bone Cement Halloysite Composites

In this project, another bone cement, tricalcium phosphate, was also studied for its mechanical properties when add halloysite to make composites. Tricalcium phosphate bone cement will be prepared by mixing 1 gram of powdered β-tricalcium phosphate halloysite mixture with 0.35 ml of 20% citric acid solution. Then the sample will be placed into molds with the desired shape and dried for one day before testing.

Halloysite tricalcium phosphate bone cements were prepared by interaction of β-tricalcium phosphate with citric acid solution. 4 grams of the powder containing a mixture of halloysite and β-tricalcium phosphate was thoroughly mixed with 1.4 ml of 20% citric acid solution and left one day for complete hardening. Original calcium phosphate cement has a white color that turns creamy yellow upon the addition of halloysite (Figure 6-17). The addition of 10-20 wt% halloysite into calcium phosphate cement gives a reasonably good distribution within the cement matrix. Formation of a microfibrous network in halloysite admixed calcium phosphate cement significantly improves the mechanical properties of the cement. SEM images indicate calcium phosphate fibers of ca. 50 micron length with an aspect ratio of close to 100.

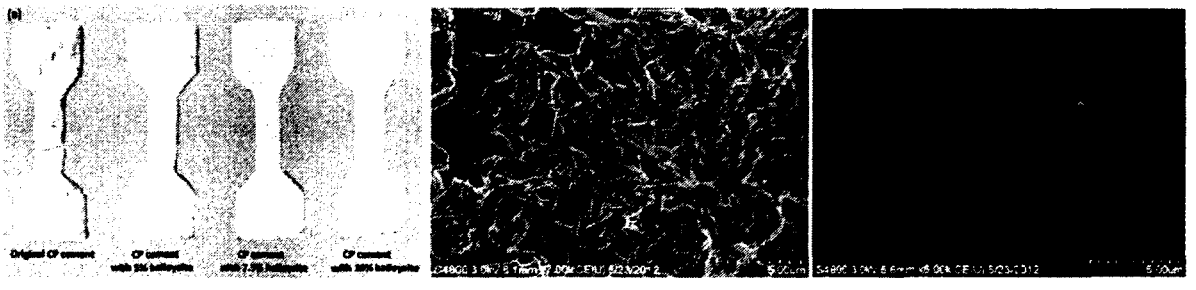

Figure 6-17: Tricalciumphosphate bone cement composites (a). Halloysite initiates non-isotropic crystallization of calcium phosphate yielding fibers of 50 microns length and 0.5 micron diameter (b-c).

Mechanical strength of tricalciumphosphate bone cement composites was compressed to determine the maximum force needed to break the composite. Figure 6-18 shows that the peak force needed to break the composite significantly increased from 25±5 N to 200±20 N. Figure 6-19 shows the strain-stress curve of halloysite/tricalciumphosphate bone cement composites.

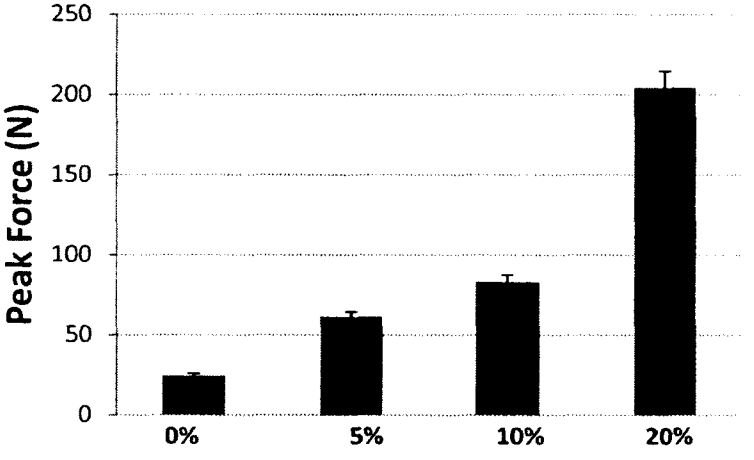

Figure 6-18: Peak force needed to break halloysite/tricalciumphosphate bone cement composites.

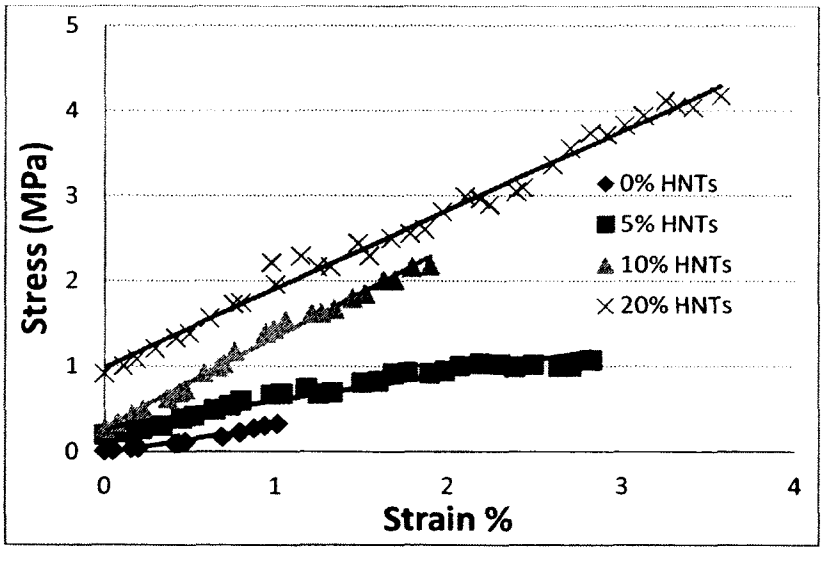

Figure 6-19: Strain-Stress curve of halloysite/tricalciumphosphate bone cement composites.

6.4 Conclusions

We have shown that PMMA bone cement doped with 5-7 wt% gentamicin-loaded halloysite nanotubes provides for slow 100-300 hours release of gentamicin without compromising the mechanical strength of the composite. There is only a slight difference between 5-7 wt% loaded halloysite/PMMA composite. The addition of PMMA/halloysite composites to bacterial cultures and the subsequent sustained gentamicin release, efficiently inhibited bacterial growth of *E. coli* and *S. aureus*. The addition of halloysite into PMMA improved the mechanical properties of the bone cement including higher tensile strength, and significant gains in adhesive strength. The flexural strength of the samples was slightly decreased at a higher ratio of halloysite content. Measurements of PMMA/halloysite adhesiveness on femoral bone showed a fivefold increase when 7 wt% halloysite was added. Based on the overall measurements, we concluded that 5 – 7.5 wt% of halloysite is the optimal amount to be added to PMMA bone cement to achieve the best mechanical and adhesive properties as well as high storage and sustained release capabilities for antimicrobial gentamicin.

A similar approach was used for halloysite loading in another commonly used bone cement- tricalcium phosphate (CP). We managed to overcome mechanical weakness of this material by increasing its tensile strength 5-6 times by doping it with halloysite nanotubes.

CHAPTER 7

CONCLUSIONS AND FUTURE WORK

7.1 Conclusions

In this dissertation, halloysite nanotubes were studied as nano-containers for loaded and sustained controlled release of drugs (antiseptics and antibiotics). Drug loaded halloysite tubes were mixed with bulk materials, such as PMMA and CP bone cements and polymeric paints, to make nanocomposites with new antibacterial properties. The polymer/halloysite composites showed synergetic improvement of materials' mechanical properties and provided a controlled release of loaded medical substances.

Usually, non-formulated drug powders dissolve in water within 10-15 minutes allowing for time-limited efficiency. However, drugs loaded in halloysite tubes release slowly for tens of hours. Because the lumen volume of halloysite is about 10-15%, the loading efficiency and release rate are controlled by the lumen size. In order to get higher loading efficiency, halloysite was modified by selective etching of the inner lumen alumina allowing an increase in the loading from 10 to 35 wt%.

Reducing drugs release rate was another important factor for this nano-formulation. An additional stopper coating was synthesized by copper-benzotriazole (BTA-Cu) coating predominantly at tube endings. Brilliant green loaded halloysite with BTA-Cu stoppers significantly (3-5 times) reduced the release rate. Brilliant green release from halloysite without a stopper reached about 70% in 3 hours; while on the other hand,

the release with BTA-Cu stopper only reached 5% in 3 hours. The additional BTA-Cu stopper also increase the loading efficiency: without a stopper it was 3%, and with a stopper - increased up to 18%. The BTA-Cu stopper formations were optimized depending on the concentration of both compounds. The higher concentration of both compounds will form a tighter coating with small pores, giving slower release. If one of the compound concentrations was much lower than the other, the coating has larger pores which led to more leakage.

Next, we studied antibacterial efficiency of encased antiseptics (brilliant green, amoxicillin, iodine). Brilliant green loaded halloysite with and without a stopper killed *S. aureus* for a 72 hour time period, while in a control experiment using on-formulated brilliant green powder only worked for 3 hours.

A similar strong increase in the efficiency was obtained for antibiotics /halloysite formulations (ciprofloxacin and gentamicin). The antibacterial effect of ciprofloxacin only lasts for 24hours, but halloysite loaded ciprofloxacin worked for 72 hours allowing for the efficient suppression of MDR (drug resistant) gangrene bacteria.

Other antibacterial nanocomposites were made using inner-tubule silver encapsulation. Halloysite can be used as a template to synthesize metal nanorods in the lumen. Silver nanorods were synthesized in 15 nm diameter halloysite lumens allowing for core-shell metal-ceramic nanostructures where metals are protected from quick oxidation. Doping encapsulated silver/clay nanorods into paint, the paint composites presented strong antimicrobial properties combined with an enhancement of the coatings tensile strength. The results show that most of the antimicrobial efficiency was located around cracks in the paint composite where enhanced release of silver ions occurred.

Another advantage of encasing silver nanorods in halloysite tube was preventing silver decomposition under intensive UV light (the paint composite preserved its color).

Further research development was the loading of halloysite with antibiotics and doping them into bone cements. The composites of polymethylmethacrylate - PMMA with halloysite solved the limitations of adding non-formulated antibiotics in PMMA bone cement (preserved antibiotics efficiency and enhanced composite strength). First, adding 5-7.5 wt% halloysite into PMMA bone cement did decrease the mechanical properties of the composites. The results show an increasing of tensile strength, and a slight decreasing of flexural strength. Surprisingly, the adhesivity of PMMA bone cement on bone surface and titanium implants significantly increased. Second, antibiotics loaded in halloysite nanotube and then mixed with PMMA bone cement provided slow 150-200 hours release of gentamicin (this one week time is a typical demand for orthopedic surgery post-treatment). Besides, if tension or crack appeared at the bone cement composite, it led to a response of faster release of antibiotics at the crack section. Third, the added halloysite in PMMA bone cement decreased the polymerization temperature from 70 to 55 °C (by references of practical surgeons in the LSU-Shreveport hospital, this will allow a decrease in tissue burning during orthopedic surgery).

A similar technique of halloysite doping into another mechanically weak bone cement - tricalcium phosphate (CP) allowed for a substantial5-7 times increase of its mechanical strength, widening applications for CP.

7.2 Future Work

7.2.1 Selective Modify Halloysite to Improve Loading and Release

One disadvantage of halloysite is the lumen volume of just about 10% which limited the loading efficiency. This dissertation gave preliminary results on sulfate acid etching of the halloysite lumen. The more etching, the larger was the lumen diameter that was obtained. However, the increase of the lumen diameter leads to faster release of the loaded substance. This work on the halloysite lumen size optimization will be preceded in Dr. Lvov's group.

Another way to improve tube loading and release is to alter its physical-chemical properties. As we know, the inner lumen of halloysite is aluminum based, and it is positively charged and hydrophilic. This is not good for a load that is positively charged or for hydrophobic substances. One can modify the surface properties of the tube lumen by reversing its charge or making it hydrophobic, for example, through silanisation. This work is also under development.

End-stoppers: the tube opening is controlling the release kinetics. In this work, BTA-Cu tube coating has already been studied, however, even though these stoppers can significantly decrease release, copper ions were noted as heavy metal and potentially harmful for biomedical applications. So, synthesis of a biocompatible stopper is needed (probably based on iron complexation).

This dissertation presents a number of simple methods for improving halloysite drug loading and extended release. For future work, one could combine and optimize these methods to reach higher loading efficiency and better controlled release.

We presented the different kinetics of the drugs release from halloysite; some of the drugs release faster, some released slowly. So, by mixing, in one formulation, halloysite loaded with different drugs, one can get the needed multidrug release pattern. In this way, we can get a series release of multiple drugs depending on time. The most important idea of the dissertation, the increased efficiency of drugs loaded into clay nanotubes, may be developed to fight multidrug resistant bacteria.

7.2.2 Metal Loaded Halloysite for X-ray Detection

X-ray is a common way to examine bone injury and recovery. In Chapter Five, a method is described on how to use halloysite as a template to make metal nanorods in the halloysite lumen. Based on this method, halloysite can be used to load some x-ray detection chemicals such as barium sulfate, then add this halloysite to PMMA bone cement, which will help to examine the bone cement using x-rays.

7.2.3 Other Biopolymer/Halloysite Composites

According to the results obtained for PMMA/halloysite composites, add loaded biocompatible natural halloysite nanotubes into biopolymers to make a composite. The composite will then provide a slow release of the loaded substance and, with the synergistic enhancement of mechanical properties, such as tensile strength, flexural strength, and adhesive strength. A similar biomaterial is artificial teeth. Dr. Lvov's group recently established contacts with LSU Dental School in New Orleans. We will work on an artificial halloysite composite for adhesive and antibacterial teeth fillings.

REFRERENCES

[1] Webb, J.; Spencer, R. *J. Bone Joint Surgery-British.* **2007**, 89, 851-857.

[2] Kühn, K-D. *Heidelberg: Springer Medizin Verlag.* **2005**, 52-59.

[3] Bayston, R.; Milner, R. *J Bone and Joint Surgery.* **1982**, 64, 460-464.

[4] Insall, J.; Thompson, F.; Brause, B. *J Bone and Joint Surgery.* **1983**, 65, 1087- 1098.

[5] Hoff, S.; Fitzgerald, R.; Kelly, P. *J Bone and Joint Surgery.* **1981**, 63, 798-804.

[6] Kim, S.; Kim, Y.; Yoon, T.; Park, S.; Cho, I.; Kim, E.; Kim, I.; Shin, J. *Biomaterials.* **2004**, 25, 5715-5723.

[7] Virto, M.; Frutos, P.; Torrado, S.; Frutos, G. *Biomaterials.* **2003**, 24, 79-87.

[8] Van, B-H.; Neut, D.; Schenk, W.; Van, H-J.; Van, M-H.; Busscher, H. *ActaOrthopaedicaScandinavica.* **2000**, 71, 625-629.

[9] Ragel, C.; Vallet-Regi, M. *J Biomed Mater Res A.* **2000**, 51, 424-429.

[10] Camire, C.; Saint-Jean, S.; Mochales, C.; Nevsten, P.; Wang, J.; Lidgren, L.; McCarthy, I.; Ginebra M. *J Biomed Mater Res B ApplBiomat.* **2005**, 76, 424-431

[11] Joussein, E; Petit, S; Churchman, J.; Theng, B.; Righi, D.; Delvaux, B. *Clay Minerals.* **2005**, 40, 383-426.

[12] White, S.R.; Sottos, N.R.; Geubelle, P.H.; Moore, J.S.; Kessler, M.R.; Sriram, S.R.; Brown, E.N.; Viswanatan, S. *Nature.* **2001**, 409, 794-797.

[13] Brown, E.N.; Sottos, N.R.; White, S.R. *Exp. Mech.* **2002**, 42, 372-379.

[14] Moll, J.L.; White, S.R.; Sottos, N.R. *J. Compos. Mater.* **2010**, 44, 2573-2585.

[15] Rong, M. Z.; Zhang, M.Q.; Zhang, W. *Adv. Compos. Lett.* **2007**, 16, 167-172.

[16] Beiermann, B.A.; Keller, M.W. Sottos, N.R. *Smart Mater. Struct.* **2009**, 18, 085001

[17] Suryanarayana, C.; Rao, K.C.; Kumar, D. *Progr. Org. Coat.* **2008**, 63, 72-78.

[18] Grigoriev, D.O.; Köhler, K.; Skorb, E.; Shchukin, D.G.; Möhwald, H. *Soft Matter.* **2009**, 5, 1426-1432.

[19] Lvov, Y.; Shchukin, D.; Möhwald, H.; Price, R. *ACS Nano.* **2008**, 2, 814-820.

[20] Bates, T.; Hilderbrand. F.; Swineford, A. *Amer Miner.* **1950**, 35, 463-485.

[21] Du, M.; Guo, B.; Jia, D. *Polymer Intern.* **2010**, 59, 574-595.

[22] Price, R.; Gaber, B.; Lvov, Y. *J Microencap.* **2001**, 18, 713-723.

[23] Abdullayev, E.; Lvov, Y. *J Mater Chem.* **2010**, 20, 6681-6687.

[24] Abdullayev, E.; Lvov, Y. *J Nanoscience Nanotech.* **2011**, 11, 10007-10026.

[25] Yelleswarapu, C.; Gu, G.; Abdullayev, E.; Lvov, Y.; Rao, D. *Opt Comm.* **2010**, 283, 438-441.

[26] Abdullayev, E.; Price, R.; Shchukin, D.; Lvov, Y. *Appl Mater & Interf.* **2009**, 2, 1437-1442.

[27] Kirkman, JH. *Clays Clay Miner.* **1981**, 29, 1-9.

[28] Lu, D.; Chen, H.; Wu, J.; Chan, C. *J NanosciNanotechnol.* **2011**, 11, 7789-7793.

[29] Singh, B. *Clays Clay Miner.* **1996**, 44, 191-196.

[30] Singh, B.; Mackinnon, I. *Clays Clay Miner.* **1996**, 44, 825-834.

[31] Abdullayev, E.; Shchukin, D.; Lvov, Y. Polym Mater SciEng. **2008**, 99, 331-332.

[32] Churchman, GJ.; Carr, RM. *Clays Clay Miner.* **1975**, 23, 382-388.

[33] Bergaya, F.; Theng, BKG.; Lagaly, G. *Amsterdam: Elsevier.* **2006**.

[34] Vergaro,V.; Abdullayev, E.;Lvov,Y.; Zeitoun, A.; Cingolani, R.;Rinaldi, R.; Leporatti, S.*Biomacromolecules.* **2010**, 11, 820–826.

[35] Tazaki, K.*Clays Clay Miner.* **2005**, 53, 224-233.

[36] Carr, RM.; Chaikum, N.; Patterson, N. *Clays Clay Miner.* **1978**, 26, 144-152.

[37] Abdullayev, E.; Joshi, A.; Wei, W.; Zhao, Y.; Lvov, Y.*ACS Nano.* **2012**, 6, 7216–7226.

[38] Yah, W.; Takahara, A.; Lvov, Y. *J. Am. Chem. Soc.* **2012**, 134, 1853–1859.

[39] Kommireddy, D.; Ichinose, I.; Lvov, Y.; Mills, D. *J. Biomed Nanotechnol.* **2005**, 1, 286-290.

[40] Suh, Y.; Kil, D.; Chung, K.; Abdullayev, E.; Lvov, Y.; Torchilin, V. *J. NanosciNanotechnol.* **2010**, 10, 3687-3700.

[41] Vollet, D. R.; Macedo, J. D.; Mascarenhas, Y. P. *Appl. Clay Sci.* **1994**, 8, 397–404.

[42] Tazaki, K. *Clays Clay Miner.* **2005**, 53, 224–233.

[43] Shchukin, D.; Price, R.; Sukhorukov, G.; Lvov, Y. *Small.* **2005**, 5, 510-513.

[44] Abdullayev, E.; Abbasov, V.; Lvov, Y. *J. Petrochem Oil Ref.* **2010**, 23, 234-246.

[45] Veerabadran, N.; Price, R.; Lvov, Y. *Polym Mater SciEng.* **2008**, 99, 566-567.

[46] Abdullayev, E.; Sakakibara, K.; Okamoto, K.; Wei, W.; Ariga, K.; Lvov, Y. *ACS Appl Mater Interf.* **2011**, 3, 4040-4048.

[47] Veerabadran, N.; Lvov, Y.; Price, R. *Macrom Rap Comm.* **2009**, 24, 99-103.

[48] White, R. D.; Bavykin, D. V.; Walsh, F. C. *Nanotechnology.* **2012**, 23, 1–10.

[49] Zhang, A.; Pan, Li; Zhang, H.; Liu, S.; Ye, Y.; Xia, M.; Chen, X. *Colloids, Surf. A.* **2012**, 396, 182–188.

[50] Viseras, M. T.; Aguzzi, C.; Cerezo, P.; Cultrone, G.; Viseras, C. *J. Microencapsulation.* **2009**, 26, 279–286.

[51] Liu, M.; Guo, B.; Zou, Q.; Du, M.; Jia, D. *Nanotechnology.* **2008**, 19, 205709.

[52] Aglietti, E. F.; Porto Lopez, J. M.; Pereira, E. *Appl. Clay Sci.* **1988**, 3, 155–163.

[53] Yah, W.; Xu, H.; Soejima, H.; Ma, W.; Takahara, T.; Lvov, Y. *J. Am ChemSoc.* **2012**, 134, 12134-12137.

[54] Cavallaro, G.; Lazzara, G.; Milioto, S. *J. Phys. Chem.* **2012**, 116, 21932–21938.

[55] Du, M.; Guo, B.; Jia, D. *Polym. Int.* **2010**, 59, 574-582.

[56] Li, C.; Liu, J.; Qu, X.; Guo, B.; Yang, Z. *J. Appl. Polym. Sci.* **2008**, 110, 3638–3646.

[57] Wang, L.; Wang, Y.; Pei, X.; Peng, B. *React. Funct. Polym.* **2008**, 68, 649–655.

[58] Matsuno, R.; Yamamoto, K.; Otsuka, H.; Takahara, A. *Chem. Mater.* **2002**, 15, 3–5.

[59] Matsuno, R.; Otsuka, H.; Takahara, A. *Soft Matter.* **2006**, 2, 415–421.

[60] Ma, W.; Otsuka, H.; Takahara, A. *Chem. Commun.* **2011**, 47, 5813–5815.

[61] Ma, W.; Yah, W. O.; Otsuka, H.; Takahara, A. *J. Mater. Chem.* **2012**, 22, 11887–11892.

[62] Terayama, Y.; Kikuchi, M.; Kobayashi, M.; Takahara, A. *Macromolecules.* **2010**, 44, 104–111.

[63] Horiuchi, S.; Hanada, T.; Ebisawa, M.; Matsuda, Y.; Kobayashi, M.; Takahara, A. *ACS Nano.* **2009**, 3, 1297–1304.

[64] Guo, B.; Lei, Y.; Chen, F.; Liu, X.; Du, M.; Jia, D. *Appl. Surf. Sci.* **2008**, 255, 7329–7336.

[65] Lecouvet, B.; Gutierrez, J.; Sclavons, M.; Bailly, C. *Polym. Degrad. Stab.* **2011**, 96, 226–235.

[66] Ye, Y.; Chen, H.; Wu, J.; Ye, L. *Polymer.* **2007**, 48, 6426–6433.

[67] Du, M.; Guo, B.; Liu, M.; Jia, D. *Polym. Comp.* **2007**, 15, 321–328.

[68] Cavallaro, G.; Donato, D.; Lazzara, G.; Milioto, S. *J. Phys.Chem.C.* **2011**, 115, 20491–20498.

[69] Chang, P. R.; Xie, Y.; Wu, D.; Ma, X. *Carbohydr. Polym.* **2011**, 84, 1426–1429.

[70] Shamsi, M. H.; Geckeler, D. V. *Nanotechnology.* **2008**, 19, 075604.

[71] Cavallaro, G.; Lazzara, G.; Milioto, S. *Langmuir.* **2011**, 27, 1158-63.

[72] Lvov, Y.; Price, R.; Gaber, B.; Ichinose, I. *Col Surf Eng.* **2002**, 198, 375-382.

[73] Kommireddy, D.; Sriram, S.; Lvov, Y. Mills, D. *Biomaterials.* **2006**, 27, 4296–4303.

[74] Hoffmann, I.; Heunemann, P.; Prévost, S.; Schweins, R.; Wagner, N. J.; Gradzielski, M. *Langmuir.* **2011**, 27, 4386–4396.

[75] Bilalov, A.; Leal, C.; Lindman, B. *J. Phys. Chem. B.* **2004**, 108, 15408–15414.

[76] Zheng, Y.; Wang, A. *J Macromol Sci A: Pure ApplChem.* **2010**, 47, 33-38.

[77] Xie, Y.; Chang, P.; Wang, S.; Yu, J.; Ma, X. *Carbohyd Polym.* **2011**, 83, 186–191.

[78] Voon, H.; Bhat, R.; Easa, A.; Liong, M.; Karim, A. *Food Bioproc Tech.* **2012**, 5, 1766-1774.

[79] Cui, T.; Hua, F.; Lvov, Y. *Trans Electr Dev.* **2004**, 51, 503-507.

[80] Fennouh, S.; Guyon, S.; Livage, J.; Roux, C. *J Sol-Gel Sci Technol.* **2000**, 19, 647-649.

[81] Konnova, S.; Sharipova, I.; Ilinskaya, O.; Lvov, Y.; Fakhrullin, R. *Chem Comm.* **2013**, 23, 476-479.

[82] Kelly, H.; Deasy, P.; Ziaka, E.; Claffey. N. *Int J Pharm.* **2004**, 274, 167-183.

[83] Wei, W.; Abdullayev, E.; Hollister, A.; Mills, D.; Lvov, Y. *Macromol Mater Eng.* **2012**, 297, 645–653.

[84] Levis, S.; Deasy, P. *Int. J. Pharm.* **2003**, 253, 145–157.

[85]Moats, W.A.; Kinner, J.A.; Maddox, S.E. *Applied Microbiology.* **1974**, 27, 844-847.

[86] Prasad, P. *John Wiley &Sons:Canada*, **2004**, 104-107.

[87] Oskin, M.; Chong, F.; Chuang, I. L.; Kubiatowicz, J. *Proc. IEEE Comp. Soc.* **2003**, 374-385.

[88] Georgakilas, V.; Tzitzios, V.; Gournis, D.; Petridis, D. *Chem. Mater.* **2005**, 17, 1613-1617.

[89] Ariga, K.; Hill, J.; Ji, Q. *Phys. Chem. Chem. Phys.* **2007**, 9, 2319-2340.

[90] Guo, D.; Li, H. *Carbon.* **2005**, 43, 1259-1264.

[91] Guo, Y.; Hu, J.; Liang, H.; Wan, L.; Bai, C. *Chem. Mater.* **2003**, 15, 4332-4336.

[92] Schnur, J. *Science.* **1993**, 262, 1669-1676.

[93] Niemeyer, C. M.; Simon, U. *Eur. J. Inorg. Chem.* **2005**, 18, 3641-3655.

[94] Yuan, P.; Southon, P.; Liu, Z.; Green, M.; Hook, J.; Antill, S.; Kepert, C. *J. Phys. Chem. C.* **2008**, 112, 15742-15751.

[95] Zhai, J.; Sun, W.; Wang, H. *J. Nanosci. Nanotechnol.* **2006**, 6, 1968-1972.

[96] Lin, C.; Danaie, M.; Liu, Y.; Mitlin, D.; Kuznicki, S. M.; Eyring E. M. *J. Nanosci. Nanotechnol.* **2009**, 9, 4985-4987.

[97] Maiyalagan, T. *Appl. Catal. A General.* **2008**, 340, 191-195.

[98] Lu, Y.; Wang, Y.; Chen, W. *J. Power Sour.* **2011**, 196, 3033-3038.

[99] Shah, M.; Nag, M.; Kalagara, T.; Singh, S.; Manorama, S. *Chem. Mater.* **2008**, 20, 2455-2460.

[100] Kong, H.; Jang, J. *Langmuir.* **2008**, 24, 2051-2056.

[101] Chatterjee, S.; Garai, A.; Nandi, A. *Synth. Met.* **2011**, 161, 62-71.

[102] Jin, R.; Cao, Y-W.; Mirkin, C.; Kelly, K.; Schatz, G.; Zheng, J. *Science.* **2001**, 294, 1901-1903.

[103] Mock, J.; Oldenburg, S.; Smith, D.; Schultz, D.; Schultz, S. *Nano Lett.* **2002**, 2, 465-469.

[104] Du, M.; Guo, B.; Jia, D. *Polym. Int.* **2010**, 59, 574-582.

[105] Kumar, A.; Vemula, P.; Ajayani, P.; John, G. *Nat Mater.* **2008**, 7, 236-241.

[106] Logvinenko, V.; Polunina, O.; Mikhailov, Y. U.; Mikhailov, K.; Bokhonov, B. *J. Therm. Anal. Calorim.* **2007**, 90, 813-816.

[107] Joussein, E.; Petit, S.; Churchman, J.; Theng, B.; Righi, D.; Delvaux, B. *Clay Miner.* **2005**, 40, 383-426.

[108] Kirkman, *Clays Clay Miner.* **1981**, 29, 1-9.

[109] Akhavan, O.; Abdolahad, M.; Abdi, Y.; Mohajerzadeh, S. *J. Mater. Chem.* **2011**, 21, 387-393.

[110] Kawashita, M.; Toda, S; Kim, H.-M.; Kokubo, T.; Masuda, N. *J. Biomed. Mater. Res.* **2003**, 66, 266-274.

[111] Kawashita, M.; Tsuneyama, S.; Miyaji, F.; Kokubo, T.; Kozuka, H.; Yamamoto, K. *Biomaterials.* **2000**, 21, 393-398.

[112] Balamurugan, A.; Balossier, G. Laurent-Maquin, D.; Pina, S.; Rebelo, A. H.; Faure, J.; Ferreira, J. M. *Dent. Mater.* **2008**, 24, 1343-1351.

[113] Bellanstone, M.; Williams, H. D.; Hench, L. L. *Antimicrob Agents Chemoter.* **2002**, 46, 1940-1945.

[114] Park, J.; Jana, S. *Polymer.* **2003**, 44, 2091-2100.

[115] Fix, D.; Andreeva, D.; Lvov, Y.; Shchukin, D.; Möhwald, H. *AdvFunct Mater.* **2009**, 19, 1720-1727.

[116] Veerabadran, N.; Price, R.; Lvov, Y. *Nano.* **2007**, 2, 115-120.

[117] Ismail, H.; Pasbakhsh, P.; Fauzi, M.; Abu, Bakar A. *Polymer Testing.* **2008**, 27, 841-850.

[118] Diez-Pena, E.; Frutos, G.; Frutos, P.; Barrales-Rienda, J. *Chemical Pharmaceutical Bulletin.* **2002**, 50, 1201-1208.

[119] Gomoll, A.; Fitz, W.; Scott, R.; Thornhill, T.; Bellare, A. *ActaOrthopaedica.* **2008**, 79, 421–427.

[120] Furman, B.; Saha, S. *Proc 16th Southern Biomedical Engineering Conference.* **1997**, 124-133.